ACTIN NUCLEATORS IN MICROVILLAR ASSEMBLY: CORDON BLEU AS A NOVEL MICROVILLAR PROTEIN

A Dissertation

Presented to the Faculty of the Graduate School

of Cornell University

In Partial Fulfillment of the Requirements for the Degree of

Doctor of Philosophy

by

Jessica Wayt

January 2015

ACTIN NUCLEATORS IN MICROVILLAR ASSEMBLY: CORDON BLEU AS A NOVEL MICROVILLAR PROTEIN

Jessica Wayt, Ph. D

Cornell University 2015

Epithelial cells polarize through reorganization of the actin cytoskeleton which results in distinct apical and basolateral domains. At the apical domain are structures called microvilli, which are plasma membrane protrusions tethered to a bundled actin filament core. It has been shown that ERM proteins, specifically Ezrin, are important for microvilli formation in these polarized cells. Ezrin is responsible for tethering the actin core to plasma membrane proteins both directly and indirectly through the scaffolding protein EBP50. What is unclear, however, is how the actin filament core of microvilli is nucleated and assembled.

There are several classes of unbranched actin nucleators and regulators, including formins, Spire, VASp, and Cordon Bleu. Formins are involved in the nucleation and polymerization of other actin based membrane protrusions like filopodia, structures similar to microvilli. To determine a potential role for formins in microvilli formation, I used quantitative RT-PCR to quantify relative formin transcript levels in an epithelial cell line that displays abundant microvilli. The top formin candidates were then knocked down using siRNA to explore their role in microvilli formation. I saw minimal effects on microvilli and upon expression of GFP fusion proteins I found that formins were not localized to microvilli. I therefore looked at other actin regulators by examining their localization in epithelial cells.

Cordon Bleu (Cobl) is a WH2-containing protein believed to act as an actin nucleator. I show that it has a very specific localization in epithelial cells at the basal

region of microvilli, a localization unlikely to be involved in actin nucleation. The protein is localized by a central region between the N-terminal COBL domain and the three C-terminal WH2 domains. Ectopic expression of Cobl shortens apical microvilli, and this requires functional WH2 domains. Proteomic studies reveal that the COBL domain binds several BAR-containing proteins, including SNX9, PACSIN-2/Syndapin-2 and ASAP1. ASAP1 is recruited to the base of microvilli by binding the COBL domain through its SH3 domain. I propose that Cobl is localized to the basal region of microvilli to participate in both length regulation and to recruit BAR proteins that associate with the curved membrane found at the microvillar base.

BIOGRAPHICAL SKETCH

Jessica was born on the coast of Virginia, where she resided until the age of four. Her parents then moved the family to a small town in New Jersey, where she would fully develop her "Jersey Girl" attitude. Jessica's first loves were dance and playing musical instruments, activities she whole heartedly participated in from a young age. She excelled in all her academic pursuits, but it was a physics class her senior year that really peaked her interest in science. She graduated near the top of her class from Absegami high school in 2004.

In the fall of 2004, Jessica began her undergraduate career at The University of Maryland, College Park where her diverse interests prevented her from committing to a particular major. As she was in the midst of pursuing a B.S. in psychology, a required chemistry course made her realize that science was actually her true passion. She changed her major and graduated with honors with a B.S. in General Biology in 2008. Her passion for research was ignited her junior year of college when she joined Dr. Arpita Upadhyaya's lab in the department of biophysics as an undergraduate researcher, where she contributed to the development of a mathematical model used to describe T-cell spreading on different substrates. Arpita encouraged Jessica to apply to graduate school in the hopes of keeping her in the lab but was ultimately disappointed when Jessica accepted an offer to attend Cornell University.

In the summer of 2008, Jessica joined the Biochemistry, Molecular and Cellular Biology program at Cornell University. She joined Dr. Anthony Bretscher's lab in 2009, where her love for science fully matured.

To my Mom, who always made sure my feet were firmly planted on the ground.

ACKNOWLEDGEMENTS

I would like to first thank Tony Bretscher for all the help and guidance he has provided me throughout my time here at Cornell. He gave me advice when it was needed, yet gave me enough independence to let me grow and become the scientist I am today. I would also like to thank my fellow Bretscher lab members, past and present, for all their advice and help along the way. Every one of you has influenced the way I think about science and life in general. I would also like to thank my committee, Bill Brown and Bob Weiss, who always offered helpful suggestions at our yearly meetings. Finally, I would like to thank my undergraduate mentor Arpita Upadhyaya, who made me realize how very real my passion for science was when she gave me way more freedom than any biology undergraduate should be afforded in a physics lab.

I would also like to thank my family, who have always supported me in the pursuit of my dreams. I would not be where I am today without their unconditional love and guidance. I would like to thank Kelly Joseph for her continued support and friendship, her selflessness inspires me to be a better woman every day. I would also like to thank all of my friends, especially here at Cornell, who made life in graduate school easy and entirely way too much fun. The Ithaca crew made a lifetime of memories in these 6 years and I know none of us will ever forget it.

Finally, I'd like to thank my partner in life and in love, Colin. I am truly grateful for the honesty, advice and love he has given me in the decade we have spent together. We have both benefited from the challenges we constantly present each other, which has made us much better people and scientists. He will always be that special someone to pick me up when I am down. Or at the very least put a glass of wine in my hand. Thank you for always believing in me, even when I didn't always believe in myself.

TABLE OF CONTENTS

LIST OF FIGURES

LIST OF TABLES

Chapter 1

Introduction

Polarized Epithelial Cells Exhibit Distinct Apical and Basolateral Domains

The ability to polarize is an essential cellular process that is required for many functions, including neuronal signaling, embryogenesis and tissue morphogenesis. Epithelial cells have the ability to undergo apical-basolateral polarity in which the cell coordinates changes in lipid membrane composition, cytoskeletal reorganization and directed trafficking which results in a cell with two distinct domains with distinct functions. While there are many pathways involved in the transition to a polarized cell, I will touch only on a few well defined mechanisms below.

Extracellular cues must first signal the cell before the transition to polarized epithelium can occur. These cues can come from contact with the Extracellular Matrix (ECM) or contacts formed between neighboring cells (Bryant *et al.*, 2010). This initiates a complicated series of signaling cascades and feedback loops that eventually lead to a defined apical and basolateral domain. Different lipid compositions between the two domains is an essential part of signaling as certain proteins are recruited dependent on the lipid signature of the membrane. The apical domain is enriched in Phosphatidylinositol 4,5-bisphosphate (PtdIns(4,5)P_2), while the basolateral domain is enriched in PtdIns(3,4,5)P_2. These specific phosphoinositides are enriched at these membranes through regulation of PTEN (phosphatidylinositol-3,4,5-trisphosphate 3-phosphatase) at the apical domain to make PtdIns(4,5)P_2 and PI3K (phosphatidylinositol-3,4,5-trisphosphate 3-kinase) to make PtdIns(3,4,5)P_2 at the basolateral domain, the regulation of which will not be discussed here (Gassama-Diagne *et al.*, 2006; Martin-Belmonte *et al.*, 2007). These different lipid compositions

participate in the further recruitment of the early determinants of both the apical and basolateral domains.

The ubiquitously expressed PAR proteins comprised of PAR1, PAR3, PAR4, PAR5, PAR6, and aPKC control many steps in the transition to a polarized epithelium. One mechanism for establishing the apical-basal axis is through the physical exclusion of proteins from the apical or basolateral domain, which results in domain specific protein populations. Atypical Protein Kinase C (aPKC) is localized to the apical domain through a complex consisting of PAR6-Crumbs-PALS1 and can exclude proteins from the apical domain, such as lethal giant larvae (LGL), through phosphorylation, which results in their enrichment at the basolateral domain (Betschinger *et al.*, 2003; Tanentzapf and Tepass, 2003). PAR1 performs a similar function by phosphorylating apical domain specific proteins, like PAR3, which excludes them from binding basolateral domain specific proteins (Figure 1.1) (Benton and St Johnston, 2003). These actions further help to establish domains with unique protein and lipid compositions. This is of course an extremely over simplified view. There is cross talk and feedback loops between these proteins that are beyond the scope of this introduction that allow the cell to precisely coordinate this transition to a polarized epithelium. For a more complete review see (Goldstein and Macara, 2007; Rodriguez-Boulan and Macara, 2014).

The cytoskeletal network first undergoes drastic reorganization before a cell can polarize. Microtubules and actin filaments are intrinsically polarized structures and their distinct orientation within a polarized cell helps to establish and maintain polarity. Microtubules are oriented along the long axis of the polarized epithelial cell such that the growing plus ends are oriented towards the basolateral domain (Bacallao *et al.*, 1989). Another more centrally located pool of microtubules are oriented with the plus ends pointing towards the apical domain and this pool helps mediate

A

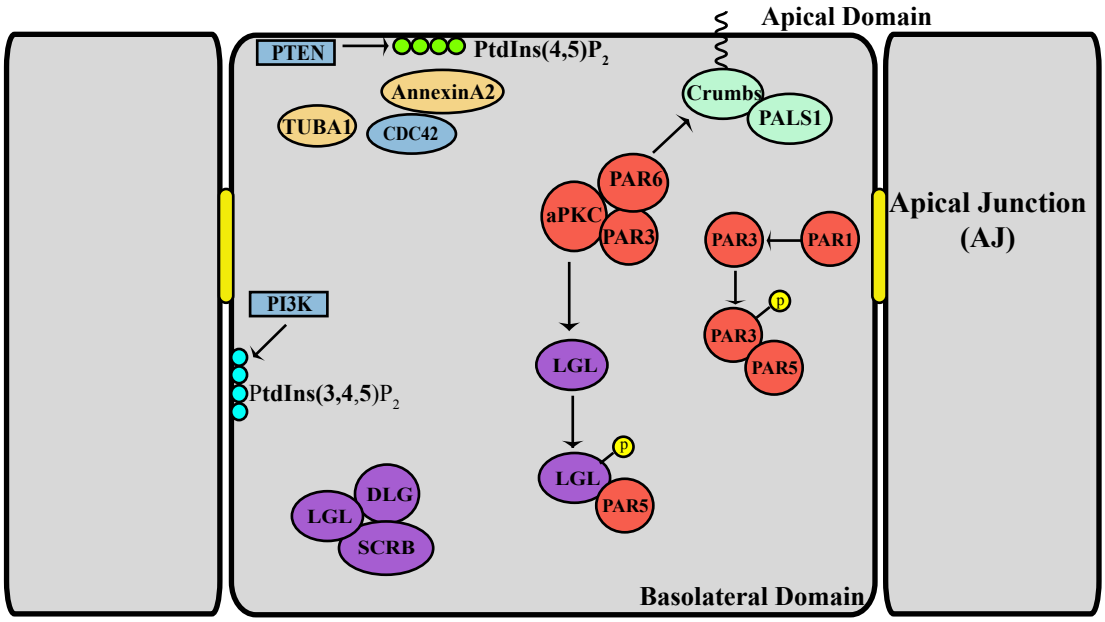

Figure 1.1 Major players in the epithelial polarity pathway. (A) Interactions and feedback loops between different members of the epithelial polarity pathway. The apical domain of polarized epithelial cells is enriched in PI(4,5)P2 through regulation by the phosphatase PTEN. The presence of PI(4,5)P2 assists in the recruitment of proteins to the apical domain. At the basolateral domain the kinase PI3K regulates the production of PI(3,4,5)P2 to recruit basolateral domain specific proteins. AnnexinA2 and PI(4,5)P2 recruit the small GTPase CDC42 to the apical domain which is activated by the Guanine Exchange Factor (GEF) Tuba. CDC42 participates in aPKC activation through PAR6. The apical domain specific transmembrane protein Crumbs recruits PALS1 which in turn recruits PAR6. The CRUMBS-PALS1-PAR6 complex recruits aPKC to the apical domain where it can exclude basolateral domain proteins, like Lethal Giant Larvae (LGL), through phosphorylation. PAR1 can also exclude apical domain specific proteins, like PAR3, from the basolateral domain through phosphorylation. This mechanism of exclusion ensures that the correct proteins are not recruited to the wrong domains. PAR5 binds to phosphorylated PAR3 and LGL as they relocate to the appropriate domain. The basolateral domain specific proteins Lethal Giant Larvae (LGL), Discs Large (DLG), and Scribble (SCRB) contribute to basolateral domain identity through interactions with PI3K and other basolateral proteins. Adapted from Rodriguez-Boulan et al. 2014.

apical oriented membrane trafficking (Weisz and Rodriguez-Boulan, 2009). The actin cytoskeleton must also reorient in the establishment of an apical and basolateral domain. Actin structures are essential for Tight Junctions (TJ) and Adherens Junctions (AJ) at the lateral domain, and these structures are thought to be regulated through the E-cadherin-catenin complex at sites of cell-cell adhesion (Drees *et al.*, 2005).

In the early establishment of the apical domain of polarized cells the Rho-GTPase CDC42 is recruited to the apical domain via AnnexinA2, PtdIns(4,5)P_2 and the guanine exchange factor (GEF) TUBA1 (Martin-Belmonte *et al.*, 2007; Bryant *et al.*, 2010). CDC42 promotes actin polymerization at the apical domain through signaling pathways that activate actin nucleation factors like the Arp2/3 complex (Johnson, 1999). The apical domain of epithelial cells is decorated with structures called microvilli, which are actin based protrusions surrounded by plasma membrane and rooted in the actin terminal web. While we know much about how microvilli are regulated (Hanono *et al.*, 2006; Zwaenepoel *et al.*, 2012), little is known about how the actin core is assembled. This thesis will focus on efforts to understand the formation and regulation of the actin core of these polarized structures.

Loss of epithelial polarity is not only detrimental at the cellular level but also is the cause of many different disease states. Loss of polarity is a hallmark of cancer and many aspects of maintaining epithelial polarity are lost in cancerous cells (Tanos and Rodriguez-Boulan, 2008). There are many other diseases besides cancer that result from loss of proper epithelial polarity. Mis-sorting of channels, like the chloride channel, and receptors, like the EGF receptor, to the wrong membrane result in diseases like Bartter's syndrome and polycystic kidney disease (PKD), respectively (Naesens *et al.*, 2004; Singla and Reiter, 2006). Improper apical recycling and intracellular protein trafficking caused by a mutation in myosin 5B (Myo5B) is responsible for

microvillus inclusion disease (MVID) which results in loss of apical-basolateral polarity and malformed microvilli (Müller *et al.*, 2008). Maintaining the correct polarity is essential for proper tissue and organ function.

Actin Filament Formation

The actin cytoskeleton is comprised of individual actin filaments (F-actin) that can be oriented into higher order structures (i.e. bundles, meshwork) that are essential for providing structural support to the cell. An actin filament is a polymer of individual actin monomer subunits (G-actin)(Holmes *et al.*, 1990). G-actin monomers are asymmetric with binding sites that allow binding to two additional actin monomers in a head to tail manner (Holmes *et al.*, 1990). Because monomer binding is oriented the resulting actin filament is polarized, such that each end exhibits distinct biochemical properties.

Formation of an actin filament is thermodynamically limited by the formation of the actin nucleation seed, which is a dimer or trimer of actin monomers (Figure 1.2A) (Wegner and Engel, 1975; Sept *et al.*, 1999). Once this actin seed is formed, the actin filament can elongate by further monomer addition at either end of the filament in a concentration dependent manner. *In vitro* studies have demonstrated that ATP-actin monomers are added preferentially to the growing (barbed end) of the actin filament at a rate of 11.6 $\mu M^{-1}s^{-1}$, which is 10x faster than addition to the minus end (Pollard, 1981). Once actin monomers are added, the ATP is rapidly hydrolyzed to ADP and Pi, with slow release of Pi to generate ADP-actin which dissociates from the minus end of the actin filament at a rate of $0.27s^{-1}$(Pollard, 1981). ATP-actin dissociates less readily from the filament than ADP-actin which directly effects the critical concentration required for further monomer addition to occur at each respective end. At a steady state concentration of actin

A

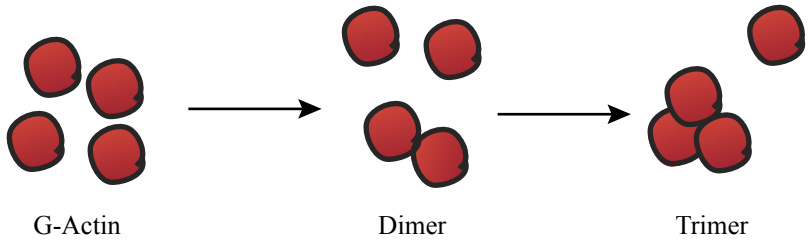

B

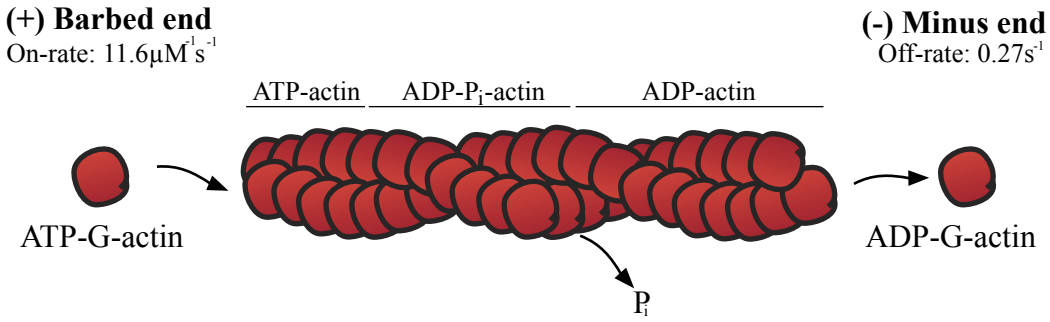

Figure 1.2 Schematic of actin filament formation and dynamics. (A) G-actin monomers are asymmetrical proteins that must form an actin nucleation seed consisting of an actin dimer or trimer before actin filament assembly can occur. (B) Actin monomers are preferentially added to the barbed (+) end of the actin filament at the rate of 11.6 µM-1s-1. (T. D. Pollard 1981). Once actin monomers are added, the ATP is rapidly hydrolyzed to ADP and Pi, with slow release of Pi to generate ADP-actin which dissociates from the minus end of the actin filament at a rate of 0.27s-1. Actin treadmilling occurs when monomer addition occurs preferentially at the barbed end and removal occurs at the pointed end but there is no net change in filament length.

monomers between the concentrations needed for addition to either end, monomer addition occurs preferentially at the barbed end and removal occurs at the pointed end but there is no net change in filament length. This effect is called actin filament treadmilling (Figure 1.2B). Actin treadmilling occurs within cells to generate a protrusive force that is thought to be important for cell motility (Le Clainche and Carlier, 2008; Bugyi and Carlier, 2010).

There is an arsenal of proteins that regulate actin filament assembly and disassembly. *In vitro* studies suggest that once the energetically unfavorable step of forming the actin nucleation seed occurs, a concentration of actin monomers above 0.1 μM will result in monomer addition at the barbed end of the actin filament, a concentration well below the level present in the cytoplasm of most cells (Pollard *et al.*, 2003). However, uncontrolled actin filament formation would be detrimental to the cell, so regulatory mechanisms exist to prevent this from occurring. The actin monomer binding profilin contributes significantly to the regulation of actin filament formation. The binding of profilin to actin monomers prevents spontaneous actin dimer or trimer formation, which in turn allows the cell to carefully regulate where actin filament formation is occurring (Kaiser *et al.*, 1999). Profilin-actin complexes are also preferentially added to the barbed end of the actin filament, which further contributes to filament polarity (Pring *et al.*, 1992). The profilin-actin is utilized during formin mediated actin filament elongation (Romero *et al.*, 2004), which will be discussed further in Chapter 2. To regulate actin filament length, capping proteins, such as CapZ, are employed to bind to the barbed end to physically block further monomer addition. Minus end capping proteins, such as tropomodulin, prevent filament depolymerization (Menna *et al.*, 2011). Actin filaments can be disassembled by the action of the severing protein cofilin, which preferentially binds to ADP-actin subunits (Blanchoin and Pollard, 1999). Binding to ADP-actin causes a structural change that causes a break in the actin filament and an increase in actin filament

free ends (Roland *et al.*, 2008). Utilizing these different proteins, a cell is better able to regulate all facets of actin filament formation.

Microvilli

At the apical domain of polarized epithelial cells are structures called microvilli, which are actin based protrusions surrounded by the plasma membrane. The presence of microvilli increases the surface area of the plasma membrane at the apical domain which is thought to be important for nutrient uptake. It has also been recently reported that cells with microvilli are better suited to resist changes in osmolality, as they use microvilli membrane stores to expand and resist bursting under osmotic stress (Pietuch *et al.*, 2013). The microvilli of the intestinal brush border have an average length of 1 μm and are evenly packed together on the apical domain. Microvilli can be dynamic structures with a lifetime on cultured cells of the order of 5-7 minutes, which includes assembly, steady state and disassembly phases (Gorelik *et al.*, 2003).

The core of microvilli consists of bundled actin filaments which are oriented with the growing, or barbed, end facing the plasma membrane at the tip. It has been demonstrated that the actin core is not static during the lifetime of a microvillus, but is actively treadmilling (Tyska and Mooseker, 2002). FRAP analysis of GFP-Actin expressed in the brush border of immortalized kidney cells demonstrate that actin subunit addition occurs at the tip of microvilli at a rate of approximately 1.5-3.0 s^{-1} (Tyska and Mooseker, 2002; Loomis *et al.*, 2003). The minus end of microvilli are anchored in an F-actin rich network called the terminal web (Tilney and Mooseker, 1971; Mooseker and Tilney, 1975), located in the apical region of the cytoplasm. An organized terminal web is essential for proper microvilli formation. Mice lacking fimbrin, which is an actin

bundling protein localized to the actin core and rootlet of microvilli, have a disorganized terminal web and as a result have shorter microvilli (Grimm-Günter *et al.*, 2009).

A single actin filament would not be able to withstand the force that the surrounding plasma membrane exerts on it in the context of a microvillus, it would buckle under the pressure (Atilgan *et al.*, 2006). This can be overcome by using parallel arrays of actin filaments and the rigidity of these filaments can be increased further by the utilization of actin bundling proteins (Tseng *et al.*, 2001; Atilgan *et al.*, 2006; Claessens *et al.*, 2006) to form higher order actin structures. The actin core of microvilli is comprised of approximately 19 actin filaments that are bundled in a paracrystalline array by three actin bundling proteins: villin, fimbrin and espin (Brown and McKnight, 2010). Villin, espin and fimbrin are all localized along the entire length of the microvilli (Bretscher and Weber, 1980a, 1980b; Bartles, 1998). Studies with single gene knockout mice have suggested that these three actin bundlers are functionally redundant (Bartles, 2000). However, a triple knockout mouse, in which all three actin bundlers are absent, is still able to form intestinal microvilli despite the presence of fewer filaments and highly disorganized F-actin core (Revenu *et al.*, 2012), Interestingly, the lack of bundling proteins has an effect on microvillus length, which shows that while microvilli can still form, the stiffness of the actin core can influence their length, and is in agreement with mathematical models of membrane protrusions (Atilgan *et al.*, 2006). The longer an actin filament, the more flexible it becomes. Without bundling proteins to add rigidity, there is a maximum distance a filament can grow before it can no longer provide the force to withstand the surrounding plasma membrane. The fact that microvilli are present in cells lacking the three known bundling proteins suggests that there are other actin binding proteins present in the microvilli that can also bundle filaments, even if that is not their primary role.

At the tip of microvilli is electron dense material just below the plasma membrane (Tilney, 1970) but all the factors that contribute to this tip complex have not been molecularly determined. One member of the tip complex is Eps8, a protein that can both cap the barbed end of actin filaments as well as bundle them (Croce *et al.*, 2004). Eps8 is another factor that contributes to microvillar length, although it is not essential to microvilli formation. In the Eps8 knockout mouse, microvilli are shorter although there was no obvious disorganization of the F-actin cytoskeleton (Tocchetti *et al.*, 2010). The case of the knockout worm is different, where loss of Eps8 results in longer microvilli although their appearance is less ordered (Croce *et al.*, 2004). This discrepancy might be due to the fact that the *C. elegans* system has a single Eps8 orthologue, while mammalian systems have four members that share functional redundancy (Offenhäuser *et al.*, 2004). Using the genetic simplicity of *C.elegans*, it was demonstrated that the bundling, not capping, function was essential for larval survival (Hertzog *et al.*, 2010). In cultured cells it is assumed that the capping activity is more important in microvilli length regulation, as over expression of an Eps8 orthologue in LLCPK1 cells causes shorter microvilli and this is attributed to the capping ability of Eps8 (Zwaenepoel *et al.*, 2012). Interestingly, the capping and bundling activity is mediated through an interaction with ezrin, an important microvillar protein discussed below (Zwaenepoel *et al.*, 2012). What is unclear, however, is why microvilli would need so many bundling proteins. The presence of so many actin regulatory proteins suggests that regulating the core of microvilli is a carefully orchestrated and important job in a polarized cell.

Tethering the actin core to the plasma membrane is another important requirement for proper microvilli formation. A class I myosin, called Myo1a, can directly tether the actin cytoskeletal core to the plasma membrane (Mooseker and Cheney, 1995). Myo1a is a plus end directed motor protein that can bind to the actin filament through the N-terminal actin binding

motor domain (Jontes *et al.*, 1995). The C-terminus contains a tail homology 1 (TH1) domain that binds directly to phospholipids at the plasma membrane through basic patches located throughout the TH1 domain (Hayden, 1990; Mazerik and Tyska, 2012). Myo1a localizes along the entire length of the actin core of brush border microvilli and provides lateral cross bridges between the actin core and plasma membrane, as seen in classic TEM images (Mooseker and Tilney, 1975; Matsudaira and Burgess, 1982; Brown and McKnight, 2010). It has been suggested that Myo1a plays an important role in regulating the high membrane tension across the apical membrane as loss of Myo1a results in a 70% reduction in membrane tension in cultured epithelial cells (Nambiar *et al.*, 2009). The Myo1a knock out mouse is still able to form microvilli at the apical domain although the microvilli are less ordered and there are regions where the plasma membrane is detached from the actin core (Tyska *et al.*, 2005). This makes a strong argument that Myo1a plays a significant role in regulating the membrane tension required for proper microvilli formation. The fact that microvilli can still form even in the absence of a major tethering protein again illustrates the enormous redundancy that is present in this system. There are several Myo1a orthologues present in microvilli, and in fact in the Myo1a knockout mouse Myo1c, which is normally basolaterally distributed, gets recruited to microvilli (Tyska *et al.*, 2005). A schematic of the actin binding proteins of microvilli can be seen in Figure 1.3.

Ezrin

As mentioned above, ezrin is another important microvilli protein that can directly tether the F-actin core of microvilli to the surrounding plasma membrane. Ezrin is a member of the ezrin, radixin, moesin (ERM) family, proteins that share high sequence similarity and functional redundancy. Ezrin is able to bind F-actin through an F-actin binding domain in the C-terminal

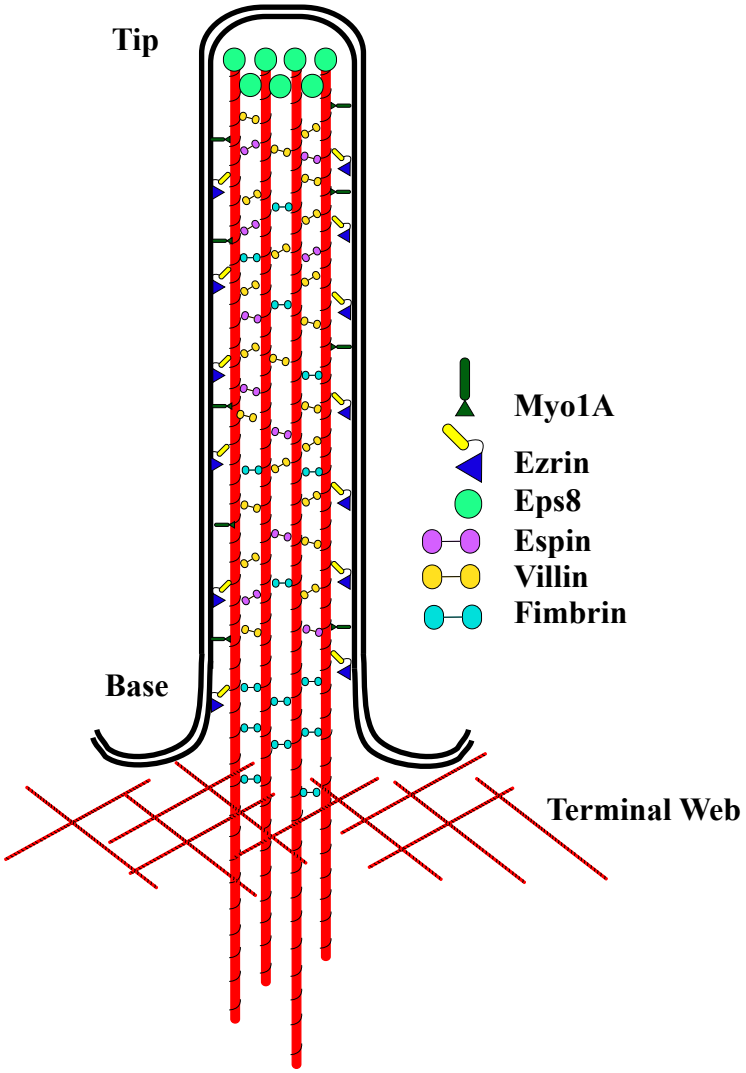

Figure 1.3 Cartoon schematic of actin binding proteins in microvilli. The actin core of microvilli consists of bundles of parallel actin filaments that are rooted in the F-actin rich terminal web which is located in the apical region of the cytoplasm. The core of microvilli is bundled by three primary actin bundling proteins: Espin, Villin and Fimbrin that localize along the entire length of microvilli, although loss of Fimbrin suggests a role in terminal web maintenance. Eps8 is an actin capping and bundling protein that localizes at the tip of microvilli at the barbed (+) end of the actin filament. The actin core is then tethered directly to the plasma membrane by the actin binding proteins myo1A and ezrin.

region of the protein called the C-ERMAD (Turunen *et al.*, 1994). The N-terminal FERM (band 4.1, ezrin, radixin, moesin) domain has affinity for the phospholipid PI(4,5)P_2 and is also able to directly bind the cytoplasmic tails of several transmembrane proteins (Yonemura *et al.*, 1998). Ezrin plays an important role in proper formation of microvilli. The ezrin knockout mouse is still able to form intestinal microvilli, a tissue where ezrin is the only ERM protein expressed, although they are shorter than normal (Saotome *et al.*, 2004). The fact that microvilli are still present suggests that other proteins can compensate for the ability of ezrin to tether the F-actin core to the plasma membrane.

Ezrin's activation, conformational change, and subsequent localization is a tightly regulated process. The C-ERMAD of ezrin is able to bind the N-terminal FERM domain, which results in a closed protein conformation that can no longer bind F-actin (Gary and Bretscher, 1995) and whose localization is mostly cytoplasmic. Release from this autoinhibition into an open, active conformation is thought to occur first by ezrin binding to the phospholipid PI(4,5)P_2 which opens the protein sufficiently to allow subsequent phosphorylation (Figure 1.4) (Fievet *et al.*, 2004; Ben-Aissa *et al.*, 2012). A large contribution to ezrin activation occurs by the phosphorylation of threonine 567 (T567) at the interface between the FERM domain and the C-ERMAD to stabilize the open conformation of the protein by preventing binding between the two domains (Fievet *et al.*, 2004). Recent evidence suggests that the kinases responsible for phosphorylation of ezrin at T567 are LOK and SLK, which are apically localized in epithelial cells (Viswanatha *et al.*, 2012). Interestingly, a phosphomimetic ezrin mutant that is constitutively active (T567E) loses specific apical localization which suggests that ezrin must undergo cycles of phosphorylation and dephosphorylation to localize properly (Viswanatha *et al.*, 2012). The utilization of different ezrin

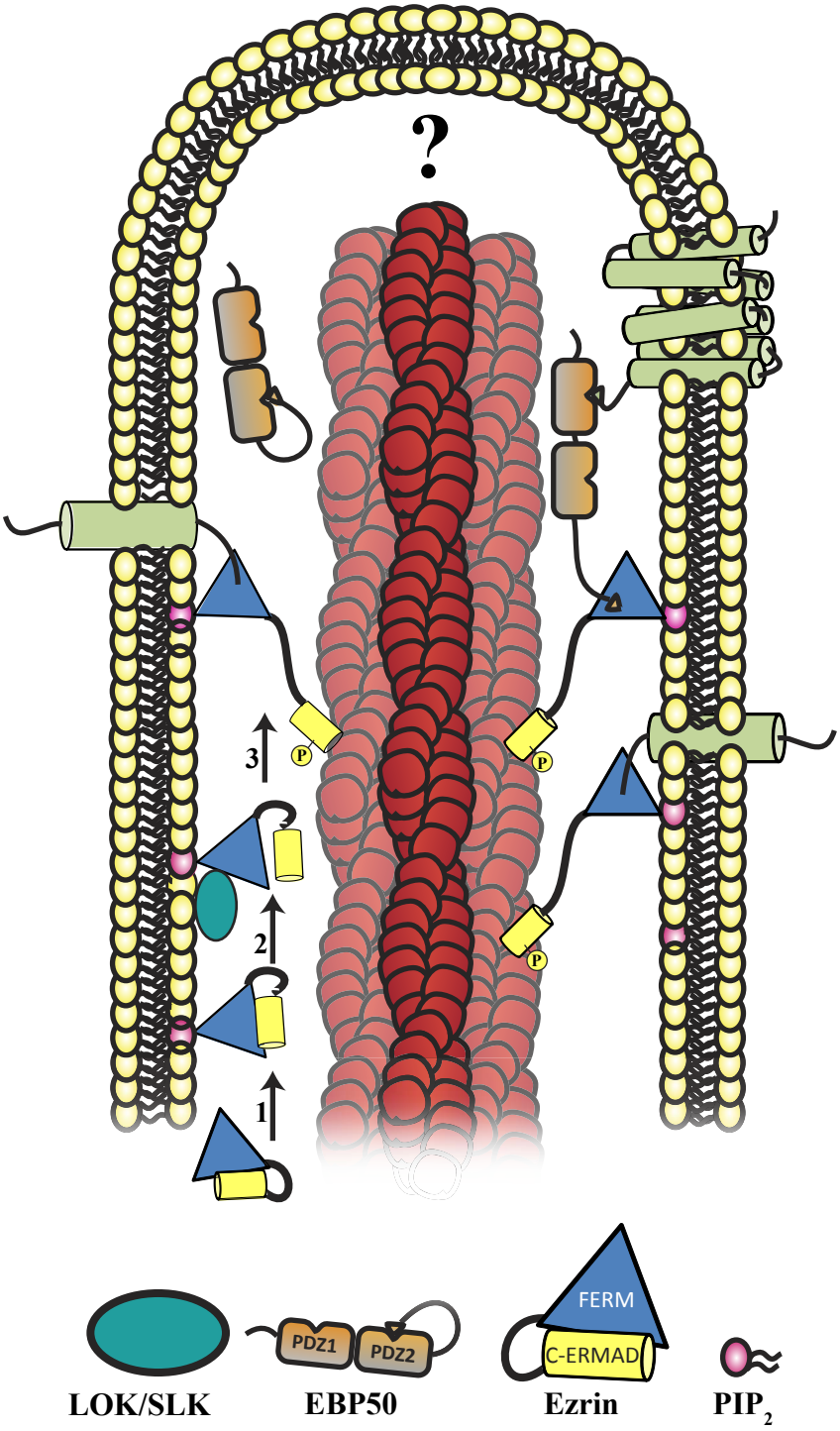
?
3
2
1
P
P
P
FERM
C-ERMAD
PDZ1
PDZ2
LOK/SLK
EBP50
Ezrin
PIP2

Figure 1.4 Simplified depiction of ezrin activation. Ezrin is cytoplasmic in the closed, auto-inhibited state. (1) Ezrin in the auto-inhibited state is recruited to $PI(4,5)P_2$ (pink) on the plasma membrane of microvilli. This recruitment induces a conformational change in which ezrin is now partially open and activated. (2) This activation is stabilized by phosphorylation of the C-ERMAD of ezrin at residue threonine 567 (T567) by the kinase LOK/SLK. (3) This open, active conformation allows the C-ERMAD to bind to F-actin and the N-terminal FERM domain to interact with transmembrane proteins at the plasma membrane. This results in a direct tether between the F-actin core and the plasma membrane. The actin core can also be indirectly tethered to the plasma membrane through the interaction between the ezrin FERM domain and the scaffolding protein EBP50. What remains to be discovered is which actin nucleator (denoted by a question mark) is involved in the formation of the actin core of microvilli, which is predicted to localize at the growing end of the F-actin filaments at the tip of microvilli. Adapted from a figure from Dr. Damien Garbett.

phosphomutants is an essential tool that will be used in Appendix A to characterize the interaction between ezrin and the formin FHOD1.

The actin core can also be indirectly tethered through the interaction between an open, activated ezrin and the scaffolding protein EBP50 (ERM phosphobinding protein)(Reczek *et al.*, 1997). The C-terminal tail of EBP50 interacts with ezrin and the N-terminal PDZ domains interact with transmembrane proteins to provide an indirect link between the plasma membrane and the actin cytoskeleton (Figure 1.4) (Fehon *et al.*, 2010). In cultured cells, EBP50 is necessary for microvilli formation (Hanono *et al.*, 2006). This function is critically dependent on ezrin, as an EBP50 mutant unable to bind ezrin cannot rescue the loss of microvilli phenotype upon EBP50 knockdown (Garbett *et al.*, 2010). Surprisingly, the EBP50 knockout mouse is able to form short brush border microvilli, although interestingly there is less actived ezrin present in the brush border (Morales *et al.*, 2004). This suggests that both ezrin and EBP50 work cooperatively to form properly organized microvilli.

As discussed above, we know a lot about how the actin core of microvilli is regulated but almost nothing is known about how the actin core is initially formed or nucleated. This work will attempt to address this issue, but I would first like to discuss the family of proteins involved in regulating the formation of actin filaments: actin nucleators.

In vivo, actin filaments are formed by a class of proteins called actin nucleators

As mentioned before, spontaneous formation of the actin dimers or trimers required to seed actin filament formation is energetically unfavorable and suppressed in the presence of actin monomer binding proteins like profilin (Vinson *et al.*, 1998). To control actin filament formation spatially and temporally cells utilize a class of proteins called actin nucleators. There are two

classes of actin nucleators that assemble two different types of actin filaments: branched and unbranched. Branched actin filaments are nucleated by the Arp2/3 complex under the regulation of nucleation promoting factors to assemble a new filament at ~70˚ angle from a pre-exisiting filament (Figure 1.5A) (Smith *et al.*, 2013). While branched filaments are crucial to many cellular processes, the actin core of microvilli is comprised of unbranched filaments so the focus of discussion will be centered on unbranched actin nucleators.

The largest class of actin nucleators that drive the assembly of unbranched filaments (Figure 1.5B) is the formin family, of which an introduction can be found in Chapter 2. There is also an emerging class of nucleators of unbranched filaments that contain the actin-monomer binding Wasp Homology 2 domain (WH2), and includes Spire, Leiomodin and Cordon Bleu. WH2 domains are variable in length (25-50AA) and contain the consensus motif LKKT, but K is often any basic amino acid, that facilitates binding to actin monomers (Paunola *et al.*, 2002). Beyond that consensus motif, the sequences of WH2 domains are poorly conserved which makes them difficult to identify. Although all WH2 domains bind actin, WH2 domains have diverse, protein specific functions (Carlier *et al.*, 2007). This can include nucleating, capping and even severing actin filaments. This wide variety of functions have made WH2 domain containing proteins a very interesting class of actin nucleators. I will focus the rest of this introduction on the WH2 domain containing actin nucleator Cordon Bleu (Cobl), which is also the focus of Chapter 3.

Cordon Bleu *in vivo*

Cordon Bleu (Cobl) was originally discovered in a LacZ-gene-trap experiment that was designed to identify novel genes involved in early mouse development (Gasca *et al.*, 1995). It was originally thought to be vertebrate specific, but recent bioinformatic studies indicate that there are

A. Branched Nucleators

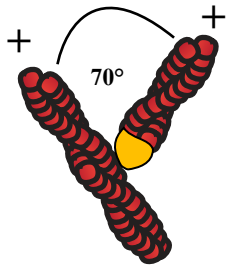

Arp2/3

B. Unbranched Nucleators

Formin

WH2 domain containing nucleators

Figure 1.5 There are two classes of actin nucleators for two types of actin filaments: branched and unbranched. (A) The Arp2/3 complex (yellow) nucleates the assembly of branched actin filaments within the cell. Under the regulation of nucleation promoting factors, the Arp2/3 complex binds to the side of a pre-existing actin filament and acts as a template to allow further monomer addition to occur at the barbed (+) end at a 70˚ angle to the pre-existing filament. (B) A major class of unbranched actin nucleators is the formin family which can both nucleate the assembly of unbranched actin filaments and increase the elongation rate of growing actin filaments. The FH2 domain (yellow arcs) must dimerize in a head to tail manner before filament elongation can occur. The protein then remains processively bound on the barbed (+) end as the filament is assembled. Another class of unbranched actin nucleators is the WH2 domain containing nucleators, which utilize WH2 domains (yellow squares) to sequester actin monomers to stabilize the energetically unfavorable actin dimer or trimer. This nucleation seed than allows actin filament elongation to occur from the barbed (+) end of actin filaments.

non-vertebrate homologs (Schultz and Terhoeven, 2013). It was named for the distinct pattern of expression along the axial midline, which looks like a blue ribbon (cordon bleu in French). The allele identified in the original gene trap experiment, CoblC101, is weakly hypomorphic with no obvious phenotype (Carroll *et al.*, 2003). When the CoblC101 allele is combined with the *Loop-tail* neurulation mutant, which has neural tube defects due to a mutation in the VANGL2 gene, there is an enhanced neural tube defect (Carroll *et al.*, 2003). This suggests a genetic interaction with VANGL2, a component of the planar cell polarity pathway (PCP), and hints at a potential role for Cobl in the PCP pathway. A Cobl knockout mouse has not been published to date, although personal communications with J. Klingensmith of Duke University suggest that Cobl knockout mice are viable with no overt phenotype.

To further understand a possible in vivo role for Cobl, the model organism zebrafish was utilized. Localization of endogenous Cobl highlights enrichment in the apical actin meshwork of ciliated epithelia (Ravanelli and Klingensmith, 2011). Loss of Cobl function results in embryonic defects, like failure in body axis elongation, that are often attributed to motile cilia defects. Indeed, depletion of Cobl results in shorter motile cilia but does not affect the total number of cilia in the Kupffer's vesicle, which is the equivalent to the node in mammals (Ravanelli and Klingensmith, 2011). As motile cilia are comprised of microtubules, not bundled actin filaments, this defect was attributed to loss of the apical actin meshwork that is directly below the cilia. How Cobl is effecting the actin cytoskeleton in this specific domain remains unclear.

Cordon Bleu is a WH2 domain containing actin nucleator and severing agent

A single Cobl gene is present in vertebrates that encodes a large (1260-1354 AA) protein that varies in length dependent on the species (Figure 1.6). The N-terminal region of Cobl consists

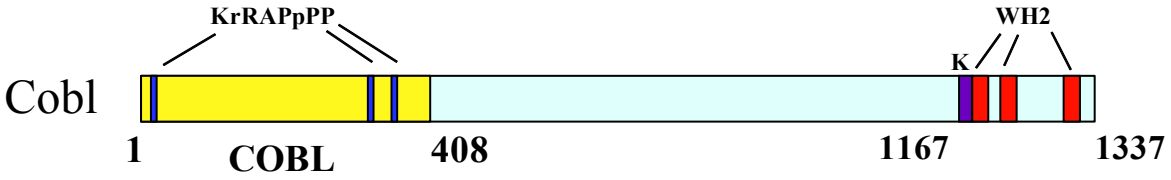

Figure 1.6 Schematic of murine Cordon Bleu. (A) At the N-terminus of Cordon Bleu (Cobl) is the canonical COBL domain which contains three polyproline KRAP motifs that are important for protein-protein interactions. At the C-terminus is three Wasp Homology 2 (WH2) domains, each of which bind an individual actin monomer. Immediately preceding the first WH2 domain is a lysine rich patch, which in conjunction with at least the first WH2 domain, is essential for nucleating the assembly of actin filaments. The region between the COBL domain and the WH2 domains is predicted to be unordered.

of the canonical COBL domain that shares 84% sequence identity among vertebrates. The COBL domain contains three proline rich KRAP motifs (Gasca *et al.*, 1995), which are important for mediating protein-protein interactions with SH3 domain containing proteins (Ahuja *et al.*, 2007). In the C-terminal region are three WH2 domains preceded by an 18 amino acid lysine rich region that is essential for regulation of the actin cytoskeleton by Cobl (Husson *et al.*, 2011). Each WH2 domain is able to bind to a single actin monomer with a 1:1 stoicheometry but not with the same affinity (Ahuja *et al.*, 2007). The region between the COBL domain and the WH2 domains is variable with no predicted structural features. A protein related to Cobl, the Cobl-like (CoblL1), harbors a COBL domain and a single WH2 domain but because they have no overlapping colocalization they are not predicted to share related functions (Carroll *et al.*, 2003).

The mechanism of Cobl mediated actin filament nucleation has not been fully established in the field. Original work demonstrated that Cobl promotes barbed end actin nucleation, but has little affinity for remaining at the barbed end, and that nucleation requires all three WH2 domains (Ahuja *et al.*, 2007). Each WH2 domain (labeled here on as A, B, C) binds an individual actin monomer, although WH2-C has weak affinity for actin monomers compared to the first two WH2 domains (Ahuja *et al.*, 2007). It was proposed that Cobl nucleates by a "template" mechanism in which the WH2 domains of Cobl bring together and stabilize the individual actin monomers to form the trimer that precedes actin filament elongation. Recent evidence suggests that this is not entirely the case. The finding that Cobl is a potent actin nucleator even when only the lysine rich patch and a single WH2 domain is present suggested that the template mechanism does not explain the mechanism of action for Cobl. It is thought that the positive lysine rich patch negates the negative charges on actin and that in combination with a single WH2 domain is enough to allow nucleation to occur. This mechanism of nucleation suggests that Cobl acts like a catalyst to make

the spontaneous formation of the actin nucleation seed more thermodynamically favorable (Husson *et al.*, 2011). A recent crystal structure of Cobl2W(WH2-A and WH2-B) in complex with two actin monomers also demonstrates that a template mechanism of actin nucleation is not possible (Chen *et al.*, 2013).

Cobl is a versatile actin regulatory protein that does not just nucleate the assembly of actin filaments but is also a potent severing protein (Husson *et al.*, 2011). This is not a novel function for WH2 domain containing proteins; the formin INF2 and the nucleator spire are also severing proteins (Chhabra and Higgs, 2006; Bosch *et al.*, 2007). Efficient severing activity by Cobl requires the lysine rich patch and the first two WH2 domains (K-WH2AB), and its activity can be abolished by mutating a critical charged patch in WH2-A, in the context of K-WH2AB (Jiao *et al.*, 2014). Structural data suggest that WH2-A is able to insert itself between actin monomers along the long pitch of an actin filament (Chen *et al.*, 2013) which is dependent on the basic charge of the lysine rich region and the first WH2 domain (Jiao *et al.*, 2014). This insertion is likely to cause structural instability in the filament resulting in filament breakage. Cobl has a higher affinity for ADP-Actin than ATP- actin (Husson *et al.*, 2011) and does not remain bound to the filament upon breakage, but sequesters ADP-actin after severing which allows for filament re-annealing to occur (Jiao *et al.*, 2014). This allows for Cobl to regulate fast F-actin dynamics but the functional consequences in the cell have yet to be determined.

Cobl has diverse functions in cells

Cobl was first described as an actin nucleator after it was discovered in a yeast 2 hybrid screen looking for novel interaction partners for Abp1 and Pacsin1, proteins that promote actin cytoskeletal reorganization (Ahuja *et al.*, 2007). Cobl plays a role in neuronal morphogenesis; in

cultured neurons overexpression of the C-terminal domain increases dendritic branch points, and decreased endogenous Cobl expression results in less dendritic branching (Ahuja *et al.*, 2007). This function is dependent on an interaction between Cobl and Pacsin1: knockdown of Pacsin1 suppresses the increased dendritic branching following Cobl overexpression (Schwintzer *et al.*, 2011). Recent work has also suggested that Cobl and Abp1 (Actin binding protein 1) work together to promote neuronal differentiation in Purkinje cells (Haag *et al.*, 2012). A mechanism was proposed in which both Abp1 and Pacsin1 were required for Cobl function, Abp1 as a recruitment factor and Pacsin1 as a plasma membrane anchor (Haag *et al.*, 2012). Interaction between Pacsin1 and Cobl has also been shown to be essential for the proper formation of ciliated sensory hair cells in zebrafish (Schüler *et al.*, 2013). More work is required to determine how Cobl is regulating the actin cytoskeleton in cells.

Project Overview

As described above, there is a large body of work contributing to our understanding of how microvilli are regulated and which factors contribute to this regulation. We understand a lot about how the actin core of microvilli is bundled and tethered to the plasma membrane but what remains a mystery is how the actin core is nucleated. The focus of this dissertation is to understand the role of two different classes of actin nucleators in microvilli formation. The formin family of unbranched actin nucleators are an attractive candidate for nucleating the assembly of the actin filament core of microvilli. In Chapter 2 I will examine the potential role of formins in microvilli formation. Recently, two proteomic analyses have identified the actin nucleator Cordon Bleu as only one of two actin nucleators present in the intestinal brush border (McConnell *et al.*, 2011; Revenu *et al.*, 2012). In Chapter 3 I will characterize Cordon Bleu in JEG-3 cells, a

choriocarcinoma line with abundant microvilli on the apical domain. This will include the dynamics of Cobl, the requirement for localization to a specific region of microvilli and possible functions of Cobl at microvilli in JEG-3 cells. This work provides novel insight on Cobl function within cells.

Finally, in Appendix A I characterize the interaction between ezrin and the formin FHOD1 in JEG-3 cells and through utilization of recombinant proteins. Appendix B will highlight results from recent proteomic analysis of the localization domain of Cordon Bleu.

References

Ahuja, R., Pinyol, R., Reichenbach, N., Custer, L., Klingensmith, J., Kessels, M. M., and Qualmann, B. (2007). Cordon-bleu is an actin nucleation factor and controls neuronal morphology. Cell *131*, 337–350.

Atilgan, E., Wirtz, D., and Sun, S. X. (2006). Mechanics and dynamics of actin-driven thin membrane protrusions. Biophys. J. *90*, 65–76.

Bacallao, R., Antony, C., Dotti, C., Karsenti, E., Stelzer, E. H., and Simons, K. (1989). The subcellular organization of Madin-Darby canine kidney cells during the formation of a polarized epithelium. J. Cell Biol. *109*, 2817–2832.

Bartles, J. R. (1998). Small Espin: A Third Actin-bundling Protein and Potential Forked Protein Ortholog in Brush Border Microvilli. J. Cell Biol. *143*, 107–119.

Bartles, J. R. (2000). Parallel actin bundles and their multiple actin-bundling proteins. Curr. Opin. Cell Biol. *12*, 72–78.

Ben-Aissa, K., Patino-Lopez, G., Belkina, N. V, Maniti, O., Rosales, T., Hao, J.-J., Kruhlak, M. J., Knutson, J. R., Picart, C., and Shaw, S. (2012). Activation of moesin, a protein that links actin cytoskeleton to the plasma membrane, occurs by phosphatidylinositol 4,5-bisphosphate (PIP2) binding sequentially to two sites and releasing an autoinhibitory linker. J. Biol. Chem. *287*, 16311–16323.

Benton, R., and St Johnston, D. (2003). Drosophila PAR-1 and 14-3-3 inhibit Bazooka/PAR-3 to establish complementary cortical domains in polarized cells. Cell *115*, 691–704.

Betschinger, J., Mechtler, K., and Knoblich, J. A. (2003). The Par complex directs asymmetric cell division by phosphorylating the cytoskeletal protein Lgl. Nature *422*, 326–330.

Blanchoin, L., and Pollard, T. D. (1999). Mechanism of Interaction of Acanthamoeba Actophorin (ADF/Cofilin) with Actin Filaments. J. Biol. Chem. *274*, 15538–15546.

Bosch, M., Le, K. H. D., Bugyi, B., Correia, J. J., Renault, L., and Carlier, M.-F. (2007). Analysis of the function of Spire in actin assembly and its synergy with formin and profilin. Mol. Cell *28*, 555–568.

Bretscher, A., and Weber, K. (1980a). Fimbrin, a new microfilament-associated protein present in microvilli and other cell surface structures. J. Cell Biol. *86*, 335–340.

Bretscher, A., and Weber, K. (1980b). Villin is a major protein of the microvillus cytoskeleton which binds both G and F actin in a calcium-dependent manner. Cell *20*, 839–847.

Brown, J. W., and McKnight, C. J. (2010). Molecular model of the microvillar cytoskeleton and organization of the brush border. PLoS One *5*, e9406.

Bryant, D. M., Datta, A., Rodríguez-Fraticelli, A. E., Peränen, J., Martín-Belmonte, F., and Mostov, K. E. (2010). A molecular network for de novo generation of the apical surface and lumen. Nat. Cell Biol. *12*, 1035–1045.

Bugyi, B., and Carlier, M.-F. (2010). Control of actin filament treadmilling in cell motility. Annu. Rev. Biophys. *39*, 449–470.

Carlier, M.-F., Hertzog, M., Didry, D., Renault, L., Cantrelle, F.-X., van Heijenoort, C., Knossow, M., and Guittet, E. (2007). Structure, function, and evolution of the beta-thymosin/WH2 (WASP-Homology2) actin-binding module. Ann. N. Y. Acad. Sci. *1112*, 67–75.

Carroll, E. A., Gerrelli, D., Gasca, S., Berg, E., Beier, D. R., Copp, A. J., and Klingensmith, J. (2003). Cordon-bleu is a conserved gene involved in neural tube formation. Dev. Biol. *262*, 16–31.

Chen, X., Ni, F., Tian, X., Kondrashkina, E., Wang, Q., and Ma, J. (2013). Structural basis of actin filament nucleation by tandem W domains. Cell Rep. *3*, 1910–1920.

Chhabra, E. S., and Higgs, H. N. (2006). INF2 Is a WASP homology 2 motif-containing formin that severs actin filaments and accelerates both polymerization and depolymerization. J. Biol. Chem. *281*, 26754–26767.

Claessens, M. M. A. E., Bathe, M., Frey, E., and Bausch, A. R. (2006). Actin-binding proteins sensitively mediate F-actin bundle stiffness. Nat. Mater. *5*, 748–753.

Le Clainche, C., and Carlier, M.-F. (2008). Regulation of actin assembly associated with protrusion and adhesion in cell migration. Physiol. Rev. *88*, 489–513.

Croce, A., Cassata, G., Disanza, A., Gagliani, M. C., Tacchetti, C., Malabarba, M. G., Carlier, M.-F., Scita, G., Baumeister, R., and Di Fiore, P. P. (2004). A novel actin barbed-end-capping activity in EPS-8 regulates apical morphogenesis in intestinal cells of Caenorhabditis elegans. Nat. Cell Biol. *6*, 1173–1179.

Drees, F., Pokutta, S., Yamada, S., Nelson, W. J., and Weis, W. I. (2005). Alpha-catenin is a molecular switch that binds E-cadherin-beta-catenin and regulates actin-filament assembly. Cell *123*, 903–915.

Fehon, R. G., McClatchey, A. I., and Bretscher, A. (2010). Organizing the cell cortex: the role of ERM proteins. Nat. Rev. Mol. Cell Biol. *11*, 276–287.

Fievet, B. T., Gautreau, A., Roy, C., Del Maestro, L., Mangeat, P., Louvard, D., and Arpin, M. (2004). Phosphoinositide binding and phosphorylation act sequentially in the activation mechanism of ezrin. J. Cell Biol. *164*, 653–659.

Garbett, D., LaLonde, D. P., and Bretscher, A. (2010). The scaffolding protein EBP50 regulates microvillar assembly in a phosphorylation-dependent manner. J. Cell Biol. *191*, 397–413.

Gary, R., and Bretscher, A. (1995). Ezrin self-association involves binding of an N-terminal domain to a normally masked C-terminal domain that includes the F-actin binding site. Mol. Biol. Cell *6*, 1061–1075.

Gasca, S., Hill, D. P., Klingensmith, J., and Rossant, J. (1995). Characterization of a gene trap insertion into a novel gene, cordon-bleu, expressed in axial structures of the gastrulating mouse embryo. Dev. Genet. *17*, 141–154.

Gassama-Diagne, A., Yu, W., ter Beest, M., Martin-Belmonte, F., Kierbel, A., Engel, J., and Mostov, K. (2006). Phosphatidylinositol-3,4,5-trisphosphate regulates the formation of the basolateral plasma membrane in epithelial cells. Nat. Cell Biol. *8*, 963–970.

Goldstein, B., and Macara, I. G. (2007). The PAR proteins: fundamental players in animal cell polarization. Dev. Cell *13*, 609–622.

Gorelik, J. *et al.* (2003). Dynamic assembly of surface structures in living cells. Proc. Natl. Acad. Sci. U. S. A. *100*, 5819–5822.

Grimm-Günter, E.-M. S., Revenu, C., Ramos, S., Hurbain, I., Smyth, N., Ferrary, E., Louvard, D., Robine, S., and Rivero, F. (2009). Plastin 1 binds to keratin and is required for terminal web assembly in the intestinal epithelium. Mol. Biol. Cell *20*, 2549–2562.

Haag, N., Schwintzer, L., Ahuja, R., Koch, N., Grimm, J., Heuer, H., Qualmann, B., and Kessels, M. M. (2012). The Actin Nucleator Cobl Is Crucial for Purkinje Cell Development and Works in Close Conjunction with the F-Actin Binding Protein Abp1. J. Neurosci. *32*, 17842–17856.

Hanono, A., Garbett, D., Reczek, D., Chambers, D. N., and Bretscher, A. (2006). EPI64 regulates microvillar subdomains and structure. J. Cell Biol. *175*, 803–813.

Hayden, S. M. (1990). Binding of brush border myosin I to phospholipid vesicles. J. Cell Biol. *111*, 443–451.

Hertzog, M. *et al.* (2010). Molecular basis for the dual function of Eps8 on actin dynamics: bundling and capping. PLoS Biol. *8*, e1000387.

Holmes, K. C., Popp, D., Gebhard, W., and Kabsch, W. (1990). Atomic model of the actin filament. Nature *347*, 44–49.

Husson, C., Renault, L., Didry, D., Pantaloni, D., and Carlier, M.-F. (2011). Cordon-Bleu uses WH2 domains as multifunctional dynamizers of actin filament assembly. Mol. Cell *43*, 464–477.

Jiao, Y., Walker, M., Trinick, J., Pernier, J., Montaville, P., and Carlier, M.-F. (2014). Mutagenetic and electron microscopy analysis of actin filament severing by Cordon-Bleu, a WH2 domain protein. Cytoskeleton (Hoboken). *71*, 170–183.

Johnson, D. I. (1999). Cdc42: An essential Rho-type GTPase controlling eukaryotic cell polarity. Microbiol. Mol. Biol. Rev. *63*, 54–105.

Jontes, J. D., Wilson-Kubalek, E. M., and Milligan, R. A. (1995). A 32 degree tail swing in brush border myosin I on ADP release. Nature *378*, 751–753.

Kaiser, D. A., Vinson, V. K., Murphy, D. B., and Pollard, T. D. (1999). Profilin is predominantly associated with monomeric actin in Acanthamoeba. J. Cell Sci. *112 (Pt 2*, 3779–3790.

Loomis, P. A., Zheng, L., Sekerková, G., Changyaleket, B., Mugnaini, E., and Bartles, J. R. (2003). Espin cross-links cause the elongation of microvillus-type parallel actin bundles in vivo. J. Cell Biol. *163*, 1045–1055.

Martin-Belmonte, F., Gassama, A., Datta, A., Yu, W., Rescher, U., Gerke, V., and Mostov, K. (2007). PTEN-mediated apical segregation of phosphoinositides controls epithelial morphogenesis through Cdc42. Cell *128*, 383–397.

Matsudaira, P. T., and Burgess, D. R. (1982). Organization of the cross-filaments in intestinal microvilli. J. Cell Biol. *92*, 657–664.

Mazerik, J. N., and Tyska, M. J. (2012). Myosin-1A targets to microvilli using multiple membrane binding motifs in the tail homology 1 (TH1) domain. J. Biol. Chem. *287*, 13104–13115.

McConnell, R. E., Benesh, A. E., Mao, S., Tabb, D. L., and Tyska, M. J. (2011). Proteomic analysis of the enterocyte brush border. Am. J. Physiol. Gastrointest. Liver Physiol. *300*, G914–26.

Menna, E., Fossati, G., Scita, G., and Matteoli, M. (2011). From filopodia to synapses: the role of actin-capping and anti-capping proteins. Eur. J. Neurosci. *34*, 1655–1662.

Mooseker, M. S., and Cheney, R. E. (1995). Unconventional myosins. Annu. Rev. Cell Dev. Biol. *11*, 633–675.

Mooseker, M. S., and Tilney, L. G. (1975). Organization of an actin filament-membrane complex. Filament polarity and membrane attachment in the microvilli of intestinal epithelial cells. J. Cell Biol. *67*, 725–743.

Morales, F. C., Takahashi, Y., Kreimann, E. L., and Georgescu, M.-M. (2004). Ezrin-radixin-moesin (ERM)-binding phosphoprotein 50 organizes ERM proteins at the apical membrane of polarized epithelia. Proc. Natl. Acad. Sci. U. S. A. *101*, 17705–17710.

Müller, T. *et al.* (2008). MYO5B mutations cause microvillus inclusion disease and disrupt epithelial cell polarity. Nat. Genet. *40*, 1163–1165.

Naesens, M., Steels, P., Verberckmoes, R., Vanrenterghem, Y., and Kuypers, D. (2004). Bartter's and Gitelman's syndromes: from gene to clinic. Nephron. Physiol. *96*, p65–78.

Nambiar, R., McConnell, R. E., and Tyska, M. J. (2009). Control of cell membrane tension by myosin-I. Proc. Natl. Acad. Sci. U. S. A. *106*, 11972–11977.

Offenhäuser, N., Borgonovo, A., Disanza, A., Romano, P., Ponzanelli, I., Iannolo, G., Di Fiore, P. P., and Scita, G. (2004). The eps8 family of proteins links growth factor stimulation to actin reorganization generating functional redundancy in the Ras/Rac pathway. Mol. Biol. Cell *15*, 91–98.

Paunola, E., Mattila, P. K., and Lappalainen, P. (2002). WH2 domain: a small, versatile adapter for actin monomers. FEBS Lett. *513*, 92–97.

Pietuch, A., Brückner, B. R., and Janshoff, A. (2013). Membrane tension homeostasis of epithelial cells through surface area regulation in response to osmotic stress. Biochim. Biophys. Acta *1833*, 712–722.

Pollard, T. D. (1981). Direct measurement of actin polymerization rate constants by electron microscopy of actin filaments nucleated by isolated microvillus cores. J. Cell Biol. *88*, 654–659.

Pollard, T. D., Blanchoin, L., and Mullins, R. D. (2003). Molecular mechanisms controlling actin filament dynamics in nonmuscle cells.

Pring, M., Weber, A., and Bubb, M. R. (1992). Profilin-actin complexes directly elongate actin filaments at the barbed end. Biochemistry *31*, 1827–1836.

Ravanelli, A. M., and Klingensmith, J. (2011). The actin nucleator Cordon-bleu is required for development of motile cilia in zebrafish. Dev. Biol. *350*, 101–111.

Reczek, D., Berryman, M., and Bretscher, A. (1997). Identification of EBP50: A PDZ-containing phosphoprotein that associates with members of the ezrin-radixin-moesin family. J. Cell Biol. *139*, 169–179.

Revenu, C. *et al.* (2012). A new role for the architecture of microvillar actin bundles in apical retention of membrane proteins. Mol. Biol. Cell *23*, 324–336.

Rodriguez-Boulan, E., and Macara, I. G. (2014). Organization and execution of the epithelial polarity programme. Nat. Rev. Mol. Cell Biol. *15*, 225–242.

Roland, J., Berro, J., Michelot, A., Blanchoin, L., and Martiel, J.-L. (2008). Stochastic severing of actin filaments by actin depolymerizing factor/cofilin controls the emergence of a steady dynamical regime. Biophys. J. *94*, 2082–2094.

Romero, S., Le Clainche, C., Didry, D., Egile, C., Pantaloni, D., and Carlier, M.-F. (2004). Formin is a processive motor that requires profilin to accelerate actin assembly and associated ATP hydrolysis. Cell *119*, 419–429.

Saotome, I., Curto, M., and McClatchey, A. I. (2004). Ezrin is essential for epithelial organization and villus morphogenesis in the developing intestine. Dev. Cell *6*, 855–864.

Schüler, S., Hauptmann, J., Perner, B., Kessels, M. M., Englert, C., and Qualmann, B. (2013). Ciliated sensory hair cell formation and function require the F-BAR protein syndapin I and the WH2 domain-based actin nucleator Cobl. J. Cell Sci. *126*, 196–208.

Schultz, J., and Terhoeven, N. (2013). The bilaterian roots of cordon-bleu. BMC Res. Notes *6*, 393.

Schwintzer, L., Koch, N., Ahuja, R., Grimm, J., Kessels, M. M., and Qualmann, B. (2011). The functions of the actin nucleator Cobl in cellular morphogenesis critically depend on syndapin I. EMBO J. *30*, 3147–3159.

Sept, D., Elcock, A. H., and McCammon, J. A. (1999). Computer simulations of actin polymerization can explain the barbed-pointed end asymmetry. J. Mol. Biol. *294*, 1181–1189.

Singla, V., and Reiter, J. F. (2006). The primary cilium as the cell's antenna: signaling at a sensory organelle. Science *313*, 629–633.

Smith, B. A., Daugherty-Clarke, K., Goode, B. L., and Gelles, J. (2013). Pathway of actin filament branch formation by Arp2/3 complex revealed by single-molecule imaging. Proc. Natl. Acad. Sci. U. S. A. *110*, 1285–1290.

Tanentzapf, G., and Tepass, U. (2003). Interactions between the crumbs, lethal giant larvae and bazooka pathways in epithelial polarization. Nat. Cell Biol. *5*, 46–52.

Tanos, B., and Rodriguez-Boulan, E. (2008). The epithelial polarity program: machineries involved and their hijacking by cancer. Oncogene *27*, 6939–6957.

Tilney, L. G. (1970). Factors controling the reassembly of the microvillous border of the small intestine of the salamander. J. Cell Biol. *47*, 408–422.

Tilney, L. G., and Mooseker, M. (1971). Actin in the brush-border of epithelial cells of the chicken intestine. Proc. Natl. Acad. Sci. U. S. A. *68*, 2611–2615.

Tocchetti, A. *et al.* (2010). Loss of the actin remodeler Eps8 causes intestinal defects and improved metabolic status in mice. PLoS One *5*, e9468.

Tseng, Y., Fedorov, E., McCaffery, J. M., Almo, S. C., and Wirtz, D. (2001). Micromechanics and ultrastructure of actin filament networks crosslinked by human fascin: a comparison with alpha-actinin. J. Mol. Biol. *310*, 351–366.

Turunen, O., Wahlström, T., and Vaheri, A. (1994). Ezrin has a COOH-terminal actin-binding site that is conserved in the ezrin protein family. J. Cell Biol. *126*, 1445–1453.

Tyska, M. J., Mackey, A. T., Huang, J.-D., Copeland, N. G., Jenkins, N. A., and Mooseker, M. S. (2005). Myosin-1a is critical for normal brush border structure and composition. Mol. Biol. Cell *16*, 2443–2457.

Tyska, M. J., and Mooseker, M. S. (2002). MYO1A (Brush Border Myosin I) Dynamics in the Brush Border of LLC-PK1-CL4 Cells. Biophys. J. *82*, 1869–1883.

Vinson, V. K., De La Cruz, E. M., Higgs, H. N., and Pollard, T. D. (1998). Interactions of Acanthamoeba profilin with actin and nucleotides bound to actin. Biochemistry *37*, 10871–10880.

Viswanatha, R., Ohouo, P. Y., Smolka, M. B., and Bretscher, A. (2012). Local phosphocycling mediated by LOK/SLK restricts ezrin function to the apical aspect of epithelial cells. J. Cell Biol. *199*, 969–984.

Wegner, A., and Engel, J. (1975). Kinetics of the cooperative association of actin to actin filament. Biophys. Chem. *3*, 215–225.

Weisz, O. A., and Rodriguez-Boulan, E. (2009). Apical trafficking in epithelial cells: signals, clusters and motors. J. Cell Sci. *122*, 4253–4266.

Yonemura, S., Hirao, M., Doi, Y., Takahashi, N., Kondo, T., and Tsukita, S. (1998). Ezrin/radixin/moesin (ERM) proteins bind to a positively charged amino acid cluster in the juxta-membrane cytoplasmic domain of CD44, CD43, and ICAM-2. J. Cell Biol. *140*, 885–895.

Zwaenepoel, I., Naba, A., Da Cunha, M. M. L., Del Maestro, L., Formstecher, E., Louvard, D., and Arpin, M. (2012). Ezrin regulates microvillus morphogenesis by promoting distinct activities of Eps8 proteins. Mol. Biol. Cell *23*, 1080–1094.

Chapter 2
Exploring whether formins nucleate the assembly of microvilli in JEG-3 cells

Overview and Introduction

As described in the introduction, de novo actin filament formation does not occur spontaneously within a cell. An actin seed, consisting of a dimer or trimer of monomers, must first form before filament elongation can occur. The formation of this actin seed is energetically unfavorable and the majority of free actin monomers within a cell are bound by profilin (Kaiser *et al.*, 1999), a small actin monomer binding protein, which together prevent spontaneous seed formation from happening *in vivo*. To overcome energetic and physical barriers to actin filament formation the cell must utilize a specialized class of proteins called actin nucleators.

The actin core of microvilli consists of parallel bundles of unbranched actin filaments that are oriented with the barbed, or growing end, oriented towards the plasma membrane (Mooseker and Tilney, 1975). The lifetime of a microvillus once the actin core is initially assembled is on the order of 5 minutes (Gorelik *et al.*, 2003), although the actin core is by no means static during this time. FRAP analysis of GFP-actin in brush border microvilli illustrates that the actin core is in fact dynamic with calculated actin subunit addition to be between 1.5-3.0 s^{-1} (Tyska and Mooseker, 2002; Loomis *et al.*, 2003). This is on the order of 5-10x faster than rate of actin monomer addition for treadmilling actin under steady state conditions(Pollard, 1981), as discussed in the introduction. This would suggest that an actin regulatory protein is assisting in the turnover of the actin filament core of microvilli. And because the actin filament core of microvilli is unbranched, this might implicate an unbranched actin nucleator in this process.

The formin family comprises the largest, best characterized class of unbranched actin filament nucleators. The mammalian class of formins has fifteen members that can be further classified into seven different subfamilies based on domain architecture. The defining feature of

the formin family is the presence of the FH2 (Formin Homology 2 domain),which upon forming a head to tail dimer is both necessary and sufficient for actin nucleation (Pruyne *et al.*, 2002; Sagot *et al.*, 2002b). The FH2 domain also has a high affinity for the barbed end, which along with other domains, allows the formin to also increase the rate of elongation of a growing actin filament. It does so by remaining processively attached as further monomer addition occurs, to both outcompete capping proteins and increase the rate of actin monomer addition (Romero *et al.*, 2004; Kovar *et al.*, 2006). The rate of elongation, which is determined in part by the FH1 domain, is not the same for all formins (Romero *et al.*, 2004) and not all FH2 domains are potent actin nucleators (Li and Higgs, 2003). The unique properties of different formins might contribute to the specialized functions each play within a cell.

Formins are large proteins (~120-220 kDa) with both regulatory and functional domains outside the canonical FH2 domain (Figure 2.1A). For the purpose of this introduction, the domain organization of the diaphanous related formins (DRF: Dia1-Dia3, FRL1, FRL2, DAAM1, DAAM2) will be discussed as this family encompasses a large portion of the formins that I focus on in this study, although points about other subfamilies will be made when appropriate. All mammalian formins contain a FH1 (Formin Homology 1) domain directly N-terminal to the FH2 domain. The FH1 domain contains poly-proline patches that bind profilin-actin monomers and different affinities between profilin isomers and the FH1 domain directly influence the rate of elongation (Neidt *et al.*, 2009). One possibility is that the FH1 domain might work to orient and increase the local concentration of actin monomers available for quick addition at the barbed ends. C-terminal to the FH2 domain is the Diaphanous Auto regulatory Domain (DAD) which binds to the Diaphanous Inhibitory Domain (DID) near the N-terminus to autoinhibit nucleation and elongation activity (Alberts, 2001; Nezami *et al.*, 2006). This autoinhibition can be relieved by

interaction between Rho-GTPases and the N-terminal GTPase Binding Domain (GBD)(Kühn and Geyer, 2014). Also within the N-terminal region is the Dimerization Domain (DD) and the Coiled-coil (CC) domain, which mediate the dimerization of the N-terminal portion of the protein.

Unrestricted actin filament assembly in the cytoplasm would have deleterious effects on the cell, so formins employ various mechanisms to direct actin assembly at specific subcellular localizations. Relief of autoinhibition spatially by disrupting the interaction between the DID and DAD is required before proper localization can occur. In the case of the yeast formin Bni1, phosphorylation by the kinase Fus3 is necessary and sufficient for proper localization (Matheos *et al.*, 2004). For mammalian formins, interaction between Rho-GTPases and the GBD to relieve autoinhibition can direct localization but is not sufficient (Seth *et al.*, 2006) and localization can be Rho-GTPase independent (Ang *et al.*, 2010). In the case of Dia1 and Dia2 at least, relief of autoinhibition by Rho-GTPase activation allows an electrostatic interaction with phospholipids at the plasma membrane, which is necessary for proper localization (Ramalingam *et al.*, 2010; Gorelik *et al.*, 2011). Interactions with specific ligands can also mediate localization, the interaction between IQGAP1 and Dia1 is essential for proper Dia1 targeting to phagocytic cups(Brandt *et al.*, 2007). The BAR domain containing proteins IRSP53 and Toca-1 can recruit Dia1 and DAAM1, respectively, to the proper membrane (Fujiwara *et al.*, 2000; Brandt *et al.*, 2007), although in both cases activation by a Rho-GTPase must also occur coincidently. The need for both an activator and a recruitment factor, may it be phospholipid binding or a protein-protein interactions, for proper localization suggests tight regulation for proper activation is required.

How exactly does a formin mediate the nucleation and elongation of a growing actin filament? The nucleation activity of formins is not well characterized but there is some evidence to suggest that the DAD domain contributes to nucleation by binding to and recruiting G-actin,

which in combination with the FH1 domain, can recruit enough monomers to form an actin seed like a bona fide nucleator (Gould *et al.*, 2011). Formin mediated actin filament elongation is thought to occur by both preventing capping proteins from binding to the barbed end of the filament and by increasing the rate of actin monomer addition. The FH1 domain orients and increases the local concentration of profilin-actin which gets added to the barbed end as each FH2 domain of the formin dimer "steps" along the growing actin filament (Vavylonis *et al.*, 2006). This can allow for monomer addition that is up to 15x faster than free diffusing actin monomers (Romero *et al.*, 2004). Additionally, certain formins also have the ability to bundle (Harris *et al.*, 2006) or sever (Harris *et al.*, 2004; Chhabra and Higgs, 2006) actin filaments, making formins versatile regulators of the actin cytoskeleton in cells.

What makes formins interesting for this study is the diverse roles they play in the maintenance of the actin cytoskeleton. Formins participate in such diverse functions as cell migration (Yamana *et al.*, 2006), membrane trafficking (Fernandez-Borja *et al.*, 2005), cell polarity (Sagot *et al.*, 2002a) and actin based membrane protrusions (Colombo *et al.*, 2013) (For a comprehensive review of formin function see (Goode and Eck, 2007)). Most interesting is the involvement of formins in maintaining actin based protrusions that are structurally similar to microvilli. The formins Dia1, Dia3 , FRL2, FRL3 all have been implicated in filopodia formation (Yayoshi-Yamamoto *et al.*, 2000; Block *et al.*, 2008; Harris *et al.*, 2010; Mellor, 2010), which are most similar to microvilli, but located at the basolateral domain or leading edge of cells. Dia1 has been linked to length regulation of stereocilia, actin based protrusions of the inner ear (Lynch, 1997; Manor and Kachar, 2008), although it has never been localized there. This makes formins a likely candidate for a role in either the assembly of or maintenance of microvilli.

This chapter will focus on an attempt to identify a formin involved in nucleating the assembly of the actin core of microvilli. Considering there are 15 human formins it is impossible to study all of them simultaneously. So to narrow down the number of potential candidates to study, I first sought to characterize which formins were most highly expressed in JEG-3 cells, a choriocarcinoma derived cell line with abundant microvilli on the apical domain. I use quantitative Real Time PCR (qPCR) to determine the relative amount of formin mRNA transcripts in JEG-3 cells, assuming that mRNA transcript level roughly correlates to protein expression level and use this list to target the most highly expressed formins with siRNA to assess a loss of function phenotype. I specifically assay whether depletion of formin protein results in loss of microvilli, a strong indication that a formin might be involved in the formation of microvilli. I also examine the cellular localization of both full length and constitutively active epitope-tagged formins in these cells to determine if any localize specifically to microvilli. From this I draw conclusions about the potential role formins might play in this system, as well as briefly mention possible future directions for those who might wish to pursue this interesting problem.

Materials and Methods

Antibodies and Reagents

The mouse FLAG antibody and resin was from Sigma-Aldrich (St. Louis, MO), mouse GFP antibody was from Santa Cruz Biotechnology (Santa Cruz, CA) and the mouse anti Dia1 was from BD Biosciences (San Jose, CA). The mouse anti-tubulin was from sigma. The anti-Profilin-1 antibody is from Cytoskeleton, Inc. (Denver, CO).The rabbit antisera and affinity-purified antibodies against full-length human ezrin have been described (Bretscher, 1989). Goat anti-mouse secondary antibodies conjugated to horseradish peroxidase were from Jackson ImmunoResearch Laboratories (West Grove, PA). Alexa Fluor 568 and Alexa Flour 660-conjugated donkey anti-rabbit antibodies and Alexa Fluor 660–conjugated phalloidin were from Invitrogen (Carlsbad, CA). IRDye 680- and 800-conjugated secondary antibodies were from LI-COR Biosciences. WGA-488 was from Molecular Probes (Lafayette,CO). Latrunculin B was from Sigma.

DNA Constructs and Sequence Alignments

INF1 cDNA was a kind gift from Dr. John Copeland (Ottawa University). Dia2 and Dia3 cDNA was from BD biosciences. FHOD1 cDNA was from ATCC. For N-terminal tags they were cloned into pEGFP-C2 and for C-terminal tags they were cloned into pEFGP-N2. Activated DAD deleted constructs were created by addition of a stop codon before the beginning of the DAD domain to create : GFP-FHOD1delDAD (AA 1-1053). GFP-Dia3delDAD was a kind gift from Dr. K. Rottner (Braunschweig, Germany). To create the active FHOD1 (V228E) I used the site directed mutagenesis XL kit as directed. To create actin binding dead INF1 (I180A), Dia3 (I725A) and FHOD1 (I705A) mutants alignments of the FH2 domain of Bni1, Dia1, Dia3, FHOD1 and INF1 were created and the residue essential for actin binding was identified (Xu *et al.*, 2004; Harris *et*

al., 2006) and was made with the site directed mutagenesis XL kit. siRNAs for all formins, GL2 and profilin-1 were purchased from Ambion. qPCR primers were purchased from IDT.

Cell Culture and Transfection

JEG-3 cells (American Type Culture Collection, Manassas, VA) were maintained in a 5% CO_2 humidified atmosphere at 37°C and cultured in MEM (Thermo Fisher Scientific, Lafayette, CO) with 10% fetal bovine serum (FBS), JEG-3 cells were transfected with polyethylenimine (Polysciences, Warrington, PA) and 1–2 μg plasmid DNA, as described (Hanono *et al.*, 2006). For knocking down endogenous formins, luciferase or profilin in Jeg-3 cells, cells were transfected with 10 nM of siRNA using Lipofectamine RNAiMax, allowed to grow for 72 h, then processed for immunofluorescence and microvilli measurements, or Western blot analysis.

Western Blotting and quantification

Jeg-3 cells treated with siRNA against a specific formin/formins were lysed in lysis buffer: (25 mM Tris, pH 7.4, 5% glycerol, 150 mM NaCl, 50 mM NaF, 0.1 mM Na_3VO_4, 10 mM β-glycerol phosphate, 8.7 mg/ml paranitrophenylphosphate, 0.3% Triton X-100, and protease inhibitor tablet [Roche]) , then spun at 13,000g for 10 min at 4C. Supernatants were than denatured with Laemmli buffer, resolved by SDS-PAGE, transferred to Immobilon-FL (EMD Millipore, Billerica, MA), blotted with specific antibody and visualized by ECL. To determine percentage of knockdown, Western blots were probed with specific antibody and IRDye conjugated 680 0r 800 secondary antibodies. The blot was than imaged using an Odyssey infrared imaging system (LI-COR Biosciences, Lincoln, NE). Analysis to determine percent knockdown was performed using Image

Studio Lite 4.0 (LI-COR biosciences). Samples were normalized to a loading control and knockdown was determined as a percent of the control.

Immunofluorescence

JEG-3 cells were grown on coverslips and fixed in 3.7% formaldehyde at room temperature for 15 minutes. Coverslips were then washed 3 times in phosphate-buffered saline (PBS) and permeabilized with 0.2% Triton X-100 for 5 minutes at room temperature. Coverslips were than washed 3 more times with PBS and blocked in filtered 3% FBS in PBS for 10 minutes. Primary and secondary antibodies were made up in 3% FBS in PBS. Coverslips were washed 3 times in PBS between addition of primary and secondary antibodies. Alexa Fluor conjugated Phalloidin (Invitrogen) was added to the secondary when F-actin was visualized. Cells were imaged by time-lapse microscopy on a spinning disk (CSU-X; Yokogawa, Tokyo, Japan) with a spherical aberration correction device, a 63×/1.4 numerical aperture (NA) objective (Leica, Wetzlar, Germany) with a 2x SAC (Spherical Aberration corrector) on an inverted microscope (DMI6000B; Leica) and an HQ2 CCD camera (Photometrics). Maximum intensity projections were created using Slidebook (Intelligent Imaging Innovations, Denver, CO) and exported in Adobe Illustrator.

Scoring loss of microvilli in JEG-3 cells

Transfected JEG-3 cells were scored as described previously (Hanono *et al.*, 2006). Briefly, cells were stained for ezrin as a marker for microvilli. At least 250 cells were counted for each siRNA in each of 3 replicates. Cells were scored as having normal microvilli, no microvilli or lacking/few microvilli. Statistical significance was determined by a Student's t-test.

Quantitative Real Time PCR (qPCR)

Jeg-3 and Hela cells were grown to confluence in 60mm dishes and lysed according to the manufacturers protocol for Trizol for RNA and the zymogen kit for genomic DNA. RNA was pooled from several dishes to have a homogenous pool. To create cDNA from RNA, 10ng/ul of RNA was treated with DNAse I to digest remaining DNA and then reverse transcribed using the Superscript III kit from Life Technologies. As a control, cDNA was made without Reverse transcriptase. 2x serial dilutions of genomic DNA were run alongside each cDNA sample for generation of standard curves. qPCR was run as described (Albulescu *et al.*, 2012). Briefly, The qPCR reactions were performed in a reaction volume of 10 µl, containing 10 µl of template (~10 ng of template), 10 mM Tris-HCl (pH 8.5), 50 mM KCl, 1.5 mM $MgCl_2$, 0.2 mM each dNTP, 0.25× SYBR Green, 5% DMSO, 0.7 ng *Taq* DNA polymerase, and 250 nM forward and reverse primers. Each biological sample was run in triplicate.

qPCR data analysis

For each formin specific primer a standard curve was generated by the following method: qPCR was performed on 2x serial dilutions of a known concentration of genomic DNA. The Cycle threshold (Ct), or the cycle number in which as fluorescent signal can be detected, was measured at each dilution in triplicate and the average Ct value was plotted against the log of the concentration to generate a standard curve. A line of best fit was determined for the standard curve. A slope between -3.0 and -3.5 and R>.98 were used as a measure of proper PCR amplification. A slope of -3.2 on a log based scale indicates that the cDNA was doubled each PCR cycle and that the PCR was 100% efficient. To determine the relative formin amount (RFA), the Ct was measured

in triplicate for each formin primer in cDNA generated from either JEG-3 or Hela cells. The RFA was determined by the equation:

$$\frac{(Ct-b)}{Slope} = RFA,$$

where b (y-intercept) and slope is determined from the standard curve and Ct is measured for each formin transcript. This value is than raised to the power of 10 to account for the log based standard curve. The RFA was than normalized to the most expressed formin transcript to determine nRFA.

Results

Determining the relative amount of formins in JEG-3 cells

The formin family of actin nucleators is highly redundant, with 15 different members in mammals (Figure 2.1A), although not all 15 are expressed in any given cell type (Krainer *et al.*, 2013). To determine which formin(s) might potentially be involved in microvilli formation I first sought to narrow the potential candidate list down by determining which formins are most highly expressed in a cell line that has abundant microvilli. One potential way to do this is to lyse cells that have microvilli and perform western blot analyses to determine which formin proteins are most abundantly expressed. Unfortunately, there are not enough commercial antibodies available to take this approach so an alternative approach had to be designed.

In this study I utilized Quantitative Real Time PCR (qPCR) to determine relative formin mRNA transcript levels in JEG-3 cells, which are a choriocarcinoma cell line that have abundant microvilli on their apical domain. mRNA transcript levels should roughly correlate with protein expression, so the highest transcript levels should indicate which formins are most abundant in this system. To complicate the issue, each formin has multiple functional splice isoforms. To ensure that I was accounting for all possible functional isoforms (defined here as the ability to nucleate the assembly of actin filaments), I created qPCR primers for all 15 formins that specifically targeted the FH2 region of each cDNA. The FH2 domain was targeted specifically because it is the region responsible for actin filament nucleation (Pruyne *et al.*, 2002; Zigmond, 2004) and every functional splice isoform has a single exon that coded for it. Primer specificity was verified by BLAST to prevent off-targeted amplification. Then mRNA was isolated from JEG-3 cells, which was reverse-transcribed into cDNA, and then qPCR was performed.

A

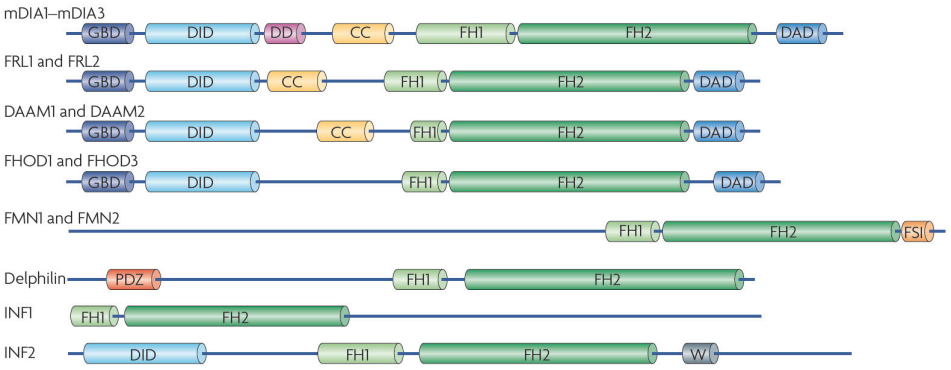

B

Formin	JEG-3 RFA (a.u)	JEG-3 nRFA	Hela RFA (a.u)	Hela nRFA
INF2	47.40	100.00	39.13	84.63
Dia1	36.80	77.65	46.22	100.00
INF1	31.38	66.20	14.25	30.95
FHOD1	22.29	47.02	23.71	51.30
Dia3	17.29	36.47	38.89	84.20
DAAM1	9.69	20.45	3.85	8.33
Dia2	3.91	8.25	20.00	43.29
FRL1	2.55	5.38	21.23	45.89
FRL2	1.74	3.67	0.27	0.58
FRL3	0.26	0.55	4.62	10.00
Delphilin	0.10	0.20	0.02	0.04
FHOD3	0.08	0.16	1.52	3.29
FMN1	0.04	0.07	0.03	0.06
DAAM2	0.02	0.04	0.01	0.02
FMN2	0.00	0.00	0.00	0.00

Figure 2.1. Determining the relative amount of formin mRNA transcripts in JEG-3 cells (A) Domain schematic of the mammalian family of formins. The fifteen members are further divided into subfamilies based on domain architecture. Figure taken from Campellone, K. and Welch, M. 2010. (B) Table listing qPCR results in which mRNA transcript levels for all fifteen formins were measured in both JEG-3 cells and Hela cells. Relative Formin Amount (RFA) is depicted in arbitrary units (a.u) and is determined by the PCR cycle threshold as described in materials and methods. The RFA was normalized to the highest expressed formin transcript (nRFA) to compare relative amounts of transcript within a cell line.

Briefly, a double stranded DNA dye is used to measure cDNA amplification at each PCR cycle. A value, known as the cycle threshold, is determined by measuring the minimum amount of cycles it requires to detect a fluorescence signal. The more start product, or the more mRNA transcript you have in your sample, the fewer number of cycles you will need to amplify the product to see a fluorescence signal. A standard curve is derived from a genomic DNA standard of 2x serial diluted concentrations, cycle threshold is plotted logarithmically against concentration and a line of best fit is determined. The cycle threshold of cDNA samples of unknown start concentration can be measured and the line of best fit can be used to determine relative formin amount (RFA). The RFA was than normalized to the highest expressed transcript to determine nRFA (Figure 2.1B).

To determine if there were differences among epithelial cell types we also performed the same analysis on Hela cells, which have short microvilli on their apical domain (Figure 2.1B). From this an ordered ranking was developed for the most expressed formin mRNA transcript in both cell lines. The similarities and differences between the two cell lines could potentially be useful to determine which formins might be utilized for specialized or shared functions in the cell. I decided that since RFA was determined from a measured cycle threshold, any formin with an RFA below 1.0 was not high enough beyond background to be sure that my measurements were accurate beyond noise levels. These also represented very low expressing formins, so they were not interesting for further study. From this, I narrowed my candidate list to nine potential formins.

Loss of individual formins does not affect microvilli formation

To determine a potential functional role for formins in microvilli formation I utilized a loss of function assay where I individually knocked out the top nine formins identified by qPCR and

assayed whether there was a reduction in the number of cells that have microvilli. Briefly, siRNA against either a non-targeting control (siLuciferase) or siRNA targeting an individual formin was used in JEG-3 cells. Using endogenous Ezrin staining as a marker for microvilli, I then counted JEG-3 cells and scored them as either having abundant or "normal" microvilli, intermediate or "less" microvilli or "none", which is the absence of microvilli (Figure 2.2A). This assay has been utilized previously as a functional readout of the involvement of a specific protein in the formation or regulation of microvilli (Hanono *et al.*, 2006; Garbett *et al.*, 2010).

Unfortunately knocking down individual formins does not show a dramatic increase in cells lacking microvilli (Figure 2.2B). For the control siLuciferase cells, there is about 35% of cells that do not have microvilli. Silencing of either the inverted formin INF1 or the ubiquitously expressed Dia1 had the greatest effect on the loss of microvilli, with an increase to 51% or 50% of cells without microvilli, respectively (Figure 2.2B).

Latrunculin B (LatB) is a small molecule that binds to monomeric G-actin to prevent F-actin filament formation in a concentration dependent manner. Use of low concentrations of LatB does not completely abolish F-actin filament formation but does make assembly of actin filaments less efficient because there are less free monomers available. A concentration of LatB was used that under normal conditions does not affect microvilli. Then, two of the top formin candidates were knocked down with siRNA and I asked if the cells were now more sensitive to LatB treatment, which I assessed by scoring loss of microvilli. The idea was that loss of a formin involved in microvilli formation might not result in loss of microvilli but may make microvilli more sensitive to perturbations to the actin cytoskeleton. Addition of Latrunculin B does not further increase the loss of microvilli phenotype for either INF1 or FHOD1 (Figure 2.2C). FHOD1 was targeted because of the discovery that it bound to the microvillar protein Ezrin (Viswanatha

A

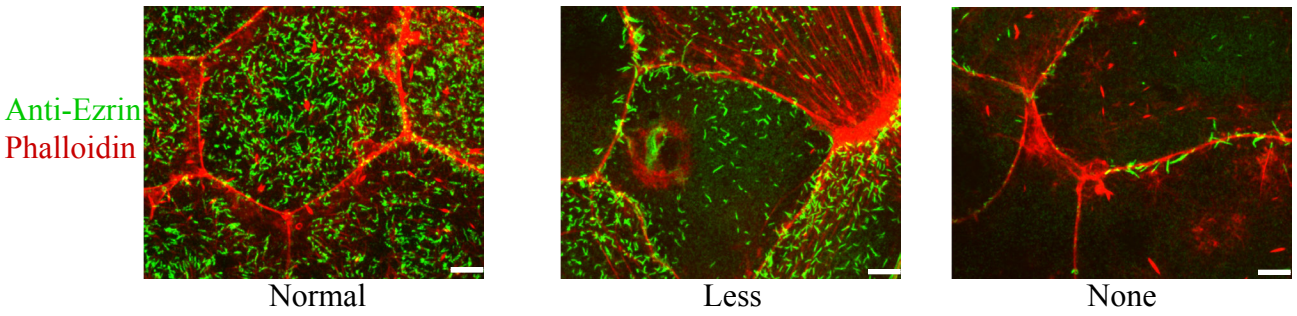
Anti-Ezrin
Phalloidin
Normal
Less
None

B

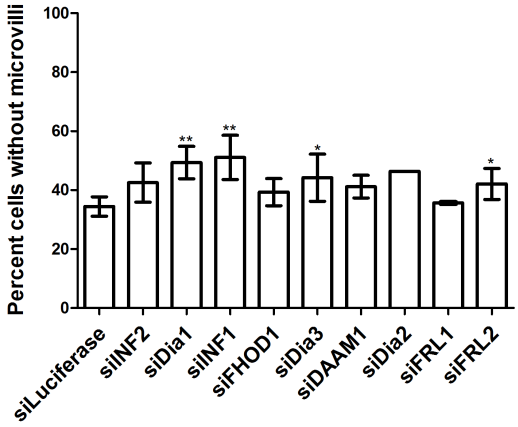
Percent cells without microvilli
100
80
60
40
20
0
**
**
*
*
siLuciferase
siINF2
siDia1
siINF1
siFHOD1
siDia3
siDAAM1
siDia2
siFRL1
siFRL2

C

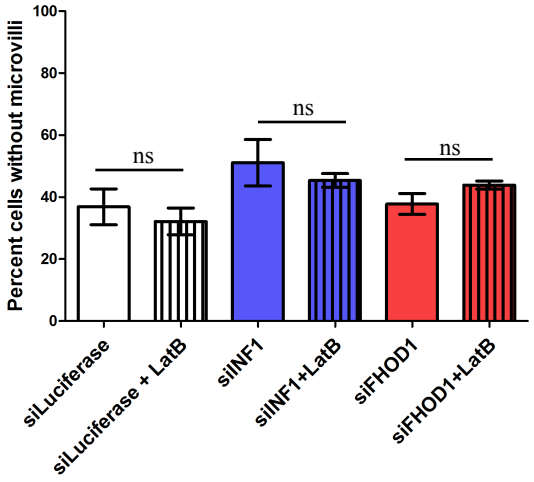
Percent cells without microvilli
100
80
60
40
20
0
ns
ns
ns
siLuciferase
siLuciferase + LatB
siINF1
siINF1+LatB
siFHOD1
siFHOD1+LatB

D

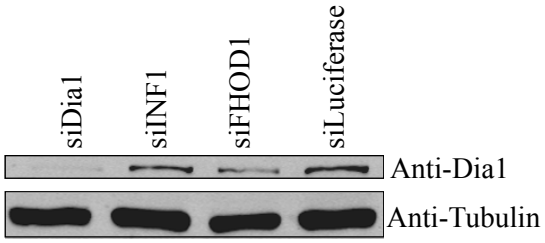
siDia1
siINF1
siFHOD1
siLuciferase
Anti-Dia1
Anti-Tubulin


Dia1 knockdown efficiency
Percentage of Dia1
100
80
60
40
20
0
siDia1
siINF1
siFHOD1
siLuciferase

E

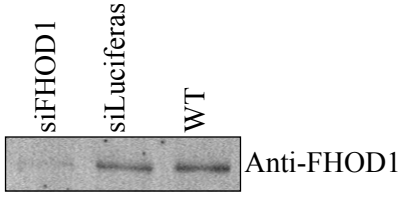
siFHOD1
siLuciferas
WT
Anti-FHOD1

Figure 2.2 Loss of individual formins does not affect microvilli formation
(A) Examples of JEG-3 cell classification used to score loss of microvilli. Maximum projections (XY) of confocal Z stacks of JEG-3 cells fixed and stained for endogenous ezrin (green) and F-actin (red) and then scored depending on the presence or absence of microvilli. "Normal" cells have abundant microvilli on the apical domain. Cells with "Less" microvilli have less than 50% of the apical domain covered with microvilli. Cells with "none" have few microvilli on the apical domain. Bars: 5µm. (B) Results of scoring microvilli phenotype after transfection with the siRNA listed, using endogenous ezrin as a microvilli marker. N=3, 100 cells each * $p<.05$, ** $p<.005$. (C) Results of scoring loss of microvilli after transfection with siRNA indicated and with or without 100 nM Latrunculin B treatment for 30 minutes. N=2, 150 cells each. ns= no statistical significance. (D) Western blot showing knock down in cells treated with siRNA against Dia1 (siDia1), INF1 (siINF1), FHOD1 (siFHOD1) or Luciferase (siLuciferase) and probed for Dia1 or tubulin (top panel). To determine Dia1 knockdown efficiency, amount of Dia1 was normalized using tubulin as a loading control and determined as a percent of the siLuciferase control (bottom panel).(E) Western blot showing knockdown in wild type (WT) cells or cells treated with siRNA against FHOD1 (siFHOD1) or Luciferase (siLuciferase) and probed for FHOD1.

et al., 2013), a topic discussed in Appendix A. This would suggest that a single formin is not solely responsible for microvilli formation in JEG-3 cells.

One caveat to this approach, as stated earlier, is that there are not enough commercial antibodies available for western blot analyses to determine if each formin is being knocked down completely. The knockdown efficiency was assessed by western when antibodies were available. In the case of Dia1 (Figure 2.2D) and FHOD1 (Figure 2.2E) the endogenous protein was significantly knocked down.

It is very likely that there is redundancy between formins in this system, and upon knocking one formin down another might compensate. In such a case, finding a formin that localizes to microvilli might be informative in trying to determine which one is potentially involved in microvilli formation.

Localization of top formin candidates is cytoplasmic

Since cloning and expressing all top nine formin candidates was not feasible due to time constraints, I utilized my knowledge from both the qPCR results and the siRNA screen to make informed decisions about which formins to localize in JEG-3 cells. Out of the top five candidates from the qPCR results, two (Dia1 and INF1) had the greatest effect on microvilli so localizing INF1 was an obvious choice. Dia1, however, is one of the most highly expressed formins in all cell types so I did not think it was a likely candidate for a specialized function like microvilli formation. I instead chose to look at the two Dia1 paralogues, Dia2 and Dia3, because they were highly expressed in JEG-3 cells and they had an intermediate effect on loss of microvilli. Dia3 is also an interesting candidate because it has also been implicated in the formation of filopodia

(Block *et al.*, 2008). I also chose to localize FHOD1 because of its interaction with Ezrin (Viswanatha *et al.*, 2013).

Utilizing endogenous ezrin as a microvilli marker, I expressed four separate formin candidates in JEG-3 cells. Because formins are barbed end actin nucleators and the barbed end of actin filaments in microvilli are oriented towards the plasma membrane, one expects to localize the potential actin nucleator of microvilli at the tip. However, INF1-GFP, which had the greatest effect on microvilli in the siRNA screen, was cytoplasmic with some localization to actin stress fibers (Figure 2.3A). Localization of both Dia2-GFP and Dia3-GFP were cytoplasmic (Figure 2.3B, C). Expression of FHOD1-GFP was cytoplasmic with some preferential localization to junctional actin (Figure 2.3D). None of the proteins expressed had any preference for the apical domain or microvilli in general.

One concern is that adding a bulky GFP tag to the C-terminal region, where the functional FH2 domain and regulatory DAD domain are, might interfere with the correct localization. However, moving the GFP tag to the N-terminus does not change the localization (data not shown.) Another possible reason for the cytoplasmic localization is that formins are autoregulated proteins (Nezami *et al.*, 2006) and most molecules in a cell exist in a closed or inactivated state within the cytoplasm. It's upon activation that the regions important for localization become accessible (Kühn and Geyer, 2014), which allows the protein to localize to a specific place. Thus expressing an activated formin might allow proper localization within the cell.

Active Dia3 localizes to the tips of filopodia in JEG-3 cells

A subset of formins are autoregulated through the interaction between the N-terminal DID and the C-terminal DAD (Figure 2.1A). Truncating the protein by removing the DAD domain

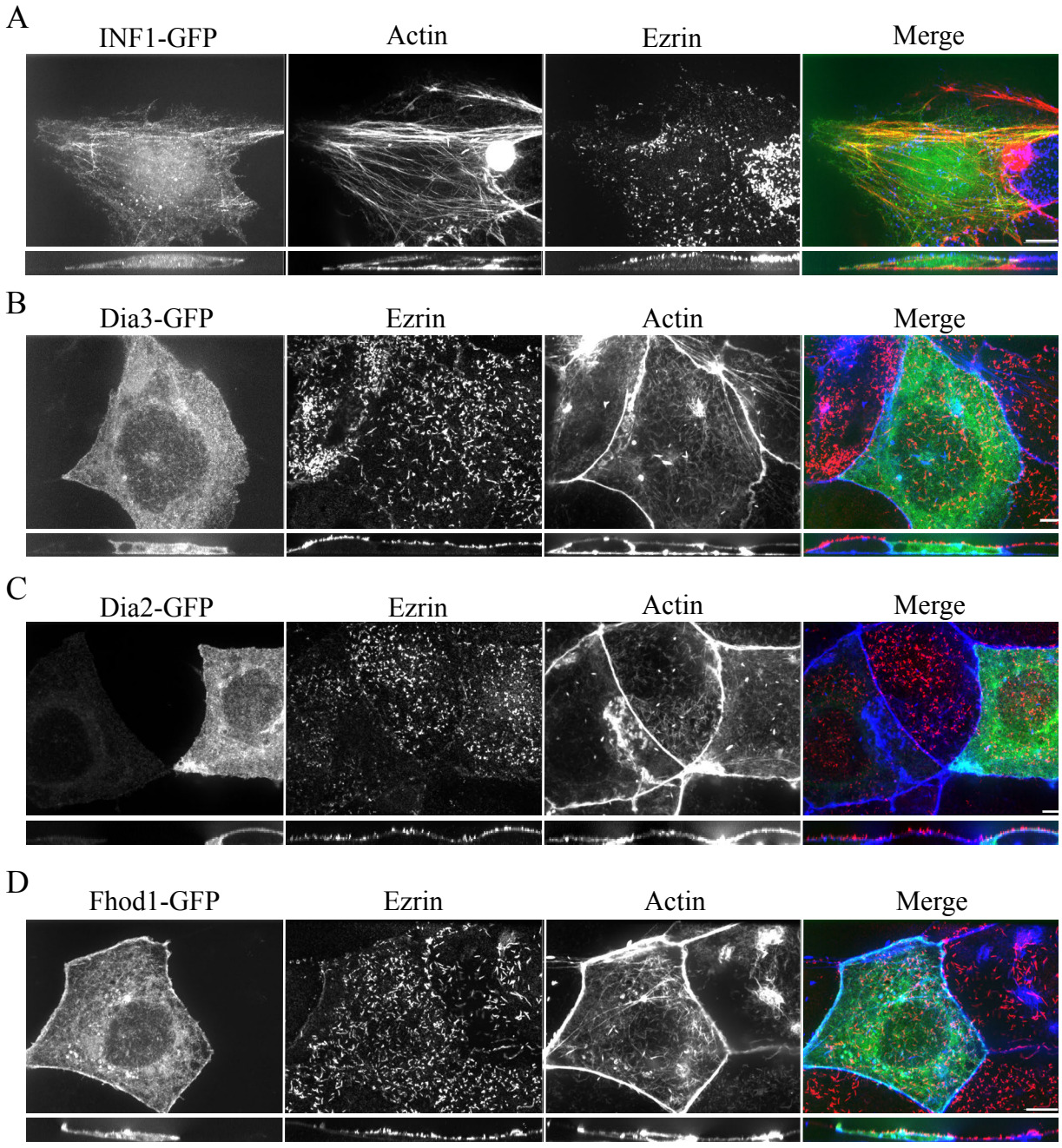

Figure 2.3 Expression of top formin candidates in JEG-3 cells is cytoplasmic
(A-D) Maximum projections (XY) of confocal Z stacks and side views (XZ) stretched 2-fold of JEG-3 cells. Cells expressing either (A) INF1-GFP, (B) Dia3-GFP, (C) Dia2-GFP or (D) FHOD1-GFP were fixed and stained for F-actin (red) and endogenous ezrin (blue) except in (A) where F-actin is (red) and endogenous ezrin is (blue). Bars: 5µm.

results in an overactive, unregulated formin (Block *et al.*, 2008). Because Dia3 is involved in filopodia formation, I decided to localize an active Dia3 in JEG-3 cells. Expression of GFP-Dia3ΔDAD resulted in aberrant ezrin positive structures, loss of normal microvilli and an increase in the formation of filopodia (Figure 2.4A). These filopodia are localized to the basolateral domain and are decorated with GFP-Dia3ΔDAD at the tips (Figure 2.4B). The filopodia are also ezrin positive, which is in agreement with the literature (Osawa *et al.*, 2009). Normal cell morphology is disrupted and the microvilli are mostly gone so it is impossible to determine if active Dia3 is also localized to the tips of microvilli. Lack of a commercial antibody decent enough for immunofluorescence also makes it impossible to localize endogenous protein.

Active Fhod1 localizes to stress fibers in JEG-3 cells

I next sought to localize active FHOD1 (GFP-FHOD1ΔDAD) in JEG-3 cells considering the demonstrated interaction with ezrin. Expression of GFP-FHOD1ΔDAD is also cytoplasmic, with some preferential localization to junctional actin (Figure 2.5A). To address the possibility that the DAD domain was playing a role in localization of FHOD1 I also expressed an active version of FHOD1 in which a single point mutation was made in the DID (V228E) that abrogates the binding between the DID and the DAD (Schulte *et al.*, 2008). This allowed me to express an active, full length protein. Expression of GFP-FHOD1V228E localized to and induces actin stress fiber formation (Figure 2.5B). Interestingly, it does seem to have some preference for the apical domain, but not specifically microvilli.

Expression of formin mutations that abrogate binding to actin have no effect on microvilli

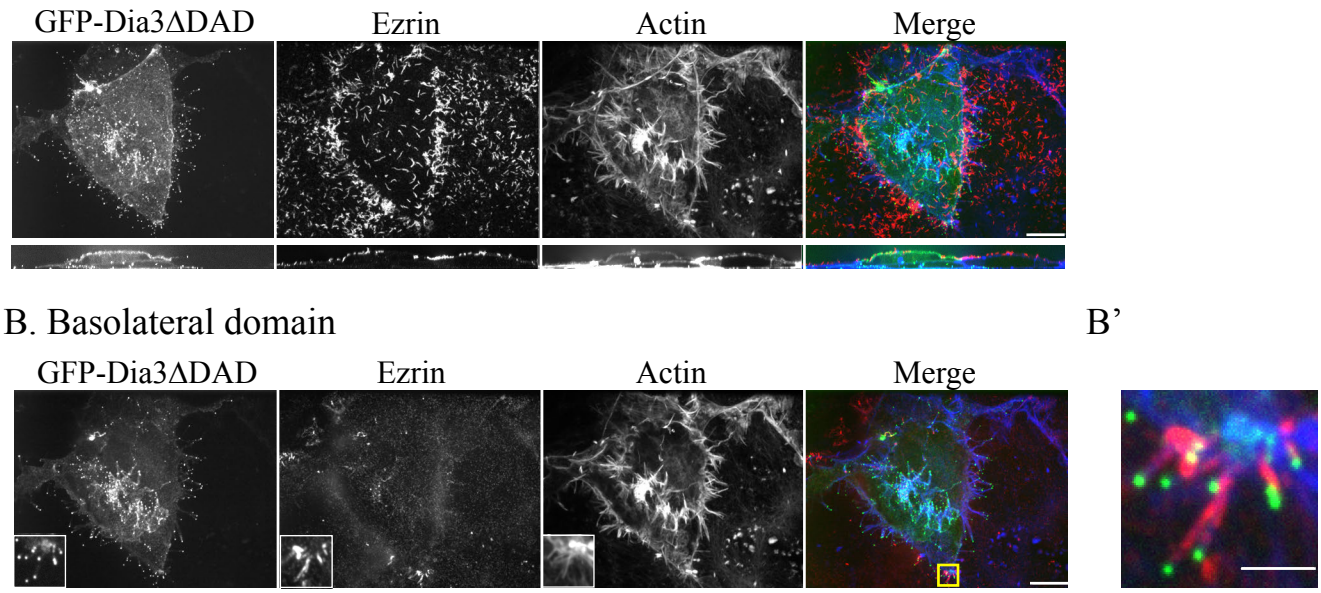

Figure 2.4 Active Dia3 localizes to the tips of filopodia in JEG-3 cells
(A) Maximum projection (XY) of confocal Z stacks and side views (XZ) stretched 2-fold of JEG-3 cells expressing active Dia3 (GFP-Dia3ΔDAD, green). Cells were fixed and stained for endogenous ezrin (red) and F-actin (blue). (B) Single confocal Z stack at the basolateral domain of JEG-3 cells expressing GFP-Dia3ΔDAD (green), and fixed and stained for endogenous ezrin (red) and F-actin (blue) Yellow box identifies the single channel insets and is shown merged in (B'). Bars: 5µm in (A-B), 2µm in (B').

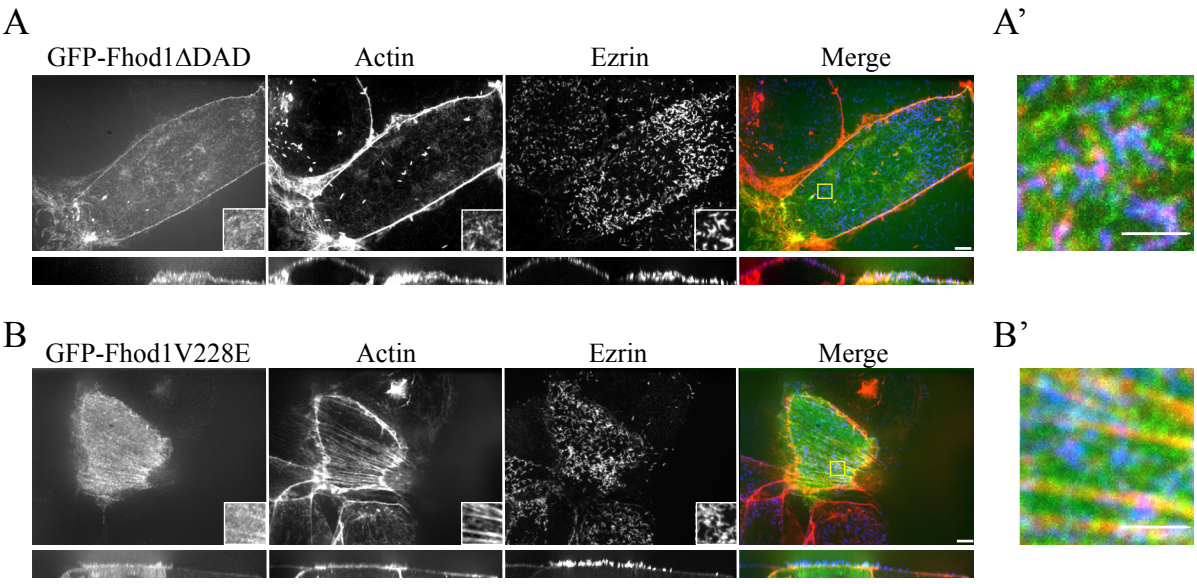

Figure 2.5 Active FHOD1 localizes to stress fibers in JEG-3 cells
(A-B) Maximum projections (XY) of confocal Z stacks and side views (XZ) stretched 2-fold of JEG-3 cells expressing active FHOD1, either GFP-FHOD1ΔDAD or GFP-FHOD1V228E. Cells were fixed and stained for F-actin (red) or endogenous ezrin (blue). Yellow boxes indentify single channel insets and is shown merged in (A'-B'). Bars: 5µm (A-B), 2µm (A'-B').

Previous work has demonstrated that mutation of a conserved isoleucine within the FH2 domain in the yeast formin Bni1p (Xu *et al.*, 2004), murine mDia2 (Harris *et al.*, 2006) or murine mDia1 (Shimada *et al.*, 2004) decreases the affinity for actin filaments. This decreases the ability of the FH2 domain to nucleate and elongate actin filaments but the protein can still dimerize and localize efficiently. I sought to create actin binding dead mutants within Dia3, FHOD1 and INF1 to create a potential dominant negative construct that could still bind endogenous protein but be non-functional as a dimer. I then assessed the effect of expressing these constructs on microvilli in JEG-3 cells.

To create the actin binding dead mutants I aligned the sequences with the previously studied actin binding dead mutants to identify the conserved isoleucine in my constructs (Figure 2.6A). I then mutated the conserved isoleucine to alanine in the context of the full length protein. Expression of GFP-Dia3(I725A) and GFP-FHOD1(I705A) was cytoplasmic with no obvious effect on microvilli (Figure 2.6B, C). Expression of GFP-INF1(I1080A) had no effect on microvilli although interestingly it is now localized to what appeared to be microtubules (Figure 2.6D). Work by others has shown that INF1 can localize and bind microtubules (Young *et al.*, 2008) but I did not see this localization until I inhibited the ability of the protein to bind actin.

Multiple formin knockdown does not reveal an obvious role for formins in microvilli formation

One possible reason for a lack of a dramatic effect on the loss of microvilli following single formin knockdown is functional redundancy between formins. To determine if multiple formins might be involved in microvilli formation an siRNA screen in which multiple formins were knocked down simultaneously was devised. Logistics made it difficult to target more than three

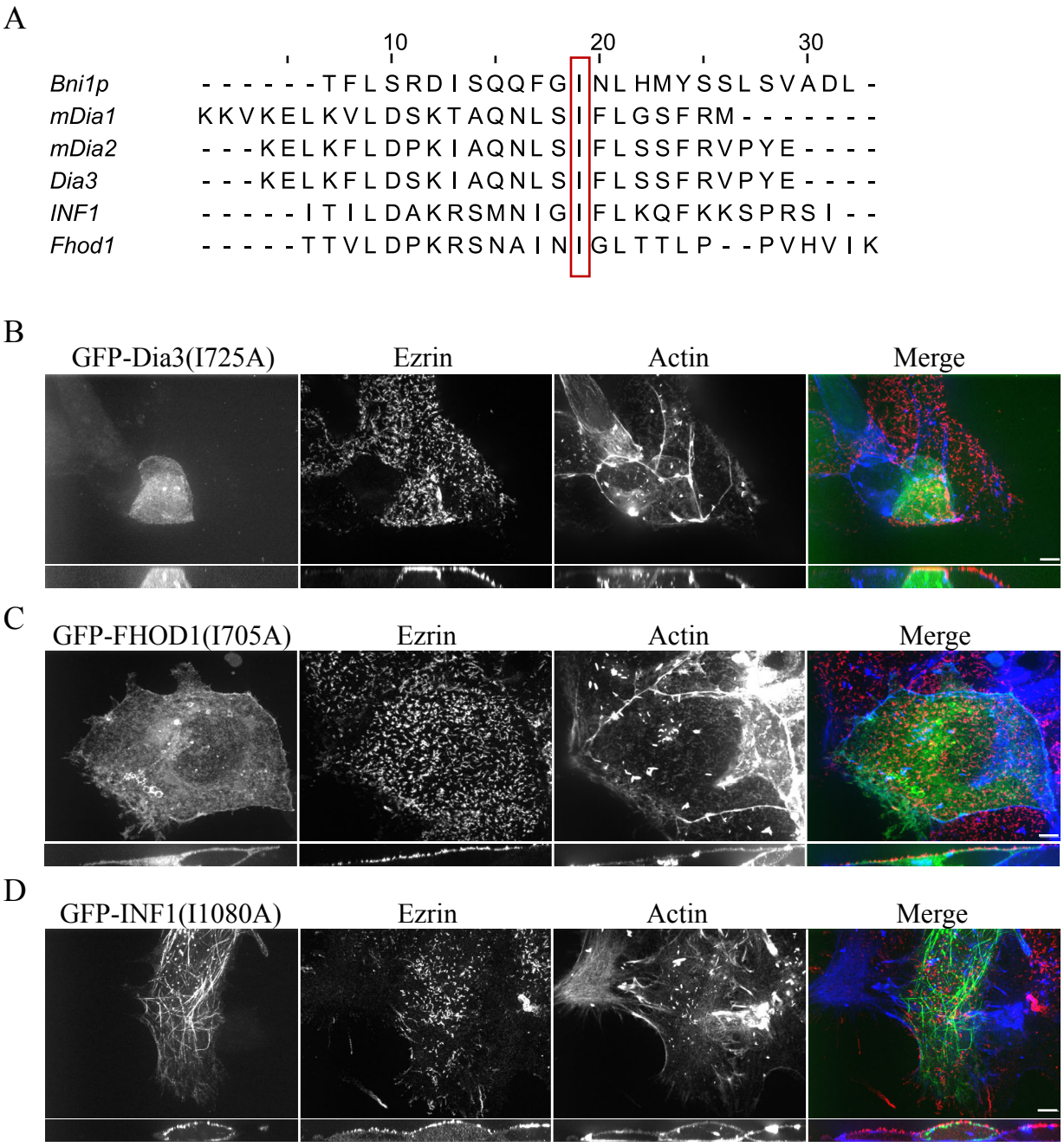

Figure 2.6 Expression of formin mutations that abrogate actin binding have no effect on microvilli

(A) Alignment of FH2 domains of proteins indicated to identify conserved isoleucines (red box) to create actin binding mutants used in (B-D). See materials and methods for details. (B-D) Maximum projections (XY) of confocal Z stacks and side views (XZ) stretched 2-fold of JEG-3 cells. Cells expressing (B) GFP-Dia3(I725A), (C) GFP-FHOD1(I705A) or (D) GFP-INF1(I1080A) were fixed and stained for endogenous ezrin (red) and F-actin (blue). Bars: 5µm.

formins at once and since there were nine potential candiates, combinatorics made it impossible to explore all discreet combinations. Thus I targeted families of closely related formins (e.g. FRL1 + FRL2) or groups of the top formin candidates from the qPCR screen (e.g. INF1 + INF2 + Dia1). Knocking down multiple formins simultaneously did not have a dramatic effect on the loss of microvilli. The most dramatic effect was still only about 50% of cells that did not have microvilli (Figure 2.7A), with the caveat that there was no way to determine if there was complete knockdown of each protein targeted (Figure 2.7B). Visually, triple formin knockdown cells did not look significantly different from control cells, although it appears that there is less actin staining at the apical domain but this does not seem to effect microvilli (Figure 2.7C).

To globally target formin activity, the actin monomer binding profilin was silenced with siRNA against profilin in JEG-3 cells. Profilin-actin binds the FH1 domain of formins and is essential for formin mediated actin filament elongation (Romero *et al.*, 2004). There are four profilin isoforms present in human cells, profilin-1 is ubiquitously expressed while the other isoforms are selectively expressed in different tissues. Profilin-2, the other main isoform, has been shown to be neuronal specific (Lambrechts *et al.*, 2000). Thus we targeted profilin-1, simply called profilin for simplicity for the rest of the chapter, for this analyses. As measured by western blot analyses, profilin was knocked down with about 90% efficiency (Figure 2.7D, bottom). However, there was no significant increase in percent of cells without microvilli as compared to luciferase treated control cells (Figure 2.7D, top). This would suggest that either the formin family of actin nucleators is not directly involved in the formation or regulation of microvilli in JEG-3 cells or that profilin is not as essential to formin mediated actin assembly as previously thought.

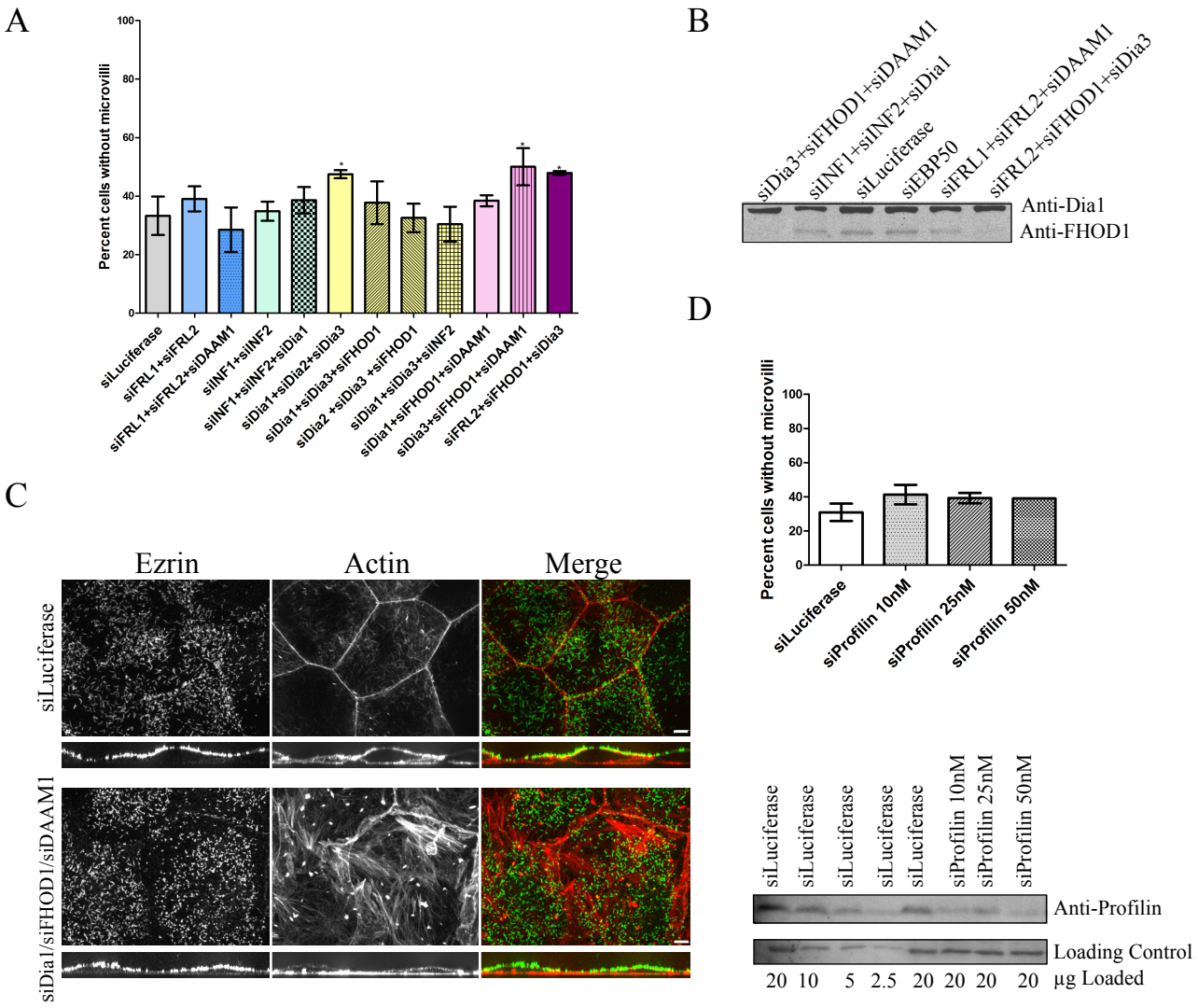

Figure 2.7 Multiple formin knockdown does not reveal an obvious role for formins in microvilli formation (A) Results of scoring microvilli phenotype after transfection with the siRNAs listed, using endogenous ezrin as a microvilli marker. N=2, 150 cells each * p<.05. (B) Western blot showing knockdown in cells transfected with the siRNA indicated and probed for Dia1 or FHOD1. (C) Maximum projection (XY) of confocal Z stacks and side views (XZ) stretched 2-fold of JEG-3 cells transfected with siRNA against either Luciferase (siLuciferase, top) or a triple siRNA transfection against Dia1, FHOD1 and DAAM1 (siDia1/siFHOD1/siDAAM1,bottom). Cells were fixed and stained for endogenous ezrin (green) and F-actin (red). Bars: 5µm. (D,top) Results of scoring microvilli phenotype after transfection with siRNA against Luciferase (siLuciferase) or different concentrations (as indicated) of siRNA against Profilin-1 (siProfilin) . N=2, 150 cells each. (D,bottom) Western blot showing knock down in cells transfected with siRNA against Luciferase (siLuciferase) or different concentrations of Profilin-1 (siProfilin) and probed for Profilin. Decreasing amounts (µg) of lysate were loaded as indicated to estimate profilin knockdown. Background band from Profilin blot was used as a loading control.

Discussion

The F-actin core of microvilli was first characterized more than 40 years again (Tilney and Mooseker, 1971) and has since been studied in great detail. However, the nucleator responsible for nucleating the assembly of the F-actin core of microvilli has remained elusive. The actin core of microvilli consists of bundled, unbranched actin filaments with the growing end oriented towards the plasma membrane (Mooseker and Tilney, 1975). This would strongly suggest that the potential actin nucleator responsible for the assembly of microvilli would nucleate unbranched filaments and would most likely localize to the growing tips of microvilli. The best characterized and most widely expressed class of unbranched actin nucleators is the formin family, which are involved in many diverse functions (Campellone and Welch, 2010). This family seemed a likely choice in which to screen for the potential nucleator responsible for assembling the core of microvilli.

Here I have utilized quantitative real time PCR (qPCR) to characterize the relative amount of mRNA transcript for each of the 15 mammalian formins in JEG-3 cells (Figure 2.1B). An ordered ranking was established and this was compared to the ordered ranking in Hela cells to compare similarities and differences between the two cell lines. Overall the top nine most expressed formins were similar between the two with the exception that INF1 was much higher in the ranking in JEG-3 cells and FRL1 was much higher ranked in Hela. Whether this difference is an indication of a specialized role for these formins in these two cell lines is unclear but would be an interesting topic of future studies.

Formins are barbed end nucleating and processive elongating factors. The barbed, or growing end, of the actin filament core of microvilli is oriented towards the plasma membrane. If a formin were indeed nucleating the actin filament core of microvilli one would expect to localize

the protein to the tip of microvilli. Expression of full length versions of four of the top formin candidates did not yield any specific localization in JEG-3 cells (Figure 2.3). However, formins are highly regulated proteins, undergoing tempo-spatial regulation to ensure that there is not aberrant actin filament formation within the cell. One way to relieve this regulation is to remove the auto-regulatory DAD region, which results in a constitutively active protein. Expression of either active Dia3 (GFP-Dia3ΔDAD) or active FHOD1 (GFP-FHOD1ΔDAD GFP-FHOD1V228E) in JEG-3 cells does not result in localization to the tips of microvilli (Figure 2.4 and Figure 2.5 respectively). In fact, GFP-Dia3ΔDAD induces filopodia formation at the basolateral domain where it is localized to the tips (Figure 2.4). This is an agreement with the current model for Dia3 function in other cell types (Block *et al.*, 2008). Expression of formin mutants that could not bind to actin filaments also had no effect on microvilli (Figure 2.6).

Cloning all top nine candidates into expression constructs was not feasible due to time constraints. Because of that, only the best candidates were chosen for localization studies. It is possible that even though I was looking at the candidates that were in relative abundance, as determined by qPCR, many copies of a single formin might not actually be necessary for such a specialized function. There is a possibility that a formin in lower abundance might be responsible for the formation of microvilli and those were excluded from my screen. Another possibility is that there is inherent problems with using overexpression vectors to localize proteins. The tag itself might interfere with the proteins natural conformation and prevent proper localization. The act of expressing a protein outside of an endogenous promoter might also interfere with potentially important interactions with other binding partners. Not enough available binding partners may lead to improper localization. Expression levels of GFP-formins were controlled whenever possible and verified by western (not shown) but it is difficult to express exogenously at endogenous levels.

There were no antibodies available for endogenous proteins that were suitable for immunofluorescence so I was unable to localize endogenous protein. So while I have not localized any specific formin, this does not exclude the possibility that a formin may be localized to microvilli.

To determine a potential functional role for formins in microvilli formation, a loss of function assay was utilized in which siRNA targeting the top nine formin candidates from the qPCR screen was used to knockdown individual formins in JEG-3 cells. A visual screen looking for an increase in the number of cells without microvilli was used as a measure of formin function in microvilli formation (Figure 2.2A, B). Knocking down a single formin only had an intermediate effect, with the most potent effect only resulting in about 50% of cells without microvilli. I was looking for an effect more similar to knocking down the microvillar protein EBP50, which results in a significant increase, to about 80%, in the percentage of cells without microvilli (Hanono *et al.*, 2006). One potential reason for an intermediate phenotype could be functional redundancy among formins. To address this potential issue I knocked out multiple formins simultaneously and asked if this increases the percentage of cells without microvilli. Unfortunately, of the combinations tested, there was no significant phenotype (Figure 2.7A). Of note, it did appear that there was less apical actin staining in Dia1/FHOD1/DAAM1 triple knockdown cells (Figure 2.7C) but the functional consequences of this have yet to be determined.

Since not all combinations of formins were targeted with siRNA I went with a more global approach for targeting formin activity. Profilin is an actin monomer binding protein that is essential to the processivity of formins at the barbed ends of actin filaments (Romero *et al.*, 2004). Profilin levels were reduced dramatically using siRNA (Figure 2.7D, bottom) which should effect the ability of all formins in the cell to nucleate the assembly of actin filaments. And yet, there was no

measurable increase in the percentage of cells that had no microvilli (Figure 2.7D, top). It is possible that profilin might be in abundance in the cell and even knocking down most of the protein might leave enough protein available for formin function. Recent reports suggest that profilin-2 is not just neuronal specific but is also expressed in many tissues other than brain, although it is not the primary profilin expressed (Mouneimne *et al.*, 2012). It's possible that profilin-2 might be upregulated in JEG-3 cells to compensate for profilin-1 knockdown, which may explain why I observe no phenotype upon loss of profilin-1. But more likely, a formin is not the sole nucleator involved in the formation of the actin filament core of microvilli.

So which actin nucleator is involved in microvilli formation? I began this work in 2008 and quietly walked away in 2011 to pursue a more promising lead in the form of the actin nucleator Cordon Bleu (the focus of Chapter 3). Three years later and no advances in the field have been made. Which isn't to say there isn't interest in this question. In a personal communication with Dr. Matt Tyska of Vanderbilt University, he suggested that he too was interested in determining the actin nucleator involved in microvilli formation but was also unable to make any headway in providing evidence that it was indeed a formin. It's possible that a formin is simply not involved in this process. It could also be that a formin is not exclusively involved but may work in concert with other actin nucleators, in a similar fashion to spire and FMN2 (Vizcarra *et al.*, 2011), or with F-bar proteins like drosophila Dia and Cip4 (Yan *et al.*, 2013). Identifying novel players in microvilli biogenesis may shed more light into which actin nucleator is involved in nucleating the assembly of the actin filament core of microvilli.

References

Alberts, A. S. (2001). Identification of a carboxyl-terminal diaphanous-related formin homology protein autoregulatory domain. J. Biol. Chem. *276*, 2824–2830.

Albulescu, L.-O., Sabet, N., Gudipati, M., Stepankiw, N., Bergman, Z. J., Huffaker, T. C., and Pleiss, J. A. (2012). A quantitative, high-throughput reverse genetic screen reveals novel connections between Pre-mRNA splicing and 5' and 3' end transcript determinants. PLoS Genet. *8*, e1002530.

Ang, S.-F., Zhao, Z., Lim, L., and Manser, E. (2010). DAAM1 is a formin required for centrosome re-orientation during cell migration. PLoS One *5*, 10.

Block, J., Stradal, T. E. B., Hänisch, J., Geffers, R., Köstler, S. A., Urban, E., Small, J. V, Rottner, K., and Faix, J. (2008). Filopodia formation induced by active mDia2/Drf3. J. Microsc. *231*, 506–517.

Brandt, D. T., Marion, S., Griffiths, G., Watanabe, T., Kaibuchi, K., and Grosse, R. (2007). Dia1 and IQGAP1 interact in cell migration and phagocytic cup formation. J. Cell Biol. *178*, 193–200.

Bretscher, A. (1989). Rapid phosphorylation and reorganization of ezrin and spectrin accompany morphological changes induced in A-431 cells by epidermal growth factor. J. Cell Biol. *108*, 921–930.

Campellone, K. G., and Welch, M. D. (2010). A nucleator arms race: cellular control of actin assembly. Nat. Rev. Mol. Cell Biol. *11*, 237–251.

Chhabra, E. S., and Higgs, H. N. (2006). INF2 Is a WASP homology 2 motif-containing formin that severs actin filaments and accelerates both polymerization and depolymerization. J. Biol. Chem. *281*, 26754–26767.

Colombo, A. *et al.* (2013). Daam1a mediates asymmetric habenular morphogenesis by regulating dendritic and axonal outgrowth. Development *140*, 3997–4007.

Fernandez-Borja, M., Janssen, L., Verwoerd, D., Hordijk, P., and Neefjes, J. (2005). RhoB regulates endosome transport by promoting actin assembly on endosomal membranes through Dia1. J. Cell Sci. *118*, 2661–2670.

Fujiwara, T., Mammoto, A., Kim, Y., and Takai, Y. (2000). Rho small G-protein-dependent binding of mDia to an Src homology 3 domain-containing IRSp53/BAIAP2. Biochem. Biophys. Res. Commun. *271*, 626–629.

Garbett, D., LaLonde, D. P., and Bretscher, A. (2010). The scaffolding protein EBP50 regulates microvillar assembly in a phosphorylation-dependent manner. J. Cell Biol. *191*, 397–413.

Goode, B. L., and Eck, M. J. (2007). Mechanism and function of formins in the control of actin assembly. Annu. Rev. Biochem. *76*, 593–627.

Gorelik, J. *et al.* (2003). Dynamic assembly of surface structures in living cells. Proc. Natl. Acad. Sci. U. S. A. *100*, 5819–5822.

Gorelik, R., Yang, C., Kameswaran, V., Dominguez, R., and Svitkina, T. (2011). Mechanisms of plasma membrane targeting of formin mDia2 through its amino terminal domains. Mol. Biol. Cell *22*, 189–201.

Gould, C. J., Maiti, S., Michelot, A., Graziano, B. R., Blanchoin, L., and Goode, B. L. (2011). The formin DAD domain plays dual roles in autoinhibition and actin nucleation. Curr. Biol. *21*, 384–390.

Hanono, A., Garbett, D., Reczek, D., Chambers, D. N., and Bretscher, A. (2006). EPI64 regulates microvillar subdomains and structure. J. Cell Biol. *175*, 803–813.

Harris, E. S., Gauvin, T. J., Heimsath, E. G., and Higgs, H. N. (2010). Assembly of filopodia by the formin FRL2 (FMNL3). Cytoskeleton (Hoboken). *67*, 755–772.

Harris, E. S., Li, F., and Higgs, H. N. (2004). The mouse formin, FRLalpha, slows actin filament barbed end elongation, competes with capping protein, accelerates polymerization from monomers, and severs filaments. J. Biol. Chem. *279*, 20076–20087.

Harris, E. S., Rouiller, I., Hanein, D., and Higgs, H. N. (2006). Mechanistic differences in actin bundling activity of two mammalian formins, FRL1 and mDia2. J. Biol. Chem. *281*, 14383–14392.

Kaiser, D. A., Vinson, V. K., Murphy, D. B., and Pollard, T. D. (1999). Profilin is predominantly associated with monomeric actin in Acanthamoeba. J. Cell Sci. *112 (Pt 2*, 3779–3790.

Kovar, D. R., Harris, E. S., Mahaffy, R., Higgs, H. N., and Pollard, T. D. (2006). Control of the assembly of ATP- and ADP-actin by formins and profilin. Cell *124*, 423–435.

Krainer, E. C., Ouderkirk, J. L., Miller, E. W., Miller, M. R., Mersich, A. T., and Blystone, S. D. (2013). The multiplicity of human formins: Expression patterns in cells and tissues. Cytoskeleton (Hoboken). *70*, 424–438.

Kühn, S., and Geyer, M. (2014). Formins as effector proteins of Rho GTPases. Small GTPases *5*.

Lambrechts, A., Braun, A., Jonckheere, V., Aszodi, A., Lanier, L. M., Robbens, J., Van Colen, I., Vandekerckhove, J., Fassler, R., and Ampe, C. (2000). Profilin II Is Alternatively Spliced, Resulting in Profilin Isoforms That Are Differentially Expressed and Have Distinct Biochemical Properties. Mol. Cell. Biol. *20*, 8209–8219.

Li, F., and Higgs, H. N. (2003). The mouse Formin mDia1 is a potent actin nucleation factor regulated by autoinhibition. Curr. Biol. *13*, 1335–1340.

Loomis, P. A., Zheng, L., Sekerková, G., Changyaleket, B., Mugnaini, E., and Bartles, J. R. (2003). Espin cross-links cause the elongation of microvillus-type parallel actin bundles in vivo. J. Cell Biol. *163*, 1045–1055.

Lynch, E. D. (1997). Nonsyndromic Deafness DFNA1 Associated with Mutation of a Human Homolog of the Drosophila Gene diaphanous. Science (80-.). *278*, 1315–1318.

Manor, U., and Kachar, B. (2008). Dynamic length regulation of sensory stereocilia. Semin. Cell Dev. Biol. *19*, 502–510.

Matheos, D., Metodiev, M., Muller, E., Stone, D., and Rose, M. D. (2004). Pheromone-induced polarization is dependent on the Fus3p MAPK acting through the formin Bni1p. J. Cell Biol. *165*, 99–109.

Mellor, H. (2010). The role of formins in filopodia formation. Biochim. Biophys. Acta *1803*, 191–200.

Mooseker, M. S., and Tilney, L. G. (1975). Organization of an actin filament-membrane complex. Filament polarity and membrane attachment in the microvilli of intestinal epithelial cells. J. Cell Biol. *67*, 725–743.

Mouneimne, G. *et al.* (2012). Differential remodeling of actin cytoskeleton architecture by profilin isoforms leads to distinct effects on cell migration and invasion. Cancer Cell *22*, 615–630.

Neidt, E. M., Scott, B. J., and Kovar, D. R. (2009). Formin differentially utilizes profilin isoforms to rapidly assemble actin filaments. J. Biol. Chem. *284*, 673–684.

Nezami, A. G., Poy, F., and Eck, M. J. (2006). Structure of the autoinhibitory switch in formin mDia1. Structure *14*, 257–263.

Osawa, H., Smith, C. A., Ra, Y. S., Kongkham, P., and Rutka, J. T. (2009). The role of the membrane cytoskeleton cross-linker ezrin in medulloblastoma cells. Neuro. Oncol. *11*, 381–393.

Pollard, T. D. (1981). Direct measurement of actin polymerization rate constants by electron microscopy of actin filaments nucleated by isolated microvillus cores. J. Cell Biol. *88*, 654–659.

Pruyne, D., Evangelista, M., Yang, C., Bi, E., Zigmond, S., Bretscher, A., and Boone, C. (2002). Role of formins in actin assembly: nucleation and barbed-end association. Science *297*, 612–615.

Ramalingam, N., Zhao, H., Breitsprecher, D., Lappalainen, P., Faix, J., and Schleicher, M. (2010). Phospholipids regulate localization and activity of mDia1 formin. Eur. J. Cell Biol. *89*, 723–732.

Romero, S., Le Clainche, C., Didry, D., Egile, C., Pantaloni, D., and Carlier, M.-F. (2004). Formin is a processive motor that requires profilin to accelerate actin assembly and associated ATP hydrolysis. Cell *119*, 419–429.

Sagot, I., Klee, S. K., and Pellman, D. (2002a). Yeast formins regulate cell polarity by controlling the assembly of actin cables. Nat. Cell Biol. *4*, 42–50.

Sagot, I., Rodal, A. A., Moseley, J., Goode, B. L., and Pellman, D. (2002b). An actin nucleation mechanism mediated by Bni1 and profilin. Nat. Cell Biol. *4*, 626–631.

Schulte, A., Stolp, B., Schönichen, A., Pylypenko, O., Rak, A., Fackler, O. T., and Geyer, M. (2008). The human formin FHOD1 contains a bipartite structure of FH3 and GTPase-binding domains required for activation. Structure *16*, 1313–1323.

Seth, A., Otomo, C., and Rosen, M. K. (2006). Autoinhibition regulates cellular localization and actin assembly activity of the diaphanous-related formins FRLalpha and mDia1. J. Cell Biol. *174*, 701–713.

Shimada, A., Nyitrai, M., Vetter, I. R., Kühlmann, D., Bugyi, B., Narumiya, S., Geeves, M. A., and Wittinghofer, A. (2004). The Core FH2 Domain of Diaphanous-Related Formins Is an Elongated Actin Binding Protein that Inhibits Polymerization. Mol. Cell *13*, 511–522.

Tilney, L. G., and Mooseker, M. (1971). Actin in the brush-border of epithelial cells of the chicken intestine. Proc. Natl. Acad. Sci. U. S. A. *68*, 2611–2615.

Tyska, M. J., and Mooseker, M. S. (2002). MYO1A (Brush Border Myosin I) Dynamics in the Brush Border of LLC-PK1-CL4 Cells. Biophys. J. *82*, 1869–1883.

Vavylonis, D., Kovar, D. R., O'Shaughnessy, B., and Pollard, T. D. (2006). Model of formin-associated actin filament elongation. Mol. Cell *21*, 455–466.

Viswanatha, R., Wayt, J., Ohouo, P. Y., Smolka, M. B., and Bretscher, A. (2013). Interactome analysis reveals ezrin can adopt multiple conformational States. J. Biol. Chem. *288*, 35437–35451.

Vizcarra, C. L., Kreutz, B., Rodal, A. A., Toms, A. V, Lu, J., Zheng, W., Quinlan, M. E., and Eck, M. J. (2011). Structure and function of the interacting domains of Spire and Fmn-family formins. Proc. Natl. Acad. Sci. U. S. A. *108*, 11884–11889.

Xu, Y., Moseley, J. B., Sagot, I., Poy, F., Pellman, D., Goode, B. L., and Eck, M. J. (2004). Crystal Structures of a Formin Homology-2 Domain Reveal a Tethered Dimer Architecture. Cell *116*, 711–723.

Yamana, N. *et al.* (2006). The Rho-mDia1 pathway regulates cell polarity and focal adhesion turnover in migrating cells through mobilizing Apc and c-Src. Mol. Cell. Biol. *26*, 6844–6858.

Yan, S., Lv, Z., Winterhoff, M., Wenzl, C., Zobel, T., Faix, J., Bogdan, S., and Grosshans, J. (2013). The F-BAR protein Cip4/Toca-1 antagonizes the formin Diaphanous in membrane stabilization and compartmentalization. J. Cell Sci. *126*, 1796–1805.

Yayoshi-Yamamoto, S., Taniuchi, I., and Watanabe, T. (2000). FRL, a Novel Formin-Related Protein, Binds to Rac and Regulates Cell Motility and Survival of Macrophages. Mol. Cell. Biol. *20*, 6872–6881.

Young, K. G., Thurston, S. F., Copeland, S., Smallwood, C., and Copeland, J. W. (2008). INF1 is a novel microtubule-associated formin. Mol. Biol. Cell *19*, 5168–5180.

Zigmond, S. H. (2004). Formin-induced nucleation of actin filaments. Curr. Opin. Cell Biol. *16*, 99–105.

Chapter 3[1]
Cordon Bleu serves as a platform at the basal region of microvilli where it regulates microvillar length through its WH2 domains

Overview

Cordon Bleu (Cobl) is a WH2-containing protein believed to act as an actin nucleator. In this chapter I show that it has a very specific localization in epithelial cells at the basal region of microvilli, a localization unlikely to be involved in actin nucleation. The protein is localized by a novel localization domain, a central region between the N-terminal COBL domain and the three C-terminal WH2 domains. Ectopic expression of Cobl shortens apical microvilli, and this requires functional WH2 domains. Proteomic studies reveal that the COBL domain binds several BAR-containing proteins, including SNX9, PACSIN-2/Syndapin-2 and ASAP1. ASAP1 is recruited to the base of microvilli by binding the COBL domain through its SH3. I propose that Cobl is localized to the basal region of microvilli to participate in both length regulation and to recruit BAR proteins that associate with the curved membrane found at the microvillar base.

[1] Parts of this chapter have been published in Wayt J. and Bretscher A.P. 2014.

Materials and Methods

Antibodies and Reagents

The mouse FLAG antibody and resin was from Sigma-Aldrich (St. Louis, MO), mouse GFP antibody was from Santa Cruz Biotechnology (Santa Cruz, CA) and the mouse E-cadherin antibody was from BD Biosciences (Mississauga, ON). The rabbit antisera and affinity-purified antibodies against full-length human ezrin have been described (Bretscher, 1989). The anti-Cobl antibody was a kind gift from J. Klingensmith (Duke University, Durham, NC). Goat anti-mouse secondary antibodies conjugated to horseradish peroxidase were from Jackson ImmunoResearch Laboratories (West Grove, PA). Alexa Fluor 568 and Alexa Flour 660-conjugated donkey anti-rabbit antibodies and Alexa Fluor 660–conjugated phalloidin were from Invitrogen (Carlsbad, CA). IRDye 680- and 800-conjugated secondary antibodies were from LI-COR Biosciences. WGA-488 was from Molecular Probes (Lafayette, CO).

DNA Constructs and Sequence Alignments

Murine GFP-Cobl-FL was a kind gift from M. Kessels (Research Institute of the FSU Jena, Jena, Germany). Cobl truncations were cloned into pEGFP-C2 (Takara Bio, Shiga, Japan) as GFP-Cobl-COBL (1-408), GFP-Cobl-CT (409-1337), GFP-Cobl-LD (648-899), GFP-Cobl-409-1167, GFP-Cobl-ΔWH2 (1-1167), GFP-Cobl 409-658, GFP-Cobl-895-1167. GFP-Cobl-FL, GFP-Cobl-COBL and GFP-Cobl-CT were cloned into a modified PQCXIP (BD Biosciences) backbone that has an N-terminal 3xFLAG to create FLAG constructs. To generate GFP-Cobl-WH2(1-3)A the WH2 domains of mouse Cobl were aligned with the WH2 domains of drosophila Spire, human SCAR, human WASP and human nWASP using ClustalW. The residues used in (Kelly *et al.*, 2006) to inactivate the WH2 domains were used as a reference to identify conserved lysines in

Cobl. The following mutations were then introduced by site directed mutagenesis of GFP-Cobl-FL using the QuickChange II XL (Agilent, Santa Clara, CA) kit: L1189A, L1202A, L1229A,L1242A, L1317A, and L1330A to generate the GFP-Cobl-WH2(1-3)A mutant. The internal deletion of the Cobl localization domain (Δ 648-899) was generated by two steps of overlapping PCR and inserted into pEGFP-C2. Murine GFP-ASAP1 in pEGFP-C1 was a kind gift from P. Randazzo (National Cancer Institute, Bethesda,MD). GFP-ASAP1ΔSH3 (AA 1-1032) was cloned from GFP-ASAP1 and placed into pEGFP-C2. GFP-Snx9 and GFP-PACSIN2 were cloned into pEGFPC-2 from human ppSumo-Snx9 and human ppSumo-PACSIN2 which were a kind gift from H. Sondermann (Cornell University, Ithaca, NY). The siRNAs targeting human Cordon Bleu (5′-AGCACGGCCUCACAACGUAtt-3′) was obtained from Ambion by Life Technologies and Luciferase GL2 (5′-CGUACGCGGAAUACUUCGA-3′) was obtained from Thermo Fisher Scientific and Applied Biosystems. The lentiCRISPR plasmid was obtained from Addgene (plasmid #49535)

Cell Culture and Transfection

JEG-3, and HEK293T cells (American Type Culture Collection, Manassas, VA) were maintained in a 5% CO_2 humidified atmosphere at 37°C. JEG-3 cells were cultured in MEM (Thermo Fisher Scientific, Lafayette, CO) with 10% fetal bovine serum (FBS), and HEK293T in DMEM with 5% FBS. JEG-3 cells were transfected with polyethylenimine (Polysciences, Warrington, PA) and 1–2 μg plasmid DNA, as described (Hanono *et al.*, 2006). HEK293T cells were transfected with Lipofectamine 2000 (Invitrogen) according to the manufacturers' instructions. For generation of stable HEK293T cell lines expressing 3xFLAG-COBL or 3xFLAG-empty vector, Phoenix-AMPHO cells were cotransfected with the above constructs in pQCXIP in addition to a plasmid

encoding VSV-G using polyethylenimine. The infected HEK293T cells were then selected and maintained with 2 μg/ml puromycin (Sigma-Aldrich). For knocking down endogenous Cobl in Jeg-3 cells, cells were transfected with 10 nM of siRNA using Lipofectamine RNAiMax, allowed to grow for 72 h, then processed for immunofluorescence and microvilli measurements, or Western blot analysis.

CRISPR Genome Edited Cell Line Generation

Creating stable genome edited CRISPR Cobl cells, in which the endogenous Cobl gene was targeted for knockout, was performed as described previously (Shalem *et al.*, 2014). The target guide sequence against the second exon of Cobl was placed into the LentiCRISPR backbone using the following Oligos: . 5' CACCGCCAAGTTCTGCTGCGACCCG 3', and 5' AAACCGGGTCGCAGCAGAACTTGGC 3'. Jeg-3 cells expressing the CRISPR system were then selected for using 2μg/ml puromycin in complete MEM for 15 days. Knockout was determined by western blot analysis.

Immunoprecipitations and Western Blotting

HEK293T cells transiently co-expressing 3xFLAG-Cobl and GFP-ASAP1 constructs for 24 hours were lysed in lysis buffer (25 mM Tris, pH 7.4, 5% glycerol, 150 mM NaCl, 50 mM NaF, 0.1 mM Na_3VO_4, 10 mM β-glycerol phosphate, 8.7 mg/ml paranitrophenylphosphate, 0.3% Triton X-100, and protease inhibitor tablet [Roche]) and immunoprecipitated with M2 FLAG resin (Sigma-Aldrich) for 2 hours. Immunoprecipates were than washed 4 times in wash buffer (Lysis buffer but with 0.2% Triton X-100 and no protease inhibitor tablet) and eluted from the FLAG resin with 200μg/ml 3xFLAG peptide. Eluates were than denatured with Laemmli buffer, resolved by SDS-

PAGE, transferred to Immobilon-FL (EMD Millipore, Billerica, MA), blotted with specific antibody and visualized by ECL.

To determine percentage of Cobl knockdown, Western blots were probed with specific antibody and IRDye conjugated 680 0r 800 secondary antibodies. The blot was than imaged using an Odyssey infrared imaging system (LI-COR Biosciences, Lincoln, NE). Analysis to determine percent Cobl knockdown was performed using Image Studio Lite 4.0 (LI-COR biosciences). Samples were normalized to the E-cadherin loading control and knockdown was determined as a percent of the control.

SILAC and mass spectrometry

For SILAC, HEK293T cells stably expressing either 3xFLAG-Empty Vector or 3xFLAG-Cobl-COBL were grown in MEM with 10% dialyzed FBS (Invitrogen) and either [^{12}C]arginine and lysine or [^{13}C]arginine and lysine, respectively, for three weeks to allow uniform labeling of all proteins. FLAG immunoprecipitations were performed as described above with modifications for mass spectrometry (Smolka *et al.*, 2007; Viswanatha *et al.*, 2012). Briefly, after immunoprecipitation, protein bound to FLAG resin was eluted in 50 mM Tris (pH 8.0) and 1% SDS and then precipitated with 50% ethanol, 49.9% acetone, and 0.1% acetic acid. Protein samples were then mixed, trypsin digested (Promega, Madison, WI) overnight at 37°C and desalted in a C18 column (Waters, Milford, MA). The tryptic peptides were dehydrated in a speed vacuum and dissolved in 80% acetonitrile and 1% formic acid for fractionation by hydrophilic interaction chromatography. The resulting fractions were dried, dissolved in 0.1% trifluoroacetic acid, and injected into a mass spectrometer (Qexactive LC-MS/MS; Thermo Fisher Scientific). The data were analyzed using Proteome Discoverer (Thermo Fisher Scientific).

Immunofluorescence

JEG-3 cells were grown on coverslips and fixed in 3.7% formaldehyde at room temperature for 15 minutes. Coverslips were then washed 3 times in phosphate-buffered saline (PBS) and permeabilized with 0.2% Triton X-100 for 5 minutes at room temperature. Coverslips were than washed 3 more times with PBS and blocked in filtered 3% FBS in PBS for 10 minutes. Primary and secondary antibodies were made up in 3% FBS in PBS. Coverslips were washed 3 times in PBS between addition of primary and secondary antibodies. Alexa Fluor conjugated Phalloidin (Invitrogen) was added to the secondary when F-actin was visualized. Cells were imaged by time-lapse microscopy on a spinning disk (CSU-X; Yokogawa, Tokyo, Japan) with a spherical aberration correction device, a 100×/1.46 numerical aperture (NA) objective (Leica, Wetzlar, Germany) on an inverted microscope (DMI6000B; Leica) and an HQ2 CCD camera (Photometrics). Maximum intensity projections were created using Slidebook (Intelligent Imaging Innovations, Denver, CO) and exported in Adobe Illustrator.

Measurements of protein localization as a function of the percent length of microvilli were performed in Slidebook. A line was drawn along the entire length of microvilli and fluorescence intensity values were exported to Excel for multiple microvilli. Data was normalized by plotting fluorescence intensity as a function of the percentage of the total length of microvilli, where 0% and 100% represents the tip and base respectively. The resulting curve was fitted with a LOWESS function in PRISM.

Microvilli Length Measurements

The length of individual microvilli was measured using Volocity® 3D image analysis software (PerkinElmer, Waltham, MA) to draw lines along the entire length of microvilli in three

dimensions through several confocal Z stacks. Confocal images were taken with 0.28um steps and endogenous ezrin staining was used as a microvilli marker in all measurements. Lengths were exported to Prism and plotted as a whisker plot. Mann-Whitney tests were performed between adjacent untransfected and transfected cells to determine if change in length was statistically significant. A bead calibration assay was performed to determine 3D accuracy in which beads of known size were measured in the manner described above and the mean bead size was plotted against the actual size of the bead. The plot was fitted with a line of best fit with the error bars representing the standard deviation.

Live-cell imaging and FRAP

Transfected JEG-3 cells were grown in 35mm glass bottom dishes (MatTek, Ashland, MA), were washed in PBS and then maintained in low-sodium bicarbonate phenol red-free MEM (Sigma-Aldrich) supplemented with 25 mM HEPES (pH 7.4), with 10% FBS and GlutaMAX (Invitrogen). Live cells were imaged by time-lapse microscopy on the spinning disk microscope at 37°C in an environmental chamber (Okolab, Ottaviano, Italy) controlled by SlideBook version 5.5 (Intelligent Imaging Innovations, Denver, CO). Regions selected for FRAP were illuminated either with a digital mirror illumination system (Mosaic; Andor Technology, Belfast, Northern Ireland) coupled to a 488-nm 400-W argon laser or with a point-scanner galvanometer-based system (Vector; Intelligent Imaging Innovations) coupled to a 473-nm, 50-mW diode-pumped solid-state laser. A region independent of the region being bleached was monitored for the duration of each experiment to control for photobleaching. Movies were processed using SlideBook and analyzed using Excel (Microsoft, Redmond, WA) and Graphpad Prism (GraphPad, La Jolla, CA). Normalized data from

multiple biological replicates were fitted to a curve and Prism was utilized to perform two-way analysis of variance.

Results

Cordon Bleu localizes to the basal region of microvilli

To determine the subcellular localization of Cobl in epithelial cells, I expressed a full length version of GFP-tagged murine Cobl (GFP-Cobl-FL) in JEG-3 cells, a choriocarcinoma cell line with abundant microvilli. Maximum projection of confocal images through the cells showed a striking and highly specific punctate distribution on the apical surface. In cells stained for the microvillar protein ezrin, actin and GFP-Cobl-FL, it was found to be specifically enriched at the basal region of microvilli (Figure 3.1A, A'). In optimal images, an ezrin rich region, GFP-Cobl-FL region and actin rich region could be discerned (Figure 3.1A"). Quantification of the normalized fluorescence intensity of GFP-Cobl-FL and endogenous ezrin along the length of the microvilli clearly revealed this relationship (Figure 3.1B).

The apparent localization of GFP-Cobl-FL at the basal region of microvilli could be complicated either by the GFP tag or possibly an effect on the distribution of ezrin. To address these issues, I expressed a FLAG-tagged construct (FLAG-Cobl-FL) and compared its localization with both ezrin and Wheat Germ Agglutinin (WGA-488), a lectin that binds to cell surface proteins and serves as a plasma membrane marker. Once again, Cobl-FL was localized to the basal region of microvilli as seen both by ezrin and plasma membrane staining (Figure 3.1C,C'). FLAG-Cobl-FL localization at the base of microvilli shows little colocalization with WGA-488 (Figure 3.1D). This suggests that Cobl has a highly specific localization at the basal region of microvilli, but not to actin filament minus ends that extend deeper into the cytoplasm.

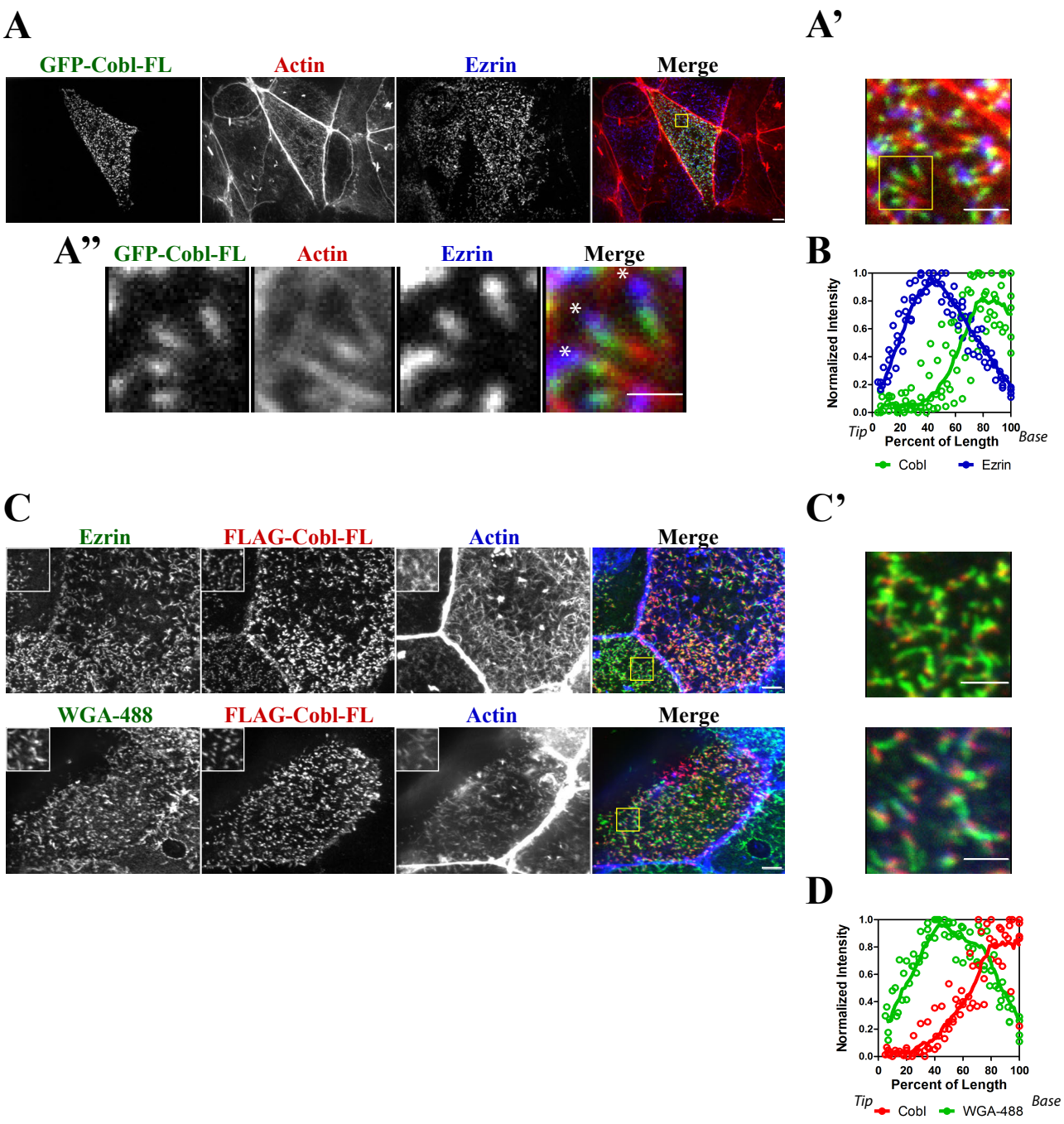
A
GFP-Cobl-FL
Actin
Ezrin
Merge
A'
A''
GFP-Cobl-FL
Actin
Ezrin
Merge
B
Normalized Intensity
1.0
0.8
0.6
0.4
0.2
0.0
Tip
0
20
40
60
80
100
Base
Percent of Length
Cobl
Ezrin
C
Ezrin
FLAG-Cobl-FL
Actin
Merge
C'
WGA-488
FLAG-Cobl-FL
Actin
Merge
D
Normalized Intensity
1.0
0.8
0.6
0.4
0.2
0.0
0
20
40
60
80
100
Percent of Length
Tip
Cobl
WGA-488
Base

Figure 3. 1. Cordon Bleu is localized to the basal region of microvilli. Maximum projections (XY) of confocal Z stacks of JEG-3 cells. (A) Localization GFP-Cobl (green), F-Actin (red) and endogenous ezrin (blue). Yellow box identifies area magnified in A'. (A") Detailed image of area defined by yellow box in A'. Asterisks indicate the tips of microvilli. (B) Normalized intensity of ezrin (blue) and Cobl (green) of several microvilli (n>5). Intensity was plotted (open circles) as a function of the percent of the total microvillar length with 0% and 100% representing tip and base respectively. The data was fitted to a LOWESS function (solid line). (C) Localization of FLAG-Cobl, F-Actin (blue), endogenous ezrin (green, upper panel) or the membrane marker WGA-488 (green, lower panel). Yellow box identifies magnified single channel insets and is shown merged in C'. (D) Normalized intensity of WGA-488 (green) and Cobl (red) of several microvilli (n>5). Intensity was plotted (open circles) as a function of the percent of the total microvillar length with 0% and 100% representing tip and base respectively. The data was fitted to a LOWESS function (solid line). Scale bars: 5μm (A, C), 2 μm (A', C') and 1 μm (A").

Cobl is localized to microvilli by a region between the COBL and WH2 domains

I next explored which region of Cobl is necessary for its localization to the base of microvilli. Cobl consists of an N-terminal COBL domain of 408 residues, with three WH2 domains in its C-terminal 170 residues (Figure 3.2A). I first made two complementary constructs, GFP-Cobl-COBL (AA 1-408) and GFP-Cobl-CT (AA 409-1337), each tagged with GFP on the N-terminal end (Figure 3.2B) to compare the localization of each in comparison with GFP-Cobl-FL (Figure 3.1A). Since the COBL domain has been shown to be essential for both protein-protein interactions and its localization to dendritic spines (Ahuja *et al.*, 2007; Haag *et al.*, 2012) I was surprised to find that GFP-Cobl-COBL was not enriched in microvilli but was cytoplasmic (Figure 3.2B, top). Conversely, expression of GFP-Cobl-CT without the COBL domain was still able to localize to microvilli (Figure 3.2B, bottom). Interestingly, GFP-Cobl-CT is not as tightly restricted to the base as full length Cobl. These data suggest that the COBL domain is not necessary for localization to microvilli.

In the C-terminal region of Cobl are three WH2 domains, each of which can bind an actin monomer (Ahuja *et al.*, 2007). These WH2 domains are able to both nucleate the assembly of actin filaments as well as act as a potent severing agent *in vitro* (Ahuja *et al.*, 2007; Husson *et al.*, 2011; Chen *et al.*, 2013; Jiao *et al.*, 2014). Adjacent to the first WH2 domain is a lysine rich patch (Figure 3.2A) that is necessary for both nucleating and severing actin filaments (Husson *et al.*, 2011; Jiao *et al.*, 2014). To see if functional WH2 domains were necessary for Cobl localization to the base of microvilli, I set out to generate mutants deficient in actin binding. Within each WH2 domain is an actin binding consensus sequence and mutations of these conserved residues can compromise this ability (Kelly *et al.*, 2006; Zuchero *et al.*, 2012). The WH2 domains of Cobl, WASP (Wiskott-Aldrich Syndrome protein), SCAR (suppressor of cyclic-AMP receptor) and Spire were aligned

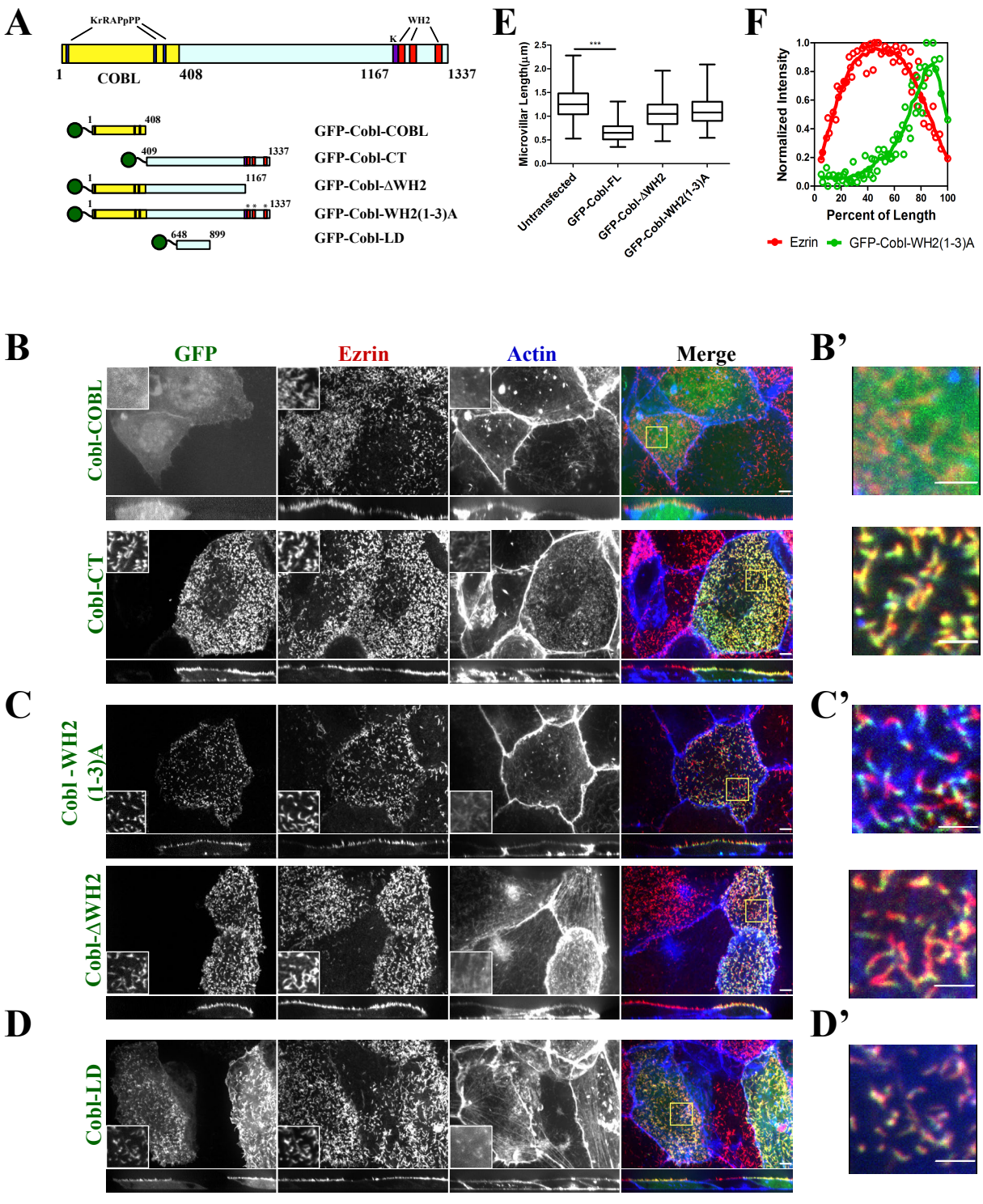
A
KrRAPpPP
WH2
K
1
COBL
408
1167
1337
GFP-Cobl-COBL
GFP-Cobl-CT
GFP-Cobl-ΔWH2
GFP-Cobl-WH2(1-3)A
GFP-Cobl-LD
E
Microvillar Length(μm)
***
Untransfected
GFP-Cobl-FL
GFP-Cobl-ΔWH2
GFP-Cobl-WH2(1-3)A
F
Normalized Intensity
Percent of Length
Ezrin
GFP-Cobl-WH2(1-3)A
B
GFP
Ezrin
Actin
Merge
B'
Cobl-COBL
Cobl-CT
C
C'
Cobl -WH2 (1-3)A
Cobl-ΔWH2
D
D'
Cobl-LD

F**igure 3.2. Cordon Bleu regulates microvilli length by its WH2 domains and is localized to microvilli independently of the COBL and WH2 domains.** (A) Schematic of Cobl and the constructs used in this study. (B-D) Maximum projections (XY) of confocal Z stacks and side views (XZ) stretched 2-fold of JEG-3 cells expressing the indicated constructs, then fixed and GFP (green), endogenous ezrin (red) and F-actin (blue) localized. Yellow boxes represent magnified single channel insets and is shown merged in (B'-D'). Scale bars: 5µm (B-D) and 2µm (B'-D'). The contrast for F-actin was increased for clarity in (C',top). (E) Length of microvilli (µm) of untransfected JEG-3 cells or transfected to express GFP-Cobl-FL, GFP-Cobl-ΔWH2, or GFP-Cobl-WH2(1-3)A. The box represents the 25th and 75th percentiles around the median and the whiskers represent the maximum and minimum. ***, $p<.0001$. (F) Normalized intensity of ezrin (red) and GPP-Cobl-WH2(1-3)A (green) of several microvilli ($n>5$). Intensity was plotted (open circles) as a function of the percent of the total microvillar length with 0% and 100% representing tip and base respectively. The data was fitted to a LOWESS function (solid line).

and conserved residues in the consensus sequence identified (Figure 3.3A). I made point mutations in each individual WH2 domain (Figure 3.3 B-D) as well as in all three WH2 domains (GFP-Cobl-WH2(1-3)A). Several of these mutations have recently been utilized and verified to affect WH2 activity in Cobl (Chen *et al.*, 2013). Expression of single WH2 mutants localized to microvilli (Figure 3.4 A-C). Expression of GFP-Cobl-WH2(1-3)A in JEG-3 cells still strongly localized to the base of microvilli (Figure 3.2C, top). Quantification of the normalized fluorescence intensity of GFP-Cobl-WH2(1-3)A and endogenous ezrin along the length of the microvilli clearly revealed this relationship (Figure 3.2F).

To further illustrate that the WH2 domains of Cobl are not essential for localization, I created a Cobl truncation mutant lacking the lysine rich patch and all three WH2 domains (GFP-Cobl-ΔWH2, AA 1-1167). GFP-Cobl-ΔWH2 localized to the basal region of microvilli just like GFP-Cobl-WH2(1-3)A (Figure 3.2C, bottom). Further removal of the COBL domain from this construct (GFP-Cobl-409-1167) still results in localization to microvilli (Figure 3.4B) and expression of just the lysine rich patch and the three WH2 domains (AA 1156-1338, Figure 3.4C) is cytoplasmic. These data suggest that the WH2 domains of Cobl play no role in the localization to the basal region of microvilli.

With neither the COBL domain nor the WH2 domains playing an essential role in localization of Cobl to the basal region of microvili, the large portion of the protein (residues 409-1167) between these, which is predicted to be unstructured, appears to harbor the localization domain. This region was further truncated into three separate 250 residue fragments, each of which was expressed individually in JEG-3 cells. One of these, comprising residues 648-899 localized to the basal region of microvilli, whereas the others did not (Figure 3.2D, 3.4D). To further demonstrate that this region is essential for the localization of Cobl I made a construct in which

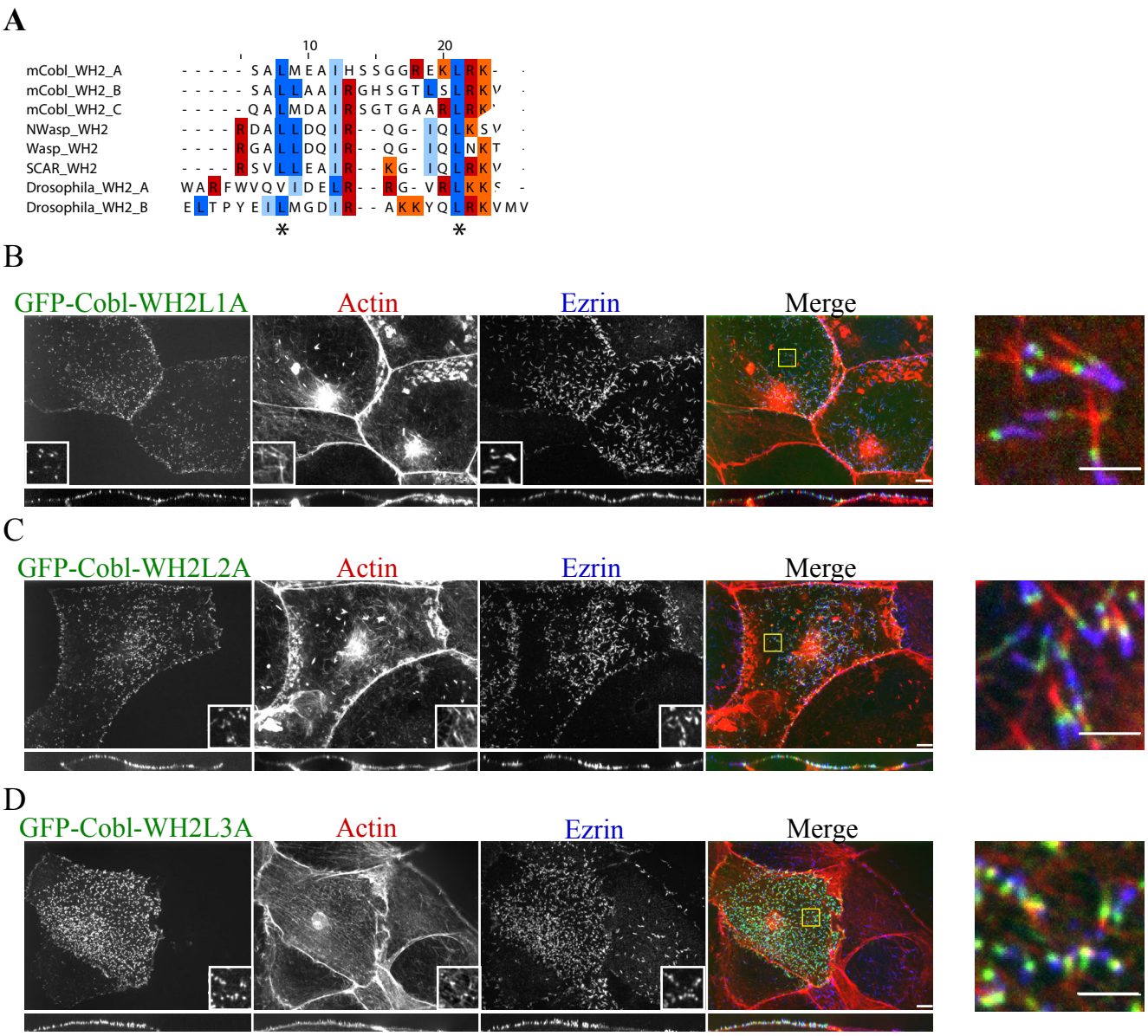

Figure 3.3 Single WH2 mutations localize to microvilli. (A) Alignment of WH2 domains to identify conserved actin binding residues (asterisks) to create GFP-Cobl -WH2(1-3)A and single WH2 domain mutants. See materials and methods for details.(B-D Maximum projections (XY) of confocal Z stacks and side views (XZ) stretched 2-fold of JEG-3 cells expressing the indicated constructs, then fixed and GFP (green), F-actin (red) and endogenous ezrin (blue) localized. Yellow boxes represent magnified single channel insets and is shown merged magnified at right. Scale bars: 5µm (B-D) and 2µm in magnified merge.

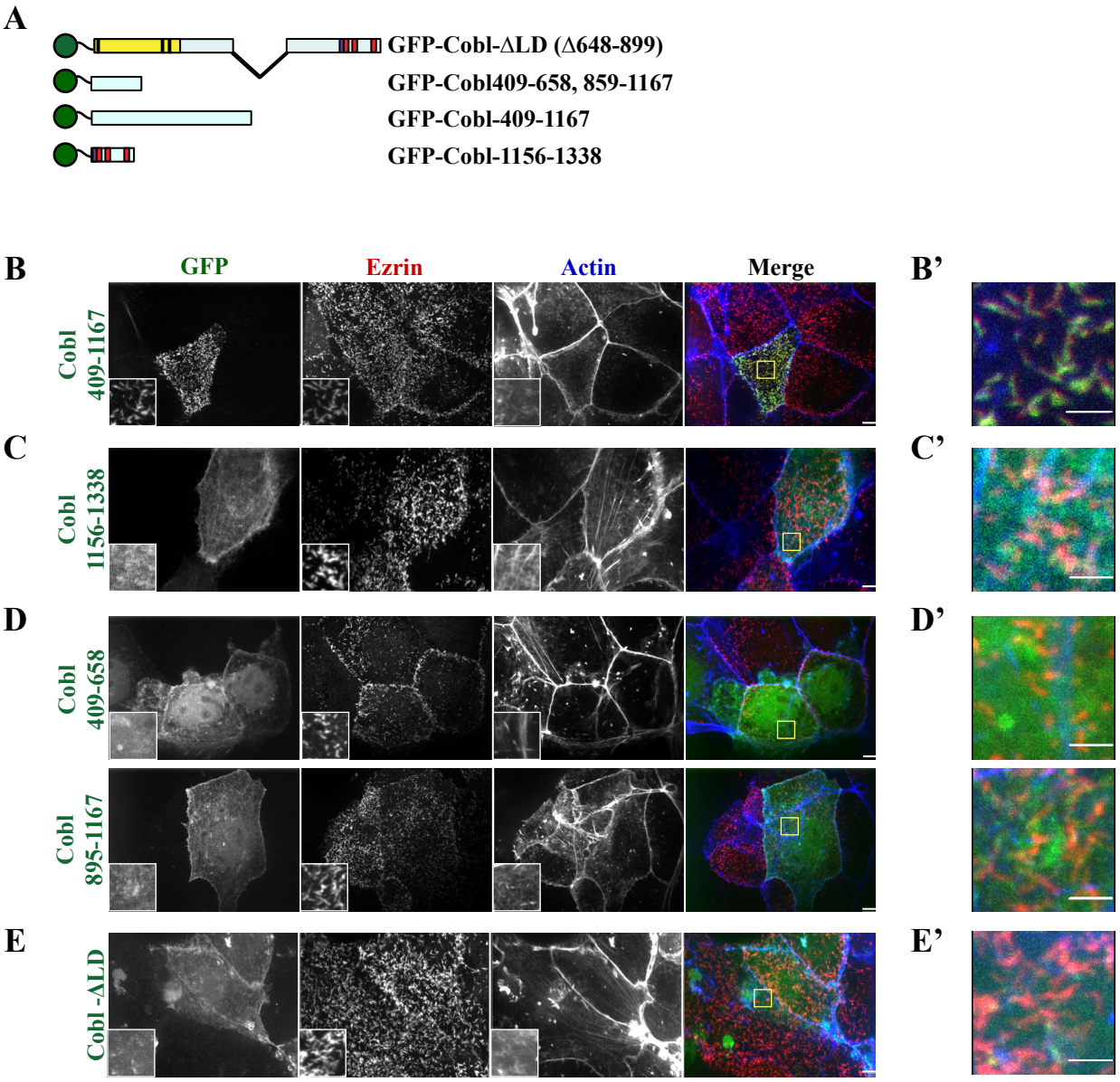

Figure 3.4 Cobl is localized to microvilli by a region between the COBL and WH2 domains. (A) Schematic of the constructs utilized in this figure. (B-E) Maximum projections (XY) of confocal Z stacks of JEG-3 cells. Cells were fixed and stained for endogenous ezrin (red) and F-actin (blue). Localization of GFP-Cobl-409-1167 (B), GFP-Cobl -1156-1338 (C), GFP-Cobl -409-658 (D,top) GFP-Cobl -895-1167 (D,bottom) or GFP-Cobl- ΔLD (E).Yellow box identifies magnified area in single channel insets. (B'-E') Detailed images of three channel merge highlighted by the yellow boxes in (B-E). Scale bars: 5µm (B-E) and 2µm (B'-E').

this region was deleted in the context of the full length protein (GFP-Cobl-ΔLD, Δ648-899) and expressed it in JEG-3 cells. GFP-Cobl-ΔLD is cytoplasmic, with no localization to microvilli (Figure 3.4E). The 648-899 region of Cobl is therefore necessary and sufficient for the localization of Cobl to the basal region of microvilli, which is outside the COBL domain, a region thought to provide the protein's specific localization in other systems (Schwintzer *et al.*, 2011; Haag *et al.*, 2012).

The Cobl WH2 domains regulate the length of microvilli

Cells expressing GFP-Cobl-FL had visibly shorter microvilli. To quantify this effect, I measured the length of microvilli in three dimensions through confocal Z stacks (Figure 3.2E). Using endogenous ezrin staining as our marker for microvillar length, I measured the length of microvilli in cells transfected with different Cobl constructs compared with adjacent untransfected cells in the same field. The median length of microvilli in untransfected cells was 1.3μm, whereas in cells expressing GFP-Cobl-FL microvilli were about half as long, with a median length of 0.6μm (Fig 3.2E), using a bead standard to verify accuracy of the measurements (Figure 3.5). To see if this length regulation was mediated by the WH2 domains, I measured the lengths of microvilli in cells expressing GFP-Cobl-ΔWH2 and GFP-Cobl-WH2(1-3)A. Expression of the constructs either lacking the WH2 domains, or containing inactivated WH2 domains, had no effect on microvillar length (Figure 3.2E). These data indicate that the WH2 domains of Cobl are necessary for the regulation of microvillar length. Since endogenous Cobl is present in Jeg-3 cells, I examined the effect of siRNA knockdown or in Cas9/CRISPR genome edited Cobl knockout cells. Neither method of lowering Cobl expression effected microvilli length (Figure 3.6)

A

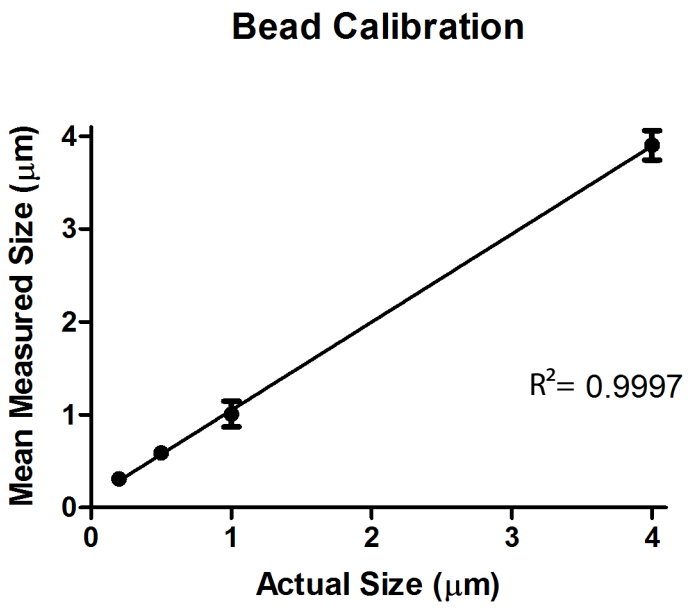

Figure 3.5. Bead measurements to determine 3D accuracy. (A) Quantification through confocal Z stacks measuring the diameter of beads of known size (n> 30, each size), using the image processing program Volocity®. Measuring protocol used was identical to one used for microvilli length measurements in Fig. 2B, see materials and methods for details. The mean of the measured diameter of the bead was plotted against the actual diameter. The plot was fitted with a line of best fit, with the R^2 value displayed. Error bars show standard deviation.

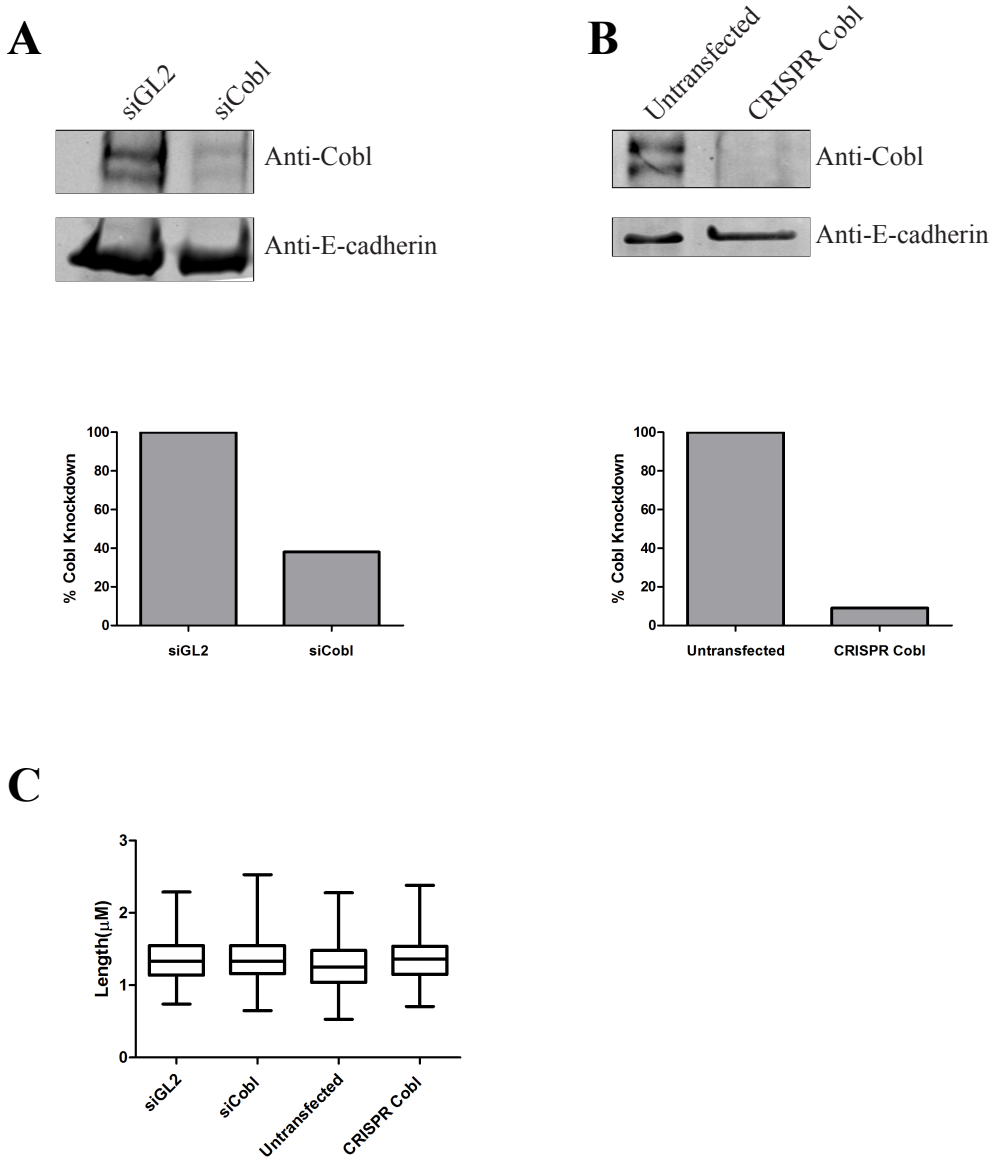

Figure 3.6. Knocking down endogenous Cobl does not affect microvilli length. (A) JEG-3 cells were transfected with siRNA against luciferase (siGL2) or Cobl (siCobl) for 72 hours and then lysed directly in 2x laemmeli sample buffer. Subsequent westerns were blotted for both endogenous Cobl and E-cadherin as a loading control (top). Percent knockdown of Cobl protein for siCobl sample was determined as a percent of the siGL2 control (bottom). (B) Untransfected JEG-3 cells or genome edited Cas9/CRISPR Cobl cells were lysed directly in 2x laemmeli sample buffer. Subsequent westerns were blotted for endogneous Cobl and E-cadherin as a loading control (top). Percent knockdown of Cobl protein for the Cas9/CRISPR Cobl sample was determined as a percent of the untransfected control (bottom). (C) Length of microvilli (μm) in JEG-3 cells for indicated experimental condition. The box represents the 25th and 75th percentile around the median and the whiskers indicate the minimum and maximum.

The localization of Cobl to the basal region of microvilli is relatively stable

Components of microvilli can have very different dynamics *in vivo*, and these dynamics are regulated (Garbett and Bretscher, 2012). Even homologous proteins, like the microvillar scaffolding proteins EBP50 and E3KARP (Na(+)/H(+) exchanger (NHE) type 3 kinase A regulatory protein), show vastly different dynamics even though they share similar localizations, but presumably somewhat distinct functions (Garbett *et al.*, 2013). I therefore examined the dynamics of Cobl to see if it is a highly dynamic or relatively stable component at the basal region of microvilli.

I explored the dynamics of Cobl using FRAP on JEG-3 cells expressing different GFP-Cobl constructs (Figure 3.7A, B). Photobleaching of GFP-Cobl-FL exhibits relatively slow recovery and only recovers to about 70% of the initial fluorescence intensity following photobleaching, just as I have seen for the relatively stable microvillar protein ezrin (Garbett and Bretscher, 2012). This suggests the Cobl undergoes a slow exchange rate between the cytosol and microvilli.

To determine if either the COBL domain, or the WH2 domains, contribute to this slow turnover, I made use of the constructs that lack the COBL domain (GFP-Cobl-CT) or contain inactive WH2 domains (GFP-Cobl-WH2(1-3)A). Expression of these constructs followed by photobleaching demonstrated that there is no significant difference in recovery curves when compared to the full length protein (Figure 3.7B, top). However, the dynamics of the localization domain alone, GFP-Cobl-LD, is much faster than that of the full length protein (Figure 3.7B, bottom). Therefore regions outside of the localization domain and C-terminal to the COBL domain must also contribute to the stabilization of Cobl at the basal region of microvilli.

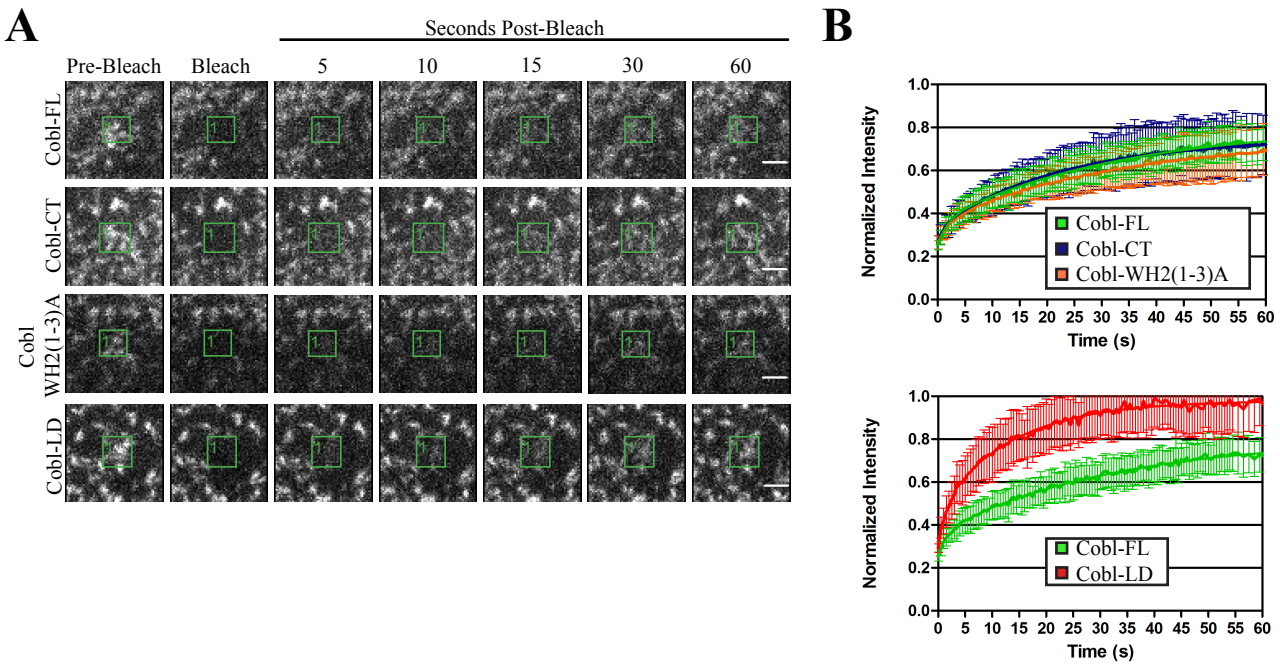

Figure 3.7. Cordon Bleu is a stable component of microvilli. (A) Images of time points after photobleaching the boxed areas of cells expressing GFP-Cobl-FL, GFP-Cobl-CT, GFP-Cobl-WH2(1-3)A and GFP-Cobl-LD. Scale bars: 2µm. (B, top) Recovery curves after photobleaching the boxed areas of cells expressing GFP-Cobl FL (n=12), GFP-Cobl-CT (n=12), GFP-Cobl-WH2(1-3)A (n=12) and (B, bottom) GFP-Cobl-FL and GFP-Cobl-LD (n=10). The recovery curves are normalized to the initial intensity in the boxed areas. Error bars show standard deviation.

Identification of Cobl interaction partners

To date, there are few known Cobl interacting partners, the best characterized of which are the Syndapin/PACSIN family of proteins and the F-actin binding protein Abp1 (Ahuja *et al.*, 2007; Schwintzer *et al.*, 2011; Haag *et al.*, 2012). I wished to identify Cobl interaction partners to provide insight into the function of Cobl.

To identify potential interacting proteins I utilized Stable Isotope Labeling of Amino acids in Cell Culture (SILAC) combined with quantitative mass spectrometry (Figure 3.8A). In outline, HEK293T cells stably expressing an empty vector control or 3x-FLAG-Cobl-COBL were used as I have so far been unable to make a line stably expressing the full length protein or the C-terminal region. FLAG-immunoprecipitation was performed on both samples and the immunoprecipitates subsequently combined and trypsin digested. The digested samples were then subjected to quantitative mass spectrometry. Peptides identified as enriched in the control sample were considered background and peptides enriched in the 3xFLAG-COBL sample were considered potential interactors of the COBL domain.

The top candidates identified by our analysis are shown in Figure 3.8B where the SILAC enrichment ratio is the quantitative measure of enrichment of peptides between heavy and light. Two are members of the PACSIN/Syndapin family and their interaction with Cobl has been described in detail (Ahuja *et al.*, 2007; Haag *et al.*, 2012). I also identified three novel Cobl binding partners including: ASAP1 (ArfGAP with SH3 domain, ankyrin repeat and PH domain 1), ASAP2 (ArfGAP with SH3 domain, ankyrin repeat and PH domain 2) and SNX9 (Sorting Nexin 9). Interestingly, all of our top candidates are BAR (Bin-Amphiphysin-Rvs167) proteins that also contain SH3 (Src Homology 3) domains (Figure 3.8C).

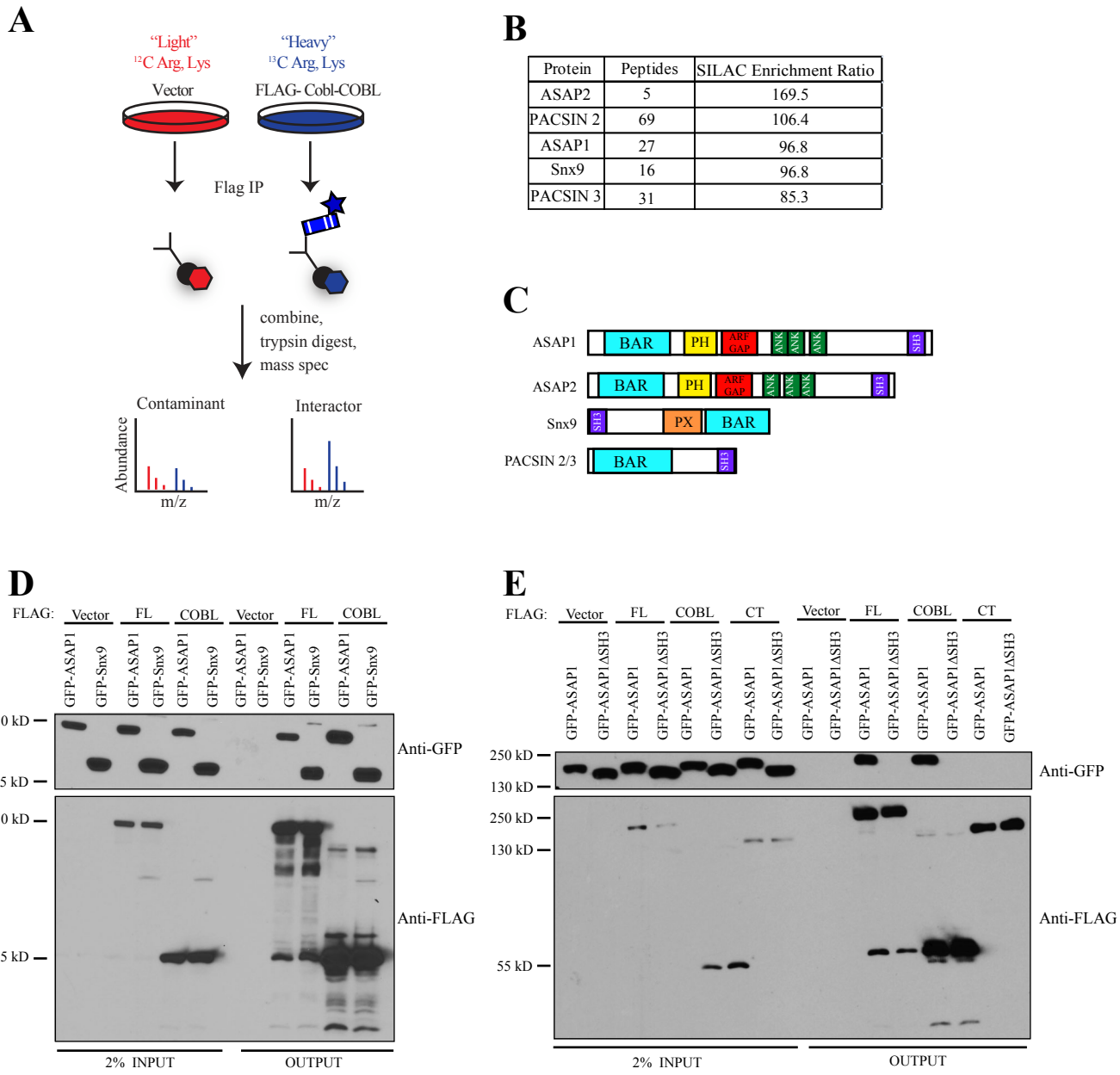

Figure 3.8. Identification of Cordon Bleu interaction partners. (A) Schematic of SILAC experiment in HK293T cells. (B) Top hits showing total number of peptides indentified for each candidate and the enrichment ratio of peptides in Heavy:Light. (C) Schematic showing domains of top SILAC hits. (D) 3x-FLAG-Cobl constructs were coexpressed in HEK293T cells with either GFP-ASAP1 or GFP-Snx9 and subjected to FLAG immunoprecipitation (IP) and then subsequently blotted for GFP and FLAG. (E) 3x-FLAG-Cobl constructs were coexpressed with either GFP-ASAP1 or GFP-ASAP1-ΔSH3 and subjected to FLAG immunoprecipitation (IP) and then subsequently blotted for GFP and FLAG.

To validate the results of the SILAC analysis I co-expressed different FLAG-Cobl variants and GFP-ASAP1 or GFP-Snx9 in HEK293T cells, and then immunoprecipitated the FLAG epitope and blotted for the GFP-tagged construct. Co-immunoprecipitations confirmed that both the full length version of Cobl as well as the COBL domain alone was able to interact with ASAP1 and Snx9 (Figure 3.8D). To determine if either of these proteins was relevant in the context of microvilli I localized GFP-tagged versions of both ASAP1 and Snx9 in JEG-3 cells. GFP-ASAP1 was localized weakly to the base of microvilli (Figure 3.9A), while GFP-Snx9 was cytoplasmic (data not shown).

I next sought to identify which region of ASAP1 interacts with the COBL domain. The interaction between Cobl and PACSIN1/2/3 is known to occur between the COBL domain and the SH3 domain of the PACSIN family (Schwintzer *et al.*, 2011). Since ASAP1 harbors an SH3 domain in its C-terminal region, it is likely to mediate the interaction with Cobl. To test this, an expression construct of ASAP1 lacking the SH3 domain, GFP- ASAP1ΔSH3, was constructed and coexpressed with FLAG-tagged full length Cobl, or its COBL domain or its C-terminal region. FLAG immunoprecipitates showed that the SH3 domain of ASAP1 is necessary for the recovery of GFP-ASAP1 by either 3xFLAG-Cobl-FL or 3xFLAG-Cobl-COBL (Figure 3.8E). Furthermore, the FLAG-Cobl-CT was not able to recover either GFP-ASAP1 or GFP-ASAP1ΔSH3 from cell lysates (Figure 3.8E). These data document that the interaction between Cobl and ASAP1 occurs between the COBL domain of Cobl and the SH3 domain of ASAP1.

Cobl serves as a platform at the base of microvilli

GFP-ASAP1 is weakly localized to microvilli when expressed alone in JEG-3 cells (Figure 3.9A, A'). However, upon co-expression with FLAG-Cobl-FL, GFP-ASAP1 is strongly enriched in microvilli (Figure 3.9B. B'). This enrichment is dependent on the interaction between the SH3

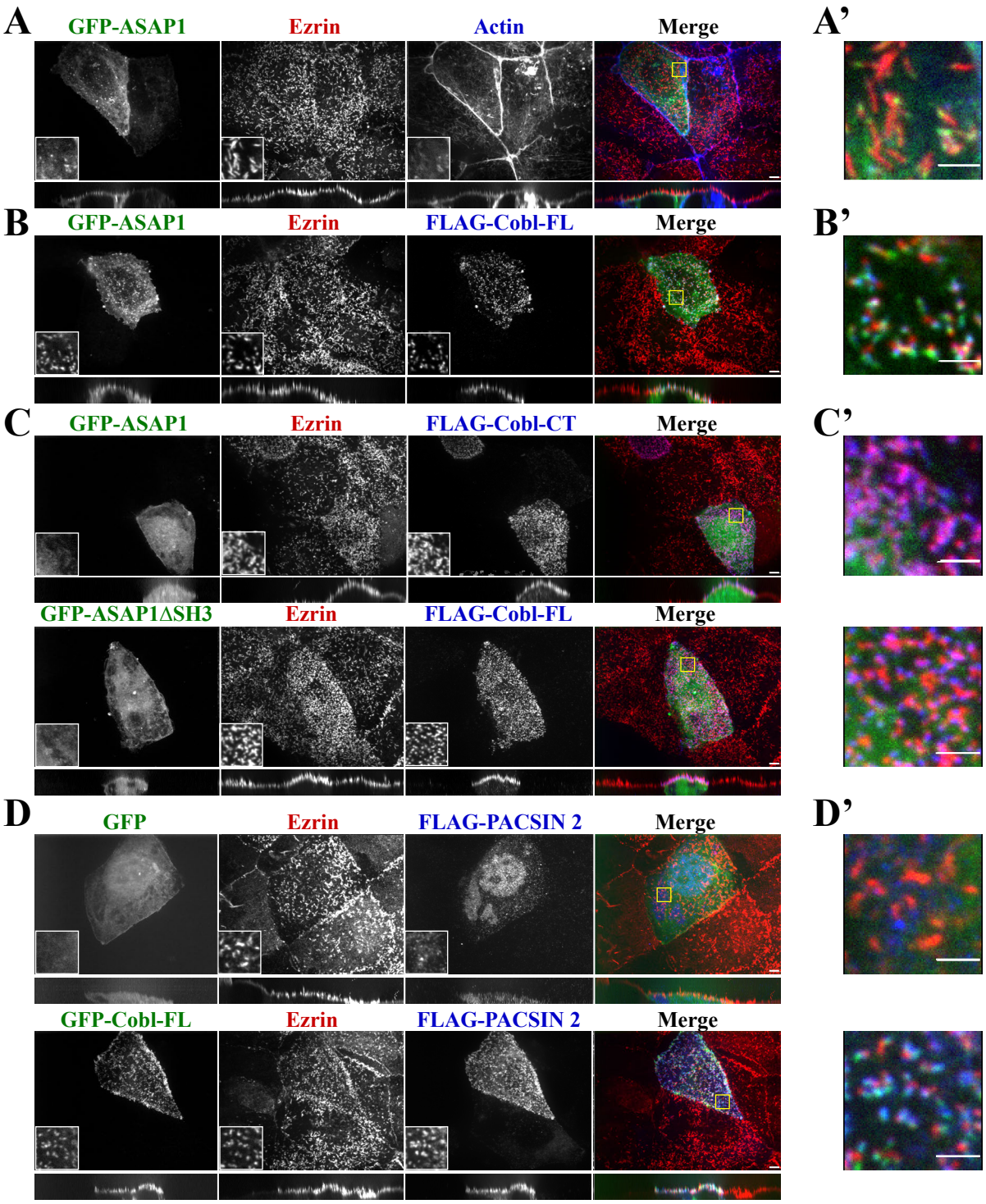
A
GFP-ASAP1
Ezrin
Actin
Merge
A'
B
GFP-ASAP1
Ezrin
FLAG-Cobl-FL
Merge
B'
C
GFP-ASAP1
Ezrin
FLAG-Cobl-CT
Merge
C'
GFP-ASAP1ΔSH3
Ezrin
FLAG-Cobl-FL
Merge
D
GFP
Ezrin
FLAG-PACSIN 2
Merge
D'
GFP-Cobl-FL
Ezrin
FLAG-PACSIN 2
Merge
E
Length(μm)
2.5
2.0
1.5
1.0
0.5
0.0
***
ns
Untransfected
GFP-Cobl-FL
GFP-ASAP1 + Flag-Cobl-FL

Figure 3.9. Cordon Bleu recruits ASAP1 and PACSIN 2 to microvilli. (A-D) Maximum projections (XY) of confocal Z stacks and side views (XZ) stretched 2-fold of JEG-3 cells. Cells expressing the indicated constructs were fixed and stained for endogenous ezrin (red) and FLAG or F-actin (blue) as indicated. Yellow boxes identify magnified single channel insets and are merged in (A'-D'). Scale bars: 5µm (A-D) and 2µm (A'-D'). (E) Length of microvilli of untransfected JEG-3 cells or transfected to express GFP-Cobl-FL, or GFP-ASAP1 and FLAG-Cobl-FL. The box represents the 25th and 75th percentiles around the median and the whiskers represent the maximum and minimum. ***, $p<.0001$

domain of ASAP1 and the COBL domain as GFP-ASAP1ΔSH3, which is normally cytoplasmic (Figure 3.10A), is not recruited with FLAG-Cobl-FL (Fig 3.9C, bottom). GFP-ASAP1 is also not recruited to microvilli with FLAG-Cobl-CT (Fig 3.9C, top) or FLAG-Cobl-COBL (Figure 3.10B). This implies that Cobl recruits ASAP1 to the basal region of microvilli. Recruitment of ASAP1 does not further effect the length of microvilli, as the median length of microvilli is the same as the length of microvilli of cells expressing Cobl alone (Fig 3.9E).

Interestingly, a similar effect is seen when FLAG-PACSIN 2 is expressed. Upon expression of FLAG-PACSIN2 alone, there is some enrichment to the apical domain but not specifically in microvilli (Figure 3.9D,D', top). Co-expression with GFP-Cobl-FL reveals significant enrichment of FLAG-PACSIN 2 in microvilli (Fig 3.9D,D', bottom), an effect not seen with co-expression of GFP-Cobl-LD (Figure 3.10C). This suggests that Cobl influences multiple proteins localization at the basal region of microvilli.

Discussion

Many studies have been dedicated to microvilli dynamics (Garbett and Bretscher, 2012; Garbett *et al.*, 2013; Yang *et al.*, 2013) and regulation (Hanono *et al.*, 2006; Zwaenepoel *et al.*, 2012), most of which focus on proteins that localize and function along the entire length of microvilli. There are few examples of proteins that localize more locally to the basal region (Hanono *et al.*, 2006; Hokanson and Bretscher, 2012; Garbett *et al.*, 2013) and even less is understood about the functional consequences of this specific localization. In this study I have demonstrated that the actin nucleator Cordon Bleu localizes to the basal region of microvilli in JEG-3 cells, but not to filament ends that extend deeper into the cytoplasm (Figure 3.1A"). This localization is not exclusive to JEG-3 cells as expressed Cobl also localizes to microvilli in Hela,

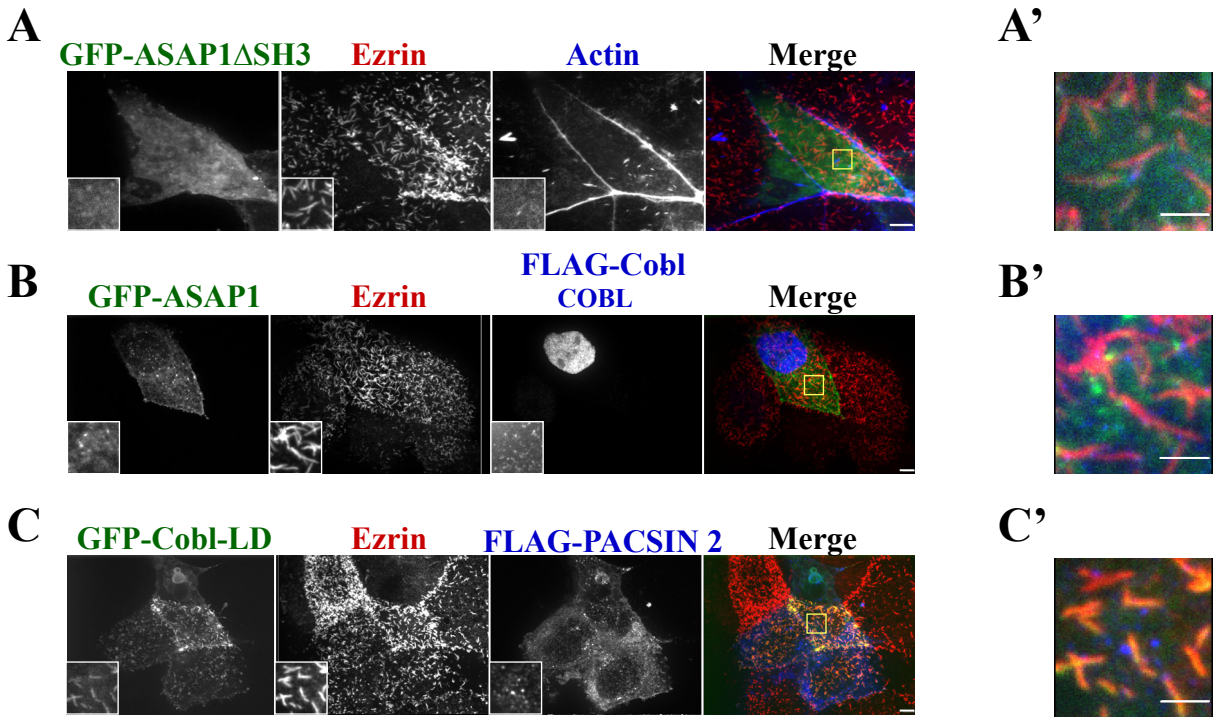

Figure 3.10 T**he COBL domain of Cobl and the SH3 domain of ASAP1 and PACSIN2 are required for their recruitment to microvilli .** (A-C) Maximum projections (XY) of confocal Z stacks of JEG-3 cells. Cells were fixed and stained for endogenous ezrin (red) and FLAG or F-actin (Blue) as indicated. Yellow boxes indentify magnified area in single channel insets. (A)Localization of GFP-ASAP1 and FLAG-Cobl-COBL in JEG-3 cells. (B) Localization of GFP-ASAP1ΔSH3 in JEG-3 cells (C). Localization of GFP-Cobl -LD and FLAG-PACSIN2. (A'-C') Detailed images of three channel merge highlighted by the yellow boxes in A-C. Scale bars: 5µm (A-C) and 2µm (A'-C').

LLCPK1 and Caco-2 cell lines (Figure 3.11A, B, D respectively) all of which are derived from different tissues. Interestingly, expression of Cobl in HEK293T cells, which normally do not have microvilli, results in localization to actin and ezrin positive structures on the apical domain (Figure 3.11C).

I quantitatively demonstrate that Cobl is localized to the basal region of microvilli by comparing the normalized fluorescence intensity of endogenous ezrin to expressed GFP-Cobl-FL along the length of a microvillus. The peak fluorescence intensity for GFP-Cobl-FL is shifted more towards the basal region than ezrin (Figure 3.1B). This shift in peak fluorescence intensity is more dramatically seen in cells expressing GFP-Cobl-WH2(1-3)A, as this construct does not shorten the overall length of microvilli but still has the ability to localize (Figure 3.2F). This localization brings into question whether Cobl acts as an actin nucleator *in vivo*, where one might expect the protein to be localized to the filament minus ends.

I have also identified a novel localization domain (AA 648-899) outside of the canonical COBL domain (Figure 3.2D), which until this point has been thought to be essential for the specific localization of Cobl in other systems (Schwintzer *et al.*, 2011; Haag *et al.*, 2012). I have attempted to determine how this region is so specifically localized by searching for interacting proteins, so far without success. Another possibility is that it might have an affinity for lipids in a highly curved region, as is found at the base of microvilli.

In this study I have also demonstrated that enhancing the concentration of Cobl is able to regulate the length of microvilli and that the WH2 domains are necessary for this function. Since WH2 domains bind actin monomers, they are likely to elevate the local monomeric actin concentration, but it is difficult to envision a simple mechanism that would shorten microvilli. A more likely scenario is that the C-terminal region acts to locally sever actin filaments, as has been

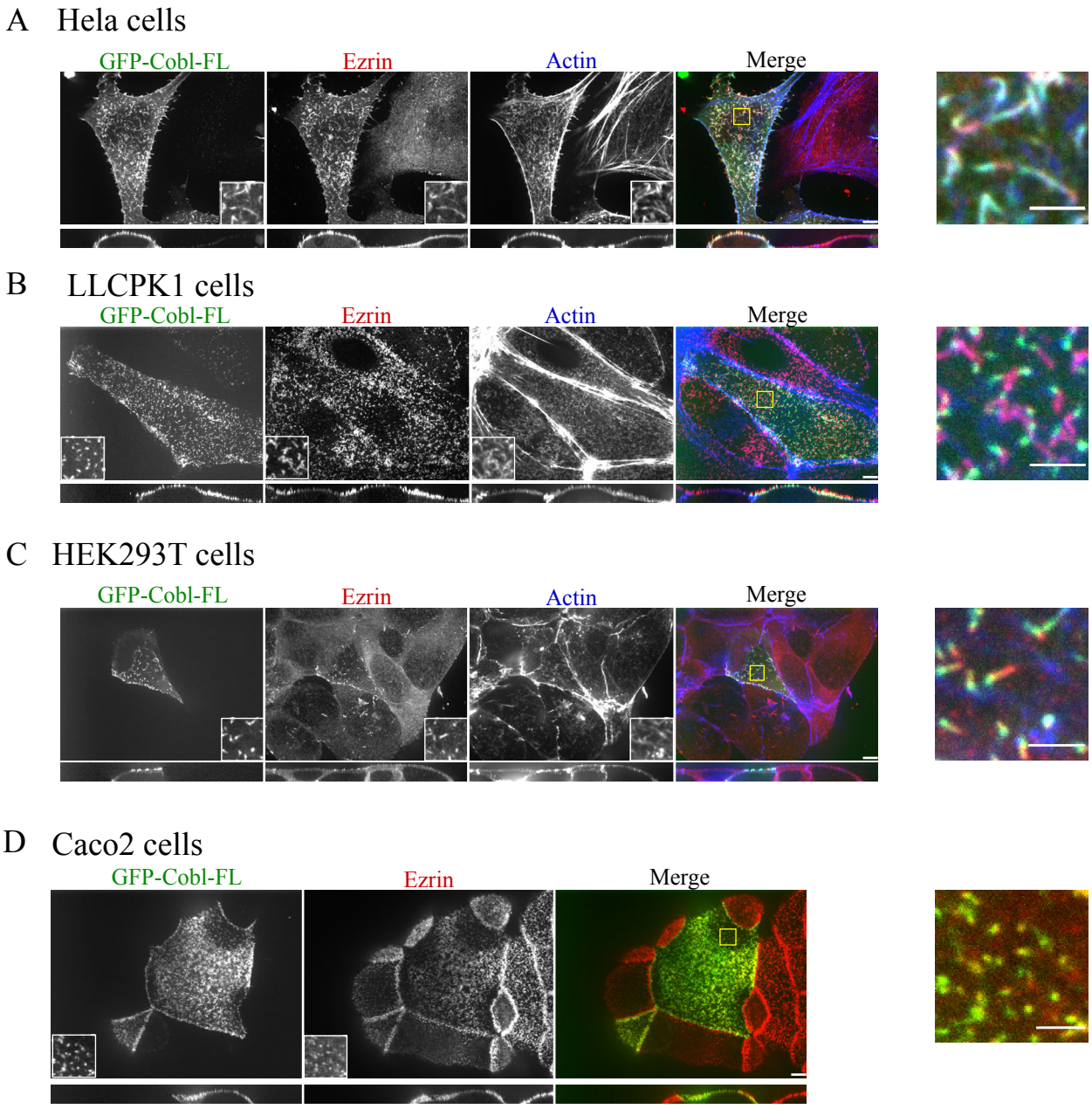

Figure 3.11 Cobl localization in other cell lines. (A-D)Maximum projections (XY) of confocal Z stacks and side views (XZ) stretched 2-fold of Hela (A), LLCKP1 (B), HEK293T (C) or Caco2 (D) cells expressing the indicated constructs, then fixed and GFP (green), endogenous ezrin (red) and F-actin (blue) localized. Yellow boxes represent magnified single channel insets and is shown merged magnified at right. Scale bars: 5µm (B-D) and 2µm in magnified merge.

seen *in vitro* (Jiao *et al.*, 2014), potentially allowing faster filament turnover, rather than a role as an actin filament nucleator. Loss of Cobl has also been shown to have a similar effect on the length of primary cilia in zebrafish (Ravanelli and Klingensmith, 2011), although primary cilia are comprised of microtubules, not actin filaments, so this is most likely an indirect consequence of loss of Cobl function.

Surprisingly knocking down Cobl, either through siRNA transfection or with Cas9/CRISPR genome edited cells, does not have a significant effect on the length of microvilli, at least not as measured by the techniques in this paper. Our microvillar measurements are taken from confocal images with a 0.28μM z-step size, which means that the difference in length between knockdown and control cells would need to be greater than this length before being considered statistically different. I do not see a difference this large (Figure 3.6). Thus reducing Cobl levels may in fact increase the length of microvilli, but I am unable to resolve such a difference at this time. There are other instances, namely in cells from the Plastin-1 or Desmoplakin knockout mice, in which the change in microvilli length was less than 0.2μM (Grimm-Günter *et al.*, 2009; Sumigray and Lechler, 2012). More work will need to be done to determine if this is the case in Cobl knock down cells. These results place Cobl on a growing list of microvilli length regulators including Desmoplakin, Plastin-1, drosophila Cad99c, and Eps8 (D'Alterio *et al.*, 2005; Grimm-Günter *et al.*, 2009; Sumigray and Lechler, 2012; Zwaenepoel *et al.*, 2012), although in no case is the mechanism of regulation known.

Using FRAP, I have demonstrated that Cobl is stably localized to the base of microvilli. Remarkably, I show that the dynamics are not determined by either the COBL domain or the WH2 domains as the dynamics of the Cobl-CT and the Cobl-WH2(1-3)A are not significantly different from full length Cobl (Figure 3.7B). This is surprising, as I had suspected that a possible reason

for the slow turnover of Cobl in microvilli might be due to protein-protein interactions mediated through the COBL domain. This suggests that there is a region outside of COBL and the localization domain that contribute to the stability of Cobl at the basal region of microvilli. Exploring which regions contribute to the dynamics of Cobl and how this influences function will be an interesting topic for future study.

Using SILAC I have identified two novel Cobl interacting partners, ASAP1 and SNX9 (Figure 3.8B). I further illustrated that the interaction between Cobl and ASAP1 occurs between the SH3 domain of ASAP1 and the COBL domain of Cobl (Figure 3.9E). Interestingly, this interaction was also necessary for localization of ASAP1 to microvilli (Figure 3.10A). I also observed a similar effect for the already established Cobl interaction partner PACSIN 2 (Figure 3.10D). These data are not in accord with the current model of Cobl recruitment. It has been suggested that in neurons the COBL domain is necessary for the specific localization of Cobl (Schwintzer *et al.*, 2011; Haag *et al.*, 2012) and that this localization is dependent on an interaction with a binding partner (Schwintzer *et al.*, 2011; Haag *et al.*, 2012). In the case of epithelial cells, the COBL domain is not necessary or sufficient for localization to the basal region of microvilli and localization can occur independent of its ability to interact with its binding partners. Also, a protein related to Cobl, Cobl-like (CoblL1), also harbors COBL domain and this protein does not localize to microvilli in JEG-3 cells (Figure 3.12).

What might be the role of Cobl at the base of microvilli? It is difficult to envision how it could drive actin assembly from that location. Our finding that it serves as a platform for BAR-containing proteins suggests that it might be part of a specific structure associated with membrane curvature. The apical membrane of epithelial cells is known to be under tension, so one possibility is that it might associate with the curved membrane and transmit the tension across the base of the

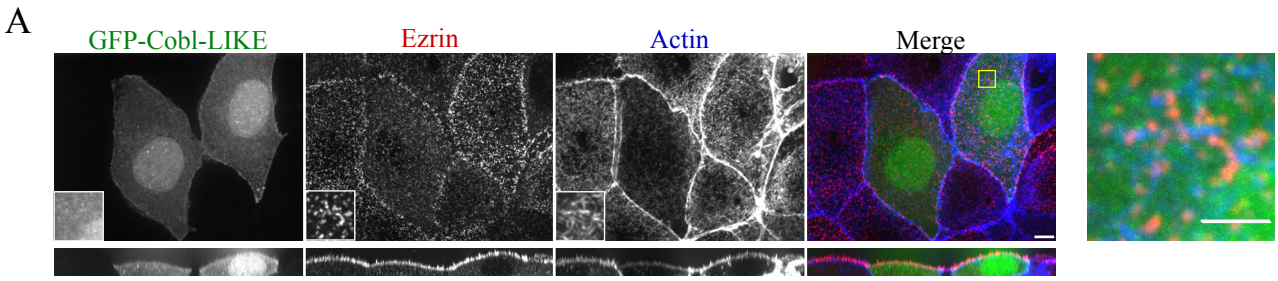

Figure 3.12. Cobl-like does not localize to microvilli in JEG-3 cells. (A) Maximum projections (XY) of confocal Z stacks and side views (XZ) stretched 2-fold of JEG-3 cells expressing the indicated constructs, then fixed and GFP (green), endogenous ezrin (red) and F-actin (blue) localized. Yellow boxes represent magnified single channel insets and is shown merged magnified at right. Scale bars: 5µm (B-D) and 2µm in magnified merge.

microvilli. Alternatively, it might represent nascent sites of endocytosis as suggested by the Cobl-binding proteins. The strong enrichment of Cobl at the basal region of microvilli newly focuses attention on this region of the apical membrane.

References

Ahuja, R., Pinyol, R., Reichenbach, N., Custer, L., Klingensmith, J., Kessels, M. M., and Qualmann, B. (2007). Cordon-bleu is an actin nucleation factor and controls neuronal morphology. Cell *131*, 337–350.

Bretscher, A. (1989). Rapid phosphorylation and reorganization of ezrin and spectrin accompany morphological changes induced in A-431 cells by epidermal growth factor. J. Cell Biol. *108*, 921–930.

Bretscher, A. (1991). Microfilament Structure and Function in the Cortical Cytoskeleton. Annu. Rev. Cell Biol. *7*, 337–374.

Carroll, E. A., Gerrelli, D., Gasca, S., Berg, E., Beier, D. R., Copp, A. J., and Klingensmith, J. (2003). Cordon-bleu is a conserved gene involved in neural tube formation. Dev. Biol. *262*, 16–31.

Chen, X., Ni, F., Tian, X., Kondrashkina, E., Wang, Q., and Ma, J. (2013). Structural basis of actin filament nucleation by tandem W domains. Cell Rep. *3*, 1910–1920.

D'Alterio, C. *et al.* (2005). Drosophila melanogaster Cad99C, the orthologue of human Usher cadherin PCDH15, regulates the length of microvilli. J. Cell Biol. *171*, 549–558.

Fehon, R. G., McClatchey, A. I., and Bretscher, A. (2010). Organizing the cell cortex: the role of ERM proteins. Nat. Rev. Mol. Cell Biol. *11*, 276–287.

Garbett, D., and Bretscher, A. (2012). PDZ interactions regulate rapid turnover of the scaffolding protein EBP50 in microvilli. J. Cell Biol. *198*, 195–203.

Garbett, D., LaLonde, D. P., and Bretscher, A. (2010). The scaffolding protein EBP50 regulates microvillar assembly in a phosphorylation-dependent manner. J. Cell Biol. *191*, 397–413.

Garbett, D., Sauvanet, C., Viswanatha, R., and Bretscher, A. (2013). The tails of apical scaffolding proteins EBP50 and E3KARP regulate their localization and dynamics. Mol. Biol. Cell *24*, 3381–3392.

Gasca, S., Hill, D. P., Klingensmith, J., and Rossant, J. (1995). Characterization of a gene trap insertion into a novel gene, cordon-bleu, expressed in axial structures of the gastrulating mouse embryo. Dev. Genet. *17*, 141–154.

Gorelik, J. *et al.* (2003). Dynamic assembly of surface structures in living cells. Proc. Natl. Acad. Sci. U. S. A. *100*, 5819–5822.

Grimm-Günter, E.-M. S., Revenu, C., Ramos, S., Hurbain, I., Smyth, N., Ferrary, E., Louvard, D., Robine, S., and Rivero, F. (2009). Plastin 1 binds to keratin and is required for terminal web assembly in the intestinal epithelium. Mol. Biol. Cell *20*, 2549–2562.

Haag, N., Schwintzer, L., Ahuja, R., Koch, N., Grimm, J., Heuer, H., Qualmann, B., and Kessels, M. M. (2012). The Actin Nucleator Cobl Is Crucial for Purkinje Cell Development and Works in Close Conjunction with the F-Actin Binding Protein Abp1. J. Neurosci. *32*, 17842–17856.

Hanono, A., Garbett, D., Reczek, D., Chambers, D. N., and Bretscher, A. (2006). EPI64 regulates microvillar subdomains and structure. J. Cell Biol. *175*, 803–813.

Heintzelman, M. B., and Mooseker, M. S. (1990). Assembly of the brush border cytoskeleton: changes in the distribution of microvillar core proteins during enterocyte differentiation in adult chicken intestine. Cell Motil. Cytoskeleton *15*, 12–22.

Hokanson, D. E., and Bretscher, A. P. (2012). EPI64 interacts with Slp1/JFC1 to coordinate Rab8a and Arf6 membrane trafficking. Mol. Biol. Cell *23*, 701–715.

Husson, C., Renault, L., Didry, D., Pantaloni, D., and Carlier, M.-F. (2011). Cordon-Bleu uses WH2 domains as multifunctional dynamizers of actin filament assembly. Mol. Cell *43*, 464–477.

Jiao, Y., Walker, M., Trinick, J., Pernier, J., Montaville, P., and Carlier, M.-F. (2014). Mutagenetic and electron microscopy analysis of actin filament severing by Cordon-Bleu, a WH2 domain protein. Cytoskeleton (Hoboken). *71*, 170–183.

Kelly, A. E., Kranitz, H., Dötsch, V., and Mullins, R. D. (2006). Actin binding to the central domain of WASP/Scar proteins plays a critical role in the activation of the Arp2/3 complex. J. Biol. Chem. *281*, 10589–10597.

McConnell, R. E., Benesh, A. E., Mao, S., Tabb, D. L., and Tyska, M. J. (2011). Proteomic analysis of the enterocyte brush border. Am. J. Physiol. Gastrointest. Liver Physiol. *300*, G914–26.

Mooren, O. L., Galletta, B. J., and Cooper, J. A. (2012). Roles for actin assembly in endocytosis. Annu. Rev. Biochem. *81*, 661–686.

Qualmann, B., and Kessels, M. M. (2009). New players in actin polymerization--WH2-domain-containing actin nucleators. Trends Cell Biol. *19*, 276–285.

Ravanelli, A. M., and Klingensmith, J. (2011). The actin nucleator Cordon-bleu is required for development of motile cilia in zebrafish. Dev. Biol. *350*, 101–111.

Reczek, D., and Bretscher, A. (1998). The Carboxyl-terminal Region of EBP50 Binds to a Site in the Amino-terminal Domain of Ezrin That Is Masked in the Dormant Molecule. J. Biol. Chem. *273*, 18452–18458.

Revenu, C. *et al.* (2012). A new role for the architecture of microvillar actin bundles in apical retention of membrane proteins. Mol. Biol. Cell *23*, 324–336.

Saotome, I., Curto, M., and McClatchey, A. I. (2004). Ezrin is essential for epithelial organization and villus morphogenesis in the developing intestine. Dev. Cell *6*, 855–864.

Schüler, S., Hauptmann, J., Perner, B., Kessels, M. M., Englert, C., and Qualmann, B. (2013). Ciliated sensory hair cell formation and function require the F-BAR protein syndapin I and the WH2 domain-based actin nucleator Cobl. J. Cell Sci. *126*, 196–208.

Schwintzer, L., Koch, N., Ahuja, R., Grimm, J., Kessels, M. M., and Qualmann, B. (2011). The functions of the actin nucleator Cobl in cellular morphogenesis critically depend on syndapin I. EMBO J. *30*, 3147–3159.

Shalem, O. *et al.* (2014). Genome-scale CRISPR-Cas9 knockout screening in human cells. Science *343*, 84–87.

Smolka, M. B., Albuquerque, C. P., Chen, S., and Zhou, H. (2007). Proteome-wide identification of in vivo targets of DNA damage checkpoint kinases. Proc. Natl. Acad. Sci. U. S. A. *104*, 10364–10369.

Sumigray, K. D., and Lechler, T. (2012). Desmoplakin controls microvilli length but not cell adhesion or keratin organization in the intestinal epithelium. Mol. Biol. Cell *23*, 792–799.

Tilney, L. G., and Mooseker, M. (1971). Actin in the brush-border of epithelial cells of the chicken intestine. Proc. Natl. Acad. Sci. U. S. A. *68*, 2611–2615.

Viswanatha, R., Ohouo, P. Y., Smolka, M. B., and Bretscher, A. (2012). Local phosphocycling mediated by LOK/SLK restricts ezrin function to the apical aspect of epithelial cells. J. Cell Biol. *199*, 969–984.

Yang, J. *et al.* (2013). NHERF2 protein mobility rate is determined by a unique C-terminal domain that is also necessary for its regulation of NHE3 protein in OK cells. J. Biol. Chem. *288*, 16960–16974.

Zuchero, J. B., Belin, B., and Mullins, R. D. (2012). Actin binding to WH2 domains regulates nuclear import of the multifunctional actin regulator JMY. Mol. Biol. Cell *23*, 853–863.

Zwaenepoel, I., Naba, A., Da Cunha, M. M. L., Del Maestro, L., Formstecher, E., Louvard, D., and Arpin, M. (2012). Ezrin regulates microvillus morphogenesis by promoting distinct activities of Eps8 proteins. Mol. Biol. Cell *23*, 1080–1094.

Chapter 4

Summary and Future Directions

Summary

As mentioned in Chapter 1, a lot is known about how the actin filament core of microvilli is bundled and tethered to the plasma membrane. What is unclear, however, is how the actin core of microvilli is nucleated and assembled. The formin family of actin nucleators are likely candidates for this function based on their involvement in nucleating the assembly of the unbranched actin filament core of structures similar to microvilli. To address if formins are involved in nucleating the assembly of the actin core of microvilli in JEG-3 cells, I performed a quantitative real time (qPCR) screen to determine which formins are most highly expressed in JEG-3 cells. I then localized the top formin candidates and found that both constitutively active and autoregulated formins do not localize to microvilli. I also determined that loss of formin protein following siRNA treatment did not result in a loss of microvilli phenotype. Finally, loss of profilin, a protein essential for formin mediated actin filament assembly, also has no effect on microvilli formation.

Because I could not determine a role for formins in microvilli formation in JEG-3 cells, I looked at other potential unbranched actin nucleators. I demonstrate that the actin nucleator Cordon Bleu (Cobl) localizes specifically to the base of microvilli via a novel localization domain outside of the canonical COBL domain or WH2 domains. Proteomic studies of this localization domain reveal novel Cobl binding partners, including AnnexinA2 and PP55alpha. I determine that Cobl has a slow turnover rate in microvilli and that the dynamics only increase upon expression of the localization domain alone. Ectopic expression of Cobl shortens apical microvilli, and this

requires functional WH2 domains. Proteomic studies reveal that the COBL domain binds several BAR-containing proteins, including SNX9, PACSIN-2/Syndapin-2 and ASAP1. ASAP1 is recruited to the base of microvilli by binding the COBL domain through its SH3, a finding that is also seen for PACSIN-2.

Future Directions

Formin mediated microvillar assembly

As discussed in Chapter 2, while I did not find a role for the formins I studied in the formation of the actin core of microvilli, this does not exclude the possibility that a formin is involved in the formation or regulation of microvilli. There are 15 human formins and exhaustive studies on each individual formin is not feasible. However, the same proteomic screens that identified Cordon Bleu also identified the formin Dia1 as the only other actin nucleator detected in the murine brush border (McConnell *et al.*, 2011; Revenu *et al.*, 2012). Dia1 interacts with the adaptor protein IRSp53 (Lim *et al.*, 2008) and is required for IRSp53 dependent filopodia formation in neurons (Goh *et al.*, 2012). An isoform of IRSp53 binds to the microvillar protein EBP50 and localizes to microvilli in JEG-3 cells (Garbett *et al.*, 2013). In light if this information, Dia1 may be an excellent candidate to study further. It will be interesting to see if both endogenous and epitope tagged expressed Dia1 localizes to microvilli. One potential problem with localization studies is that Dia1 may only be necessary for the initial formation of the actin core of microvilli but then may get competed off the barbed end of actin filaments by the major microvillar barbed end actin capping protein Eps8 for the duration of the treadmilling portion of the microvillus lifetime. To avoid this potential problem one could localize Dia1 in a Cas9/CRISPR Eps8 genome

edited knockout cell. Loss of the major microvilli capping protein would free up the barbed ends of the actin filaments, such that Dia1 could remain processive at the tips of microvilli.

I determined that knocking down Dia1 alone with siRNA did not cause a loss of microvilli in JEG-3 cells but I did notice that microvilli appeared shorter (unquantified) in Dia1 knockdown versus wild type cells. Measuring the length of microvilli, using the same technique I used for measuring microvilli in cells expressing GFP-Cobl, in Dia1 knockdown cells could implicate a formin in the regulation of microvilli. If one could localize Dia1 and then establish a potential phenotype (like shortening of microvilli) then other assays like SILAC-mass spectrometry could be done to determine potential binding partners for Dia1. This could contribute to our understanding of how the actin filament core of microvilli is nucleated and assembled.

Cordon Bleu

A hypothetical model has been created to illustrate the activity of Cobl at the base of microvilli (Figure 4.1). An intriguing result from Chapter 3 was that the COBL domain of Cordon Bleu (Cobl) binds to and recruits F-BAR proteins to the base of microvilli, specifically ASAP1 and PACSIN-2. What is unclear, however, is whether Cobl forms a ternary complex with both ASAP1 and PACSIN-2 or if there is competitive binding that occurs between proteins. One could address this question by first determining if PACSIN-2 and ASAP1 have a direct interaction and if not then one can ask if PACSIN-2 is also pulled down in an immunoprecipitation using expressed Cobl and ASAP1 and vice versa. If it is indeed a complex, asking if loss of Cobl disrupts this interaction would be important in establishing a potential role for Cobl as a scaffolding protein at the base of microvilli. If ASAP1 and PACSIN-2 are not in a complex with Cobl but are competing

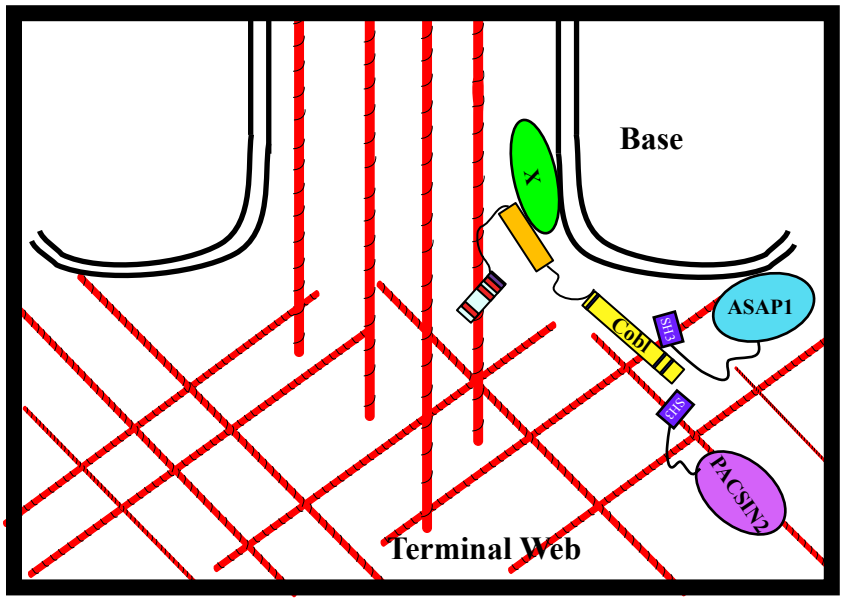

Figure 4.1 Hypothetical model of Cobl localization at the base of microvilli
Cartoon schematic of a hypothesized model for the localization of Cobl to the base of microvilli. The localization of Cobl is mediated through an interaction between the localization domain of Cobl (AA 648-899) and an unknown protein X. The lysine rich region and the WH2 domains of Cobl are then able to interact with the F-actin core of microvilli to regulate the length. The COBL domain of Cobl recruits SH3 domain containing BAR proteins like the Arf-GAP ASAP1 and PACSIN-2, which can presumably bind to and possibly regulate the high membrane curvature at the base of microvilli.

to bind to Cobl, then this could suggest that Cobl is a spatio-temporal recruitment factor for F-BAR proteins to the base of microvilli.

Another obvious question is of course what function does the recruitment of F-BAR proteins have at the base of microvilli? One possibility could be that these F-BAR proteins mediate the tension that is generated at the curved membrane at the base of microvilli. It would be interesting to determine by electron microscopy if microvilli morphology changes in CRISPR/Cas9 genome edited Cobl knockout cells, which should presumably also result in less F-BAR recruitment to the base. This might result in less curvature at the base of microvilli. It would also be interesting to see if Cobl contributes to apical membrane tension and if this tension changes upon loss of Cobl.

ASAP1, PACSIN-2 and Snx9 have all been implicated in clathrin mediated endocytosis. Could Cobl have a role in recruiting F-BAR proteins to nascent sites of endocytosis? I have optimized an assay using flow cytometry to measure EGF receptor uptake in JEG-3 cells over-expressing GFP-Cobl versus GFP alone. GFP-Cobl does not stably express and is hard to express in JEG-3 cells, so it is difficult to produce consistent results. In the CRISPR/Cas9 Cobl knockout cell line one could measure the difference in receptor uptake in cells with and without endogenous Cobl. Not having to preferentially measure EGF receptor uptake in cells that are expressing either GFP or GFP-Cobl would simplify measurements and analysis, which would in turn aid in getting more consistent results.

Proteomic studies using the Cobl localization domain (AA 648-899, Table B.1 and Table B.2) has opened the door for discovering many new potential Cobl interacting partners. I have established that Cobl can bind to AnnexinA2, a protein that has already been localized to microvilli by others (Danielsen *et al.*, 2003) and which is a component of lipid rafts/domains that exist

between brush border microvilli (Danielsen, 2003). Does AnnexinA2 influence Cobl localization or does Cobl recruit AnnexinA2? Localization studies will need to be done to better understand this interaction. AnnexinA2 is recruited to the apical membrane in a calcium dependent manner and often requires binding to S100A10 (Lewit-Bentley *et al.*, 2000; Gerke and Moss, 2002). This might make functional studies more complicated by needing to co-express S100A10 along with AnnexinA2, but potentially very interesting. Exploring other proteins that were identified by proteomics could also broadly enhance our understanding of what the function of Cobl is at the base of microvilli. Understanding a role for Cobl at this specific region of microvilli would significantly contribute to our understanding of microvilli as a whole.

References

Danielsen, E. (2003). Lipid rafts in epithelial brush borders: atypical membrane microdomains with specialized functions. Biochim. Biophys. Acta - Biomembr. *1617*, 1–9.

Danielsen, E. M., van Deurs, B., and Hansen, G. H. (2003). "Nonclassical" secretion of annexin A2 to the lumenal side of the enterocyte brush border membrane. Biochemistry *42*, 14670–14676.

Garbett, D., Sauvanet, C., Viswanatha, R., and Bretscher, A. (2013). The tails of apical scaffolding proteins EBP50 and E3KARP regulate their localization and dynamics. Mol. Biol. Cell *24*, 3381–3392.

Gerke, V., and Moss, S. E. (2002). Annexins: from structure to function. Physiol. Rev. *82*, 331–371.

Goh, W. I., Lim, K. B., Sudhaharan, T., Sem, K. P., Bu, W., Chou, A. M., and Ahmed, S. (2012). mDia1 and WAVE2 proteins interact directly with IRSp53 in filopodia and are involved in filopodium formation. J. Biol. Chem. *287*, 4702–4714.

Lewit-Bentley, A., Réty, S., Sopkova-de Oliveira Santos, J., and Gerke, V. (2000). S100-annexin complexes: some insights from structural studies. Cell Biol. Int. *24*, 799–802.

Lim, K. B., Bu, W., Goh, W. I., Koh, E., Ong, S. H., Pawson, T., Sudhaharan, T., and Ahmed, S. (2008). The Cdc42 effector IRSp53 generates filopodia by coupling membrane protrusion with actin dynamics. J. Biol. Chem. *283*, 20454–20472.

McConnell, R. E., Benesh, A. E., Mao, S., Tabb, D. L., and Tyska, M. J. (2011). Proteomic analysis of the enterocyte brush border. Am. J. Physiol. Gastrointest. Liver Physiol. *300*, G914–26.

Revenu, C. *et al.* (2012). A new role for the architecture of microvillar actin bundles in apical retention of membrane proteins. Mol. Biol. Cell *23*, 324–336.

Appendix A[1]

Characterizing the Interaction Between the Microvillar Protein Ezrin and the Actin Nucleator FHOD1

Overview and Introduction

This appendix contains experiments based on work and results from Raghuvir Viswanatha that identified FHOD1 as an interactor of a more closed conformation of ezrin by SILAC coupled with mass spectrometry (Viswanatha *et al.*, 2013). Here, I confirm the mass spectrometry results by demonstrating by both endogenous IP and Flag Immunoprecipitations that ezrin and FHOD1 interact. I also examine whether conformation of either protein effects this interaction in cells. I then map this interaction to specific regions of both ezrin and FHOD1 using truncation series for both proteins. Finally, I look at the localization of FHOD1 truncations in JEG-3 cells. The potential, unresolved consequences of this interaction are an interesting topic for future study.

As discussed in Chapter 1, the microvillar protein ezrin contains a FERM (4.1 Ezrin, Radixin Moesin domain) at the N-terminal region of the protein that is connected to the C-ERMAD through an alpha-helical region (Figure A.1A). This flexible alpha helical region allows the FERM domain to interact with the C-ERMAD which results in a closed, inactive conformation of ezrin (Gary and Bretscher, 1995). Upon phosphorylation at threonine 567 (T567) the interaction between the FERM domain and the C-ERMAD is disrupted, which results in an open, active conformation of ezrin. In JEG-3 cells, ezrin undergoes rapid phosphocycling and approximately

[1] Parts of this Appendix have been published in Viswanatha *et al*. 2013.

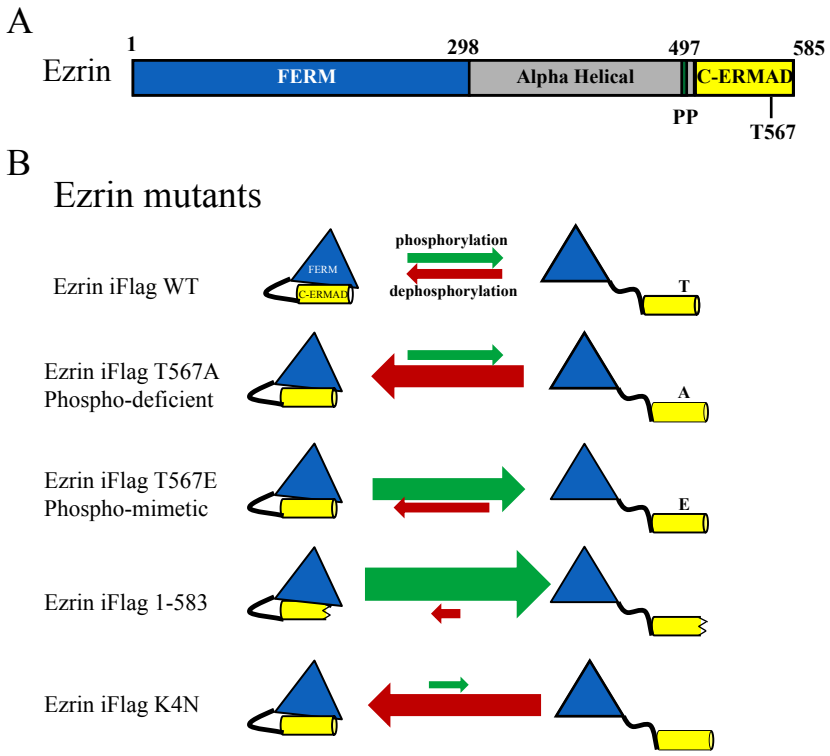

Figure A.1 Ezrin domain schematic (A) At the N-terminus of ezrin is the FERM domain, which is connected by an alpha helical domain to the C-ERMAD. Within the C-ERMAD is residue threonine 567 (T567), the phosphorylation of which plays a major role in the activation of ezrin. (B) The different ezrin mutants used in this appendix to address how protein conformation affects protein-protein interactions. In the closed, inactive state the FERM domain of ezrin binds to the C-ERMAD to block binding of F-actin by the C-ERMAD. Phosphorylation (green arrow) at T567 distrupts the interaction between the FERM and C-ERMAD which results in an open, active conformation. Cycling between phosphorylation and dephosphorylation (red arrow) makes the conformational changes of ezrin highly dynamic. In JEG-3 cells, about half of ezrin molecules are phosphorylated at a given time, which means there are roughly equal pools of open and closed ezrin. The phospho-deficient (T567A) mutant exists in a more closed conformation while the phospho-mimetic (T567E) prefers the more open conformation. The hyperactive (1-583) mutant exists almost exclusively in the open, active conformation. The ezrin K4N mutant, which has mutations that block PI(4,5)P_2 binding, exists in a mostly closed conformation.

half of the ezrin population is in the phosphorylated state at a given time (Viswanatha *et al.*, 2012). Use of ezrin phospho-mutants is a critical tool in exploring how the conformational state of ezrin effects different protein-protein interactions. The phospho-deficient ezrin mutant (T567A) exists preferentially in a closed, inactive conformation while the phospho-mimetic mutant (T567E) exists preferentially in an open, active conformation. An ezrin mutant in which the last two amino acids are removed (Ezrin 1-583) results in a hyperactive ezrin mutant that unmasks the FERM domain and exists in a mostly open conformational state (Figure A.1B). Raghuvir Viswanatha performed Stable Isotope Labeling of Amino Acids in Cell Culture (SILAC) coupled to mass spectrometry experiments using these mutants to identify novel ezrin interaction with preferences for different conformational states (Viswanatha *et al.*, 2013). FHOD1 was identified as an interacting protein that preferred the more closed conformation of ezrin. Because formins were a potential candidate for the actin nucleator involved in nucleating the assembly of the actin core of microvilli, I chose to characterize this interaction further.

Materials and Methods

Antibodies and reagents

The mouse FLAG antibody and resin were from Sigma-Aldrich (St. Louis, MO), mouse GFP antibody was from Santa Cruz Biotechnology (Santa Cruz, CA) and the mouse FHOD1 antibody was from Abcam (Canbridge, UK). The rabbit antisera and affinity-purified antibodies against full-length human ezrin have been described (Bretscher, 1989).The rabbit antisera and affinity purified antibodies against human EBP50 have been described (Reczek *et al.*, 1997) . Goat anti-mouse and Donkey anti-Rabbit secondary antibodies conjugated to horseradish peroxidase were from Jackson ImmunoResearch Laboratories (West Grove, PA). Alexa Fluor 568 donkey anti-rabbit antibodies and Alexa Fluor 660–conjugated phalloidin were from Invitrogen (Carlsbad, CA). IRDye 680– and 800–conjugated secondary antibodies were from LI-COR Biosciences (Lincoln, NE).

DNA constructs

GFP-FHOD1 was created using FHOD1 cDNA purchased from ATCC and cloned into pEGFP-C2. FHOD1 truncations were cloned into pEGFP-C2 as GFP-FHOD1-1-339, GFP-FHOD1 1-569. GFP-FHOD1 569-1164 and GFP-FHOD1ΔDAD (AA 1-1053). The V228E mutation was introduced by site-directed mutagenesis of GFP-FHOD1 WT using the QuikChange II XL kit (Agilent, Santa Clara, CA) to mutate Valine 228 to Aspartic Acid (V228E). Plasmids for stable or transient transfection of ezrin-iFLAG and variants (in pQCXIP, Clontech) have been previously described (Viswanatha *et al.*, 2012). The "K4N" mutation (Barret *et al.*, 2000) was generated by inverse PCR and inserted into PQCXIP. GFP-EBP50 has been described previously (Garbett *et al.*, 2010).

Cell Culture and Transfection

JEG-3 and HEK293T cells (American Type Culture Collection, Manassas, VA) were maintained in a 5% CO2 humidified atmosphere at 37°C. JEG-3 cells were cultured in MEM (Thermo Fisher Scientific) with 10% fetal bovine serum (FBS), and HEK293T in DMEM with 5% FBS. JEG-3 cells were transfected with polyethylenimine (Polysciences, Warrington, PA) and 1–2 μg of plasmid DNA, as described (Hanono *et al.*, 2006). HEK293T cells were transfected with Lipofectamine 2000 (Invitrogen) according to the manufacturer's instructions. For generation of stable JEG-3 cells expressing Ezrin iFlag contructs see (Viswanatha *et al.*, 2012). Stable JEG-3 cells were maintained with 2 μg/ml puromycin (Sigma-Aldrich).

Dithiobis(succinimidyl Propionate) (DSP) Cross-linking

Where DSP crosslinking is indicated, cells were grown to ~80% confluence, then washed three times with PBS and treated with 1.25 mM DSP (Thermo) at 37 °C for 2 min. The cells were then washed three times at room temperature with TBS. They were incubated in the last TBS wash for 15–20 min prior to immunoprecipation

Immunoprecipitations and western blotting

Either JEG-3 cells stably expressing ezrin iFlag mutants, stables co-expressing GFP-FHOD1 contructs or HEK293T cells co-expressing the constructs indicated were lysed in lysis buffer (25 mM Tris, pH 7.4, 5% glycerol, 150 mM NaCl, 50 mM NaF, 0.1 mM Na3VO4, 10 mM β-glycerol phosphate, 8.7 mg/ml paranitrophenylphosphate, 0.3% Triton X-100, and protease inhibitor tablet [Roche, Indianapolis, IN]) and immunoprecipitated with M2 FLAG resin (Sigma-Aldrich) for 2 h.

Immunoprecipitates were then washed four times in wash buffer (lysis buffer but with 0.2% Triton X-100 and no protease inhibitor tablet) and eluted from the FLAG resin with 200 μg/ml 3xFLAG peptide for 15 min at room temperature. Eluates were than denatured with Laemmli buffer, resolved by SDS-PAGE, transferred to Immobilon-FL (EMD Millipore, Billerica, MA), blotted with specific antibody, and visualized by enhanced chemiluminescence.

Endogenous immunprepitations were performed as described above but antibody against endogenous FHOD1 or control antibody was pre-incubated with Protein A/G beads (Sigma) before whole cell lysate was added.

GST-Pulldowns

Bacterical pellets induced to express GST-Ezrin 1-368 (FERM) or ezrin 474-586 were lysed in 150mM NaCl, 20mM Tris pH 7.4, 0.1% BME, 0.1% Triton X-100 with complete protease inhibitor by sonication, centrifuged and added to hydrated glutathione agarose (Sigma), washed, and left as a 50% slurry for binding assays. JEG-3 cells expressing either GFP-FHOD1 or GFP-EBP50 were lysed in lysis buffer: 25 mM Tris, pH 7.4, 5% glycerol, 150 mM NaCl, 50 mM NaF, 0.1 mM Na_3VO_4, 10 mM β-glycerol phosphate, 8.7 mg/ml paranitrophenylphosphate, 0.3% Triton X-100, and protease inhibitor tablet. Pulldowns were nutated at 4˚C and washed four times with wash buffer, eluates were than denatured with Laemmli buffer, resolved by SDS-PAGE, transferred to Immobilon-FL (EMD Millipore, Billerica, MA), blotted with specific antibody, and visualized by enhanced chemiluminescence.

Immunofluorescence

JEG-3 cells were grown on coverslips and fixed in 3.7% formaldehyde at room temperature for 15 min. Coverslips were then washed three times in phosphate-buffered saline (PBS) and

permeabilized with 0.2% Triton X-100 for 5 min at room temperature. Coverslips were then washed three more times with PBS and blocked in filtered 3% FBS in PBS for 10 min. Primary and secondary antibodies were made up in 3% FBS in PBS. Coverslips were washed three times in PBS between addition of primary and secondary antibodies. Alexa Fluor–conjugated phalloidin (Invitrogen) was added to the secondary when F-actin was visualized. Cells were imaged by time-lapse microscopy on a spinning disk (CSU-X; Yokogawa, Tokyo, Japan) with a spherical aberration correction device, a 100×/1.46 numerical aperture (NA) objective (Leica, Wetzlar, Germany) on an inverted microscope (DMI6000B; Leica), and an HQ2 CCD camera (Photo-metrics, Tucson, AZ). Maximum intensity projections were created using SlideBook (Intelligent Imaging Innovations, Denver, CO) and exported in Illustrator (Adobe, San Jose, CA).

Results and Discussion

Immunoprecipitations confirm that FHOD1 interacts with ezrin in JEG-3 cells

To confirm that ezrin and FHOD1 interact *in vivo,* immunoprecipitations of endogenous proteins were performed from JEG-3 cells. Endogenous FHOD1 was immunoprecipitated from JEG-3 cell lysate and the western subsequently blotted for endogenous ezrin (Figure A.2A). Endogenous FHOD1 is able to precipitate endogenous ezrin, which suggests the two proteins indeed interact *in vivo*. To confirm the results of the SILAC analysis, which suggested that FHOD1 preferentially binds to a more closed form of ezrin (ezrin T567A), I preformed Flag immunoprecipitations in JEG-3 cells stably expressing various ezrin-iFlag mutants, then blotted for endogenous FHOD1. I performed the original immunoprecipitations in the presence of DSP crosslinking because that was how the SILAC immunoprecipitations were performed, but found that this was not necessary so omitted crosslinking in later experiments. Immunoprecipitations confirmed that FHOD1 does indeed interact with ezrin, with preference for ezrin iFlagT567A over ezrin iFlagWT or ezrin iFlagT567E (Figure A.2B). Interestingly, endogenous FHOD1 does not interact at all with Ezrin iFlag 1-583, the hyperactive conformation. This is in contrast to what is seen with the well-defined interaction between ezrin and the scaffolding protein EBP50, which prefers an open ezrin conformation (Viswanatha *et al.*, 2012). This is clearly seen here, with EBP50 being precipitated with preference for ezrin iFlag1-583 versus the other ezrin conformation states (Figure A.2B). This suggests that FHOD1 interacts with a preferentially closed conformation of ezrin. Before this study, the only described interacting partner that interacts with closed ezrin is the phosphoinositide $PI(4,5)P_2$, an interaction that is essential to the activation of ezrin (Fievet *et al.*, 2004). Determining a potential function for the preference of FHOD1 to closed ezrin made characterizing the interaction between FHOD1 and ezrin potentially very interesting.

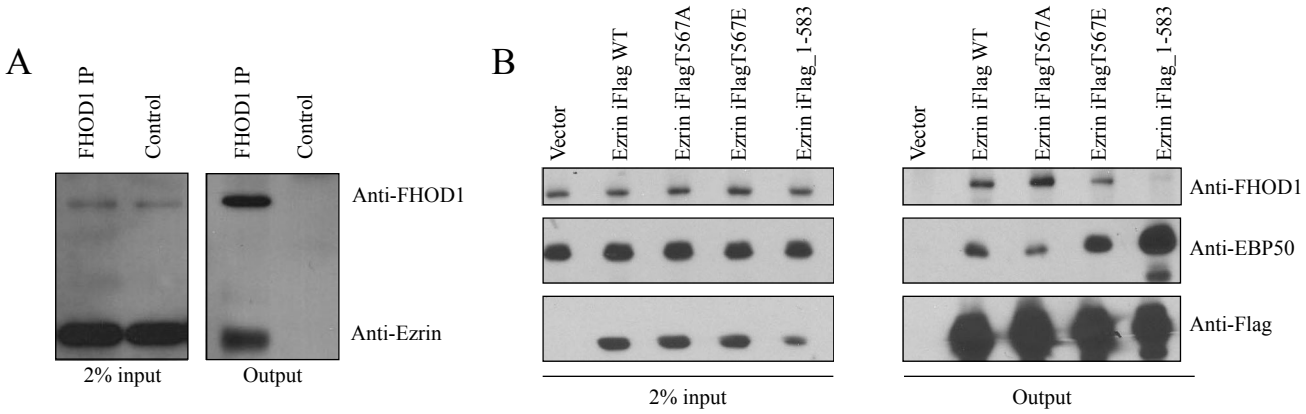

Figure A.2 Immunoprecipitations confirm that FHOD1 interacts with ezrin in JEG-3 cells. (A) Immunoprecipitations utilizing endogenous FHOD1 antibody conjugated to protein A/G beads were performed using JEG-3 whole cell lysate. Subsqequent western blots were probed using antibodies against endogenous ezrin and FHOD1. (B) EzriniFlag (internal Flag) constructs were stably expressed in JEG-3 cells, subjected to Flag immunoprecipitation (IP) and then subsequently blotted for FLAG, endogenous FHOD1 or endogenous EBP50 as a control.

The activation state of FHOD1 affects binding to ezrin

The formin FHOD1 is a diaphanous related formin whose domain architecture is described in detail in the introduction of Chapter 2. Briefly, at the N-terminus is the diaphanous inhibitory domain (DID) which interacts with the diaphanous autoregulatory domain (DAD) at the C-terminus to negatively regulate the protein (Figure A.3A) (Alberts, 2001). This auto-inhibition can be relieved by interaction with a Rho-GTPase with the GTPase binding domain (GBD) at the N-terminal region of the formin which results in an open, active conformation (Figure A.3B) (Kühn and Geyer, 2014). One way to mimic this activation state is to create a FHOD1 mutant in which the DAD domain is removed and FHOD1 can no longer be auto-inhibited (FHOD1ΔDAD, AA 1-1053). To ensure that removing the entire DAD region does not have an effect on ezrin interaction, a full length active FHOD1 mutant was created. Previous work has shown that a single point mutation in the DID domain at Valine 228 to Aspartic Acid (V228E) completely abrogates the interaction between the DID and DAD domain which results in a full length, active FHOD1 (Schulte *et al.*, 2008). Active FHOD1 mutants (Figure A.3C) were utilized to determine if the activation and conformation of FHOD1 affects the interaction with ezrin.

To determine if FHOD1 conformation effects interaction with ezrin, co-immunoprecipitations were performed in which JEG-3 cells stably expressing ezrin iFlag mutants were transfected with either GFP-FHOD1-WT, or the active mutants GFP-FHOD1ΔDAD or GFP-FHOD1V288E. The Flag epitope was immunoprecipitated and then blotted for the GFP-tagged construct. Immunoprecipitations confirm that both GFP-FHOD1ΔDAD and GFP-FHOD1V228E are recovered by both ezrin iFlagT567A and T567E better than GFP-FHOD1-WT (Figure A.3D). However, there is no preferential recovery of active FHOD1 for either T567A or T567E as both are able to precipitate the active FHOD1 mutants with about equal efficiency. I also did not see a

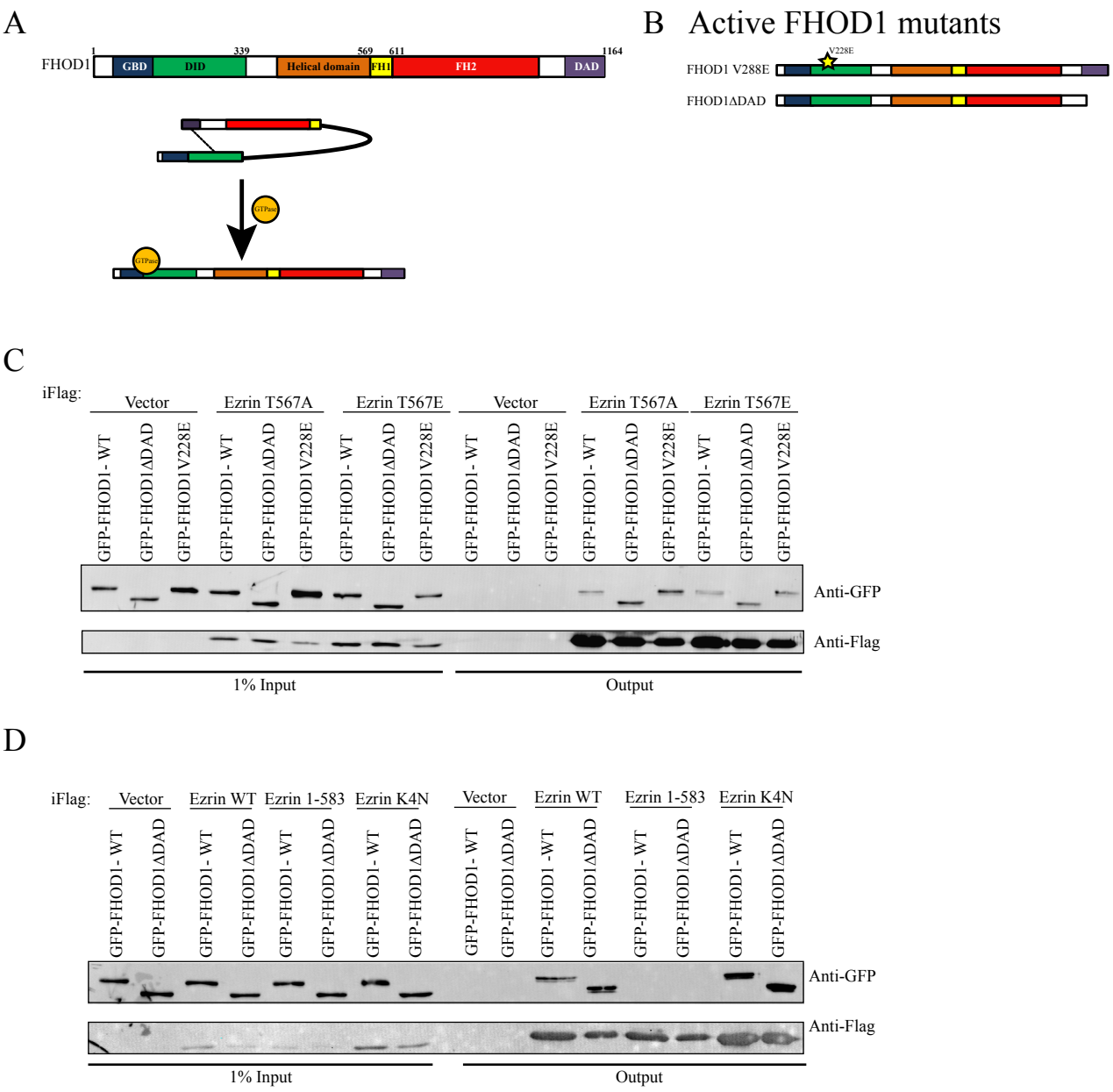
A
FHOD1
1
339
569
611
1164
GBD
DID
Helical domain
FH1
FH2
DAD
GTPase
GTPase
B Active FHOD1 mutants
V228E
FHOD1 V288E
FHOD1ΔDAD
C
iFlag:
Vector
Ezrin T567A
Ezrin T567E
Vector
Ezrin T567A
Ezrin T567E
GFP-FHOD1 - WT
GFP-FHOD1ΔDAD
GFP-FHOD1V228E
Anti-GFP
Anti-Flag
1% Input
Output
D
iFlag:
Vector
Ezrin WT
Ezrin 1-583
Ezrin K4N
Vector
Ezrin WT
Ezrin 1-583
Ezrin K4N
GFP-FHOD1 - WT
GFP-FHOD1ΔDAD
GFP-FHOD1 -WT
Anti-GFP
Anti-Flag
1% Input
Output

Figure A.3 The activation state of FHOD1 has a small effect on the interaction with ezrin
(A) Diaphanous related formins, including FHOD1, are autoregulated through an interaction between the N-terminal Diaphanous inhibitory domain (DID) and the C-terminal diaphanous autoregulatory domain (DAD). Activation occurs upon binding of a Rho GTPase to the GTPase binding domain (GBD). This results in an open, active conformation. (B) Constitutively active FHOD1 mutants used within this appendix. Mutation of Valine 228 to aspartic acid in the DID domain prevents interaction between the DID and the DAD and results in a full length active FHOD1. Removal of the DAD domain also results in a fully active protein. (C) GFP-FHOD1-WT, GFP-FHOD1ΔDAD or GFP-FHOD1V228E was expressed in JEG-3 cells stably expressing ezrin iFlag contructs, subjected to Flag immunoprecipitation (IP) and then subsequently blotted for GFP and Flag. (D) Ezrin iFlag constructs were coexpressed with either GFP-FHOD1-WT or GFP-FHOD1ΔDAD, subjected to Flag immunoprecipitations and then subsequently blotted for GFP and Flag.

difference in the recovery of GFP-FHOD1ΔDAD and GFP-FHOD1V228E by ezrin, as both were recovered the same by ezrin constructs tested. I thus performed the remaining experiments with GFP-FHOD1ΔDAD for simplicity.

To address whether FHOD1 activation state effects interactions with more dramatic conformations of ezrin, the hyperactive ezrin iFlag 1-583 and the ezrin K4N mutants were utilized. Ezrin K4N contains mutations in basic residues essential for $PI(4,5)P_2$ binding that result in a completely closed form of ezrin (Niggli *et al.*, 1995; Barret *et al.*, 2000). I do not have a stable JEG-3 cell line with the ezrin iFlag K4N mutant so I used co-transfection for immunoprecipitations. Co-transfections in JEG-3 cells often result in low protein expression levels, especially when one of the plasmids is large like FHOD1, thus immunoprecipitations were performed in HEK293T cells which express abundant amounts of protein. Flag immunoprecipitations from 293T cells demonstrate that both GFP-FHOD1-WT and GFP-FHOD1ΔDAD bind to ezrin iFlag WT, with slightly more GFP-FHOD1ΔDAD pulled down by ezrin iFlagWT than GFP-FHOD1-WT (Figure A.3E). The hyperactive ezrin iFlag 1-583 cannot pull down either GFP-FHOD1-WT or active GFP-FHOD1ΔDAD. Interestingly, the completely closed conformation of ezrin, ezrin iFlagK4N is able to precipitate both GFP-FHOD1-WT and GFP-FHOD1ΔDAD with equal efficiency.

Together these results suggest that there is a preference for active FHOD1 in the context of a specific ezrin mutant. However, it also suggests that something more complicated is happening within the cell. While comparing the ability of wild type FHOD1 versus active FHOD1 to bind a single ezrin construct there is some preference for active FHOD1. However, when comparing the ability of active FHOD1 to bind either closed ezrin (iFlag T567A) or open ezrin (iFlag T567E) it is difficult to determine if there is a measurable difference in amount of pull down. It might be that

the differences in binding are subtle and when expressing active FHOD1 the conformation state of ezrin might be less important for interaction between the two proteins. What is most interesting is that FHOD1 is able to interact with the completely closed form of ezrin (ezrin iFlagK4N), which makes a strong case that FHOD1 does in fact prefer a more closed conformation of ezrin. More work will need to be done to determine exactly how FHOD1 activation plays a role in the interaction with different ezrin conformations and what this means functionally within the cell.

The interaction between FHOD1 and ezrin occurs between the FERM domain of ezrin and the extreme N-terminus of FHOD1

Next I sought to determine which regions of FHOD1 are essential for the interaction with ezrin. A FHOD1 truncation series was created (Figure A.4A) to narrow down a potential interaction region. Immunoprecipitations were performed in HEK293T cells co-expressing GFP-FHOD1 truncations and ezrin iFlag mutants. The Flag epitope was immunoprecipitated and then blotted for the GFP-tagged construct. Flag immunoprecipitations demonstrate that the region of FHOD1 that encompasses the GBD and the DID domains (GFP-FHOD1 1-339) was sufficient to bind both ezrin iFlagWT and ezrin iFlagT567A, while a truncation of FHOD1 that does not contain this region (GFP-FHOD1 569-1164) cannot bind ezrin (Figure A.4B). To determine if the alpha helical domain of FHOD1 contributes to this interaction, a truncation of FHOD1 that contains the alpha helical domain along with the GBD and DID (GFP-FHOD1 1- 569) was created. GFP-FHOD1 1-569 is not recovered preferentially by ezrin compared to GFP-FHOD1 1-339 (Figure A.4C). Finally, the hyperactive ezrin iFlag 1-583 is still unable to bind FHOD1 truncations (Figure A.4C). This would suggest that the interaction between ezrin and FHOD1 occurs within the first 339 amino acids of FHOD1.

A

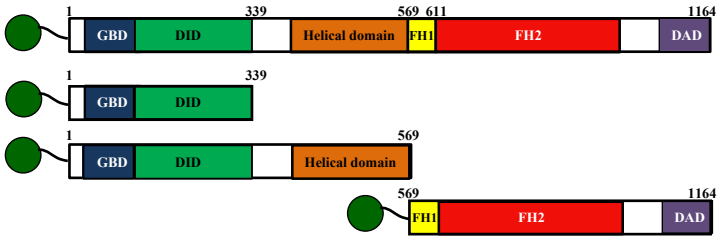
1
339
569
611
1164
GBD
DID
Helical domain
FH1
FH2
DAD
1
339
GBD
DID
1
569
GBD
DID
Helical domain
569
1164
FH1
FH2
DAD

B

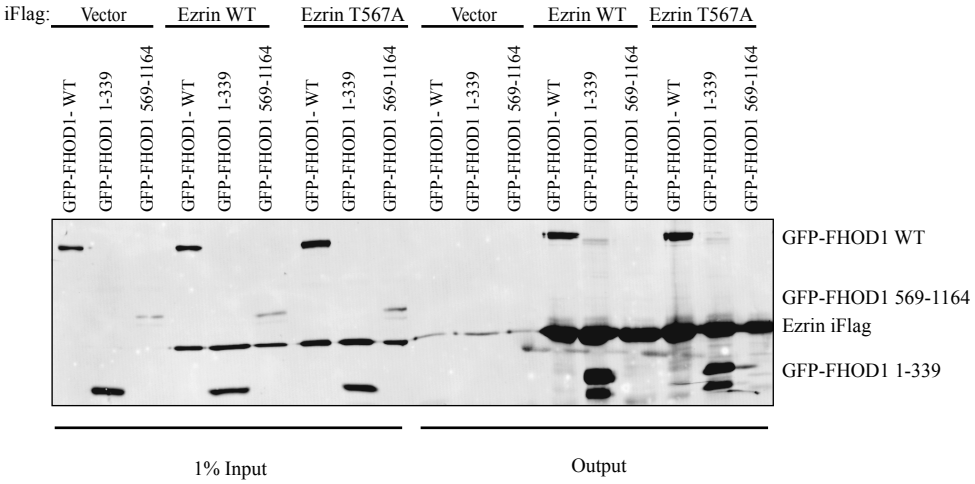
iFlag:
Vector
Ezrin WT
Ezrin T567A
Vector
Ezrin WT
Ezrin T567A
GFP-FHOD1- WT
GFP-FHOD1 1-339
GFP-FHOD1 569-1164
GFP-FHOD1 WT
GFP-FHOD1 569-1164
Ezrin iFlag
GFP-FHOD1 1-339
1% Input
Output

C

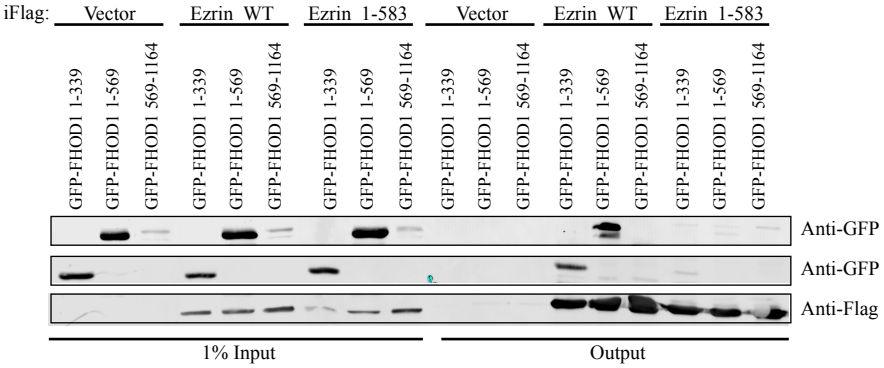
iFlag:
Vector
Ezrin WT
Ezrin 1-583
Vector
Ezrin WT
Ezrin 1-583
GFP-FHOD1 1-339
GFP-FHOD1 1-569
GFP-FHOD1 569-1164
Anti-GFP
Anti-GFP
Anti-Flag
1% Input
Output

D

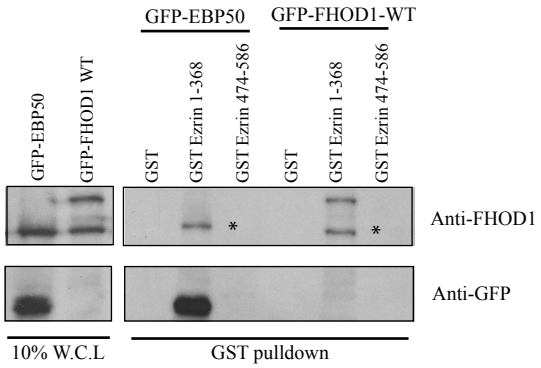
GFP-EBP50
GFP-FHOD1-WT
GFP-EBP50
GFP-FHOD1 WT
GST
GST Ezrin 1-368
GST Ezrin 474-586
GST
GST Ezrin 1-368
GST Ezrin 474-586
*
*
Anti-FHOD1
Anti-GFP
10% W.C.L
GST pulldown

Figure A.4 The interaction between ezrin and FHOD1 occurs betwwen the N-terminus of FHOD1 and the FERM domain of ezrin. (A) Schematic of the FHOD1 truncation constructs used in this figure. (B) HEK293T cells co-expressing the iFlag constructs indicated and either GFP-FHOD1-WT, GFP-FHOD1 1-339 or GFP-FHOD1 569-1164 were subjected to Flag immunoprecipitations and then subsequently blotted for GFP and Flag. (C) HEK293T cells co-expressing the ezrin iFlag construct indicated and the GFP-FHOD1 construct indicated were subjected to Flag immunoprecipitations and then subsequently blotted for GFP and Flag. (D) GST pulldowns were performed using GST-Ezrin 1-368 (FERM), GST Ezrin 474-586(C-ERMAD) or GST alone on JEG-3 cell lysate that was expressing either GFP-FHOD1 or GFP-EBP50 as a control. Subsequent blots were blotted using antibodies against GFP or endogenous FHOD1. * indicates endogenous FHOD1, while upper band is GFP-FHOD1.

To determine which region of ezrin is important for the interaction with FHOD1, GST pulldowns were performed. GST coupled to either ezrin FERM (GST-ezrin 1-368) or ezrin C-ERMAD (GST ezrin 474-586) was utilized on JEG-3 cell lysate expressing either GFP-FHOD1-WT or GFP-EBP50 as a control. Blotting with endogenous FHOD1 demonstrated that both GFP-FHOD1-WT, as well as endogenous FHOD1, was precipitated with the FERM domain (GST Ezrin 1-368) but not the C-ERMAD (GST-ezrin 474-586). GFP-EBP50 was pulled down as a positive control for FERM domain interaction (Fig.A.4D). This suggests that the interaction between ezrin and FHOD1 occurs between the FERM domain of ezrin and the N-terminus of FHOD1. This result does not, however, explain why FHOD1 does not bind to ezrin iFlag 1-583, a conformation in which the FERM domain is completely unmasked. Perhaps the hyperactive ezrin mutant is binding to other FERM domain binding partners which prevents the interaction between FHOD1 and ezrin. *In Vitro* work was attempted to classify this interaction further but the results were inconclusive (data not shown). More work, within the context of the cell and other binding partners, will need to be done.

FHOD1 truncations do not strongly localize to microvilli in JEG-3 cells

When Ezrin iFlag WT immunoprecipitations were performed more GFP-FHOD1 1-339 bound wild type ezrin than full length GFP-FHOD1 WT (Figure A.4B). To determine whether this stronger interaction with ezrin reflected a higher affinity for microvilli, I localized GFP-FHOD1 1-339 in JEG-3 cells. GFP-FHOD1 WT is cytoplasmic (See Chapter 2). Maximum projections of confocal *Z*-stacks in JEG-3 cells demonstrate that GFP-FHOD1 1-339 is mostly cytoplasmic, with some enrichment to the apical domain as seen in maximum Y projections (Figure A.5A). When looking at a single confocal z-stack, to help eliminate cytoplasmic signal, there is a slight

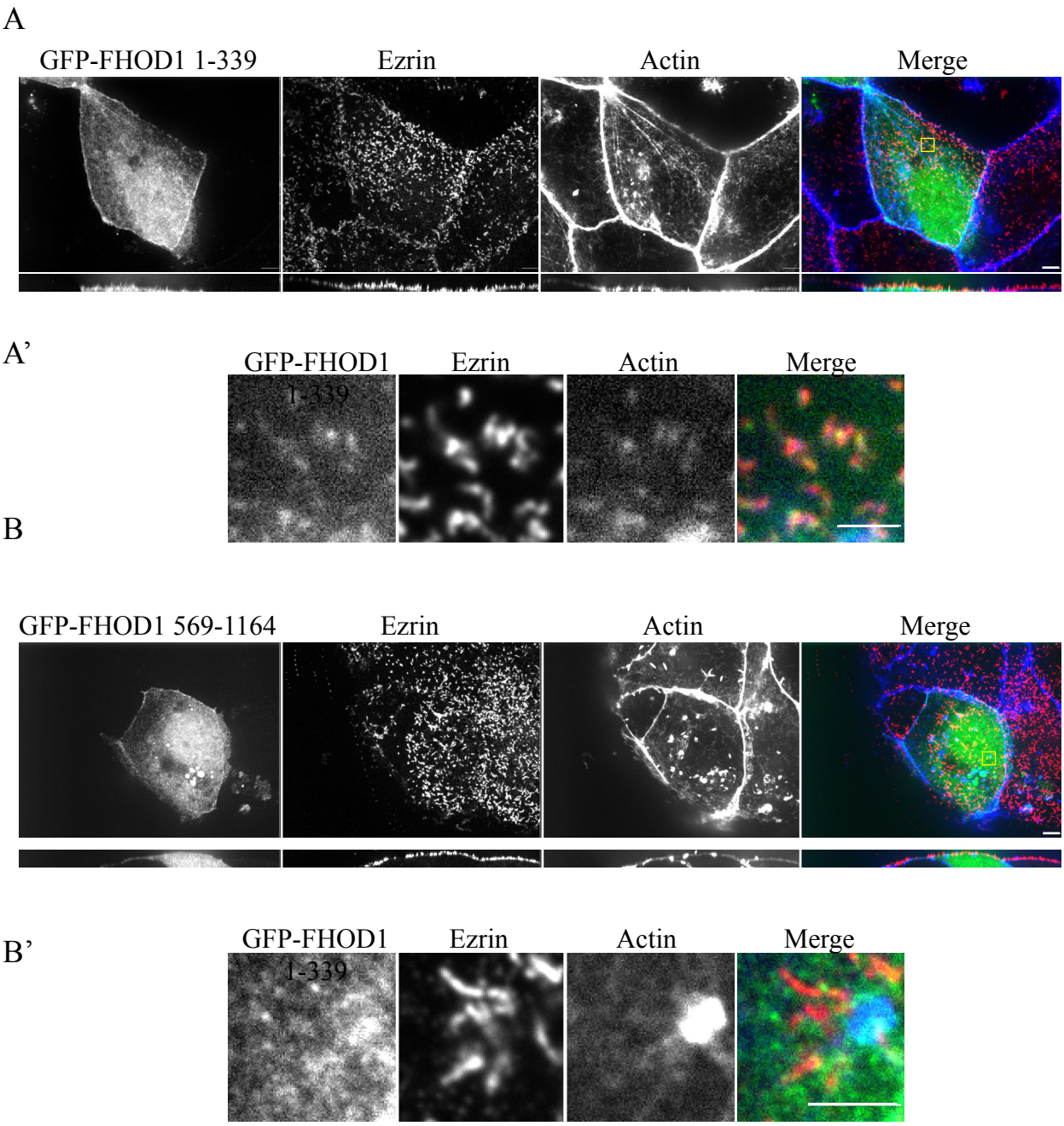

Figure A.5 FHOD1 1-339 has weak localization to microvilli in JEG-3 cells. (A-B) Maximum projections (XY) of confocal Z-stacks and side views (XZ) stretched twofold of JEG-3 cells expressing the indicated constructs, then fixed and GFP (green), endogenous ezrin (red), and F-actin (blue) localized. Yellow boxes represent a magnified single confocal Z-stack slice shown in (A'-B'). Bars: 5µm in (A, B, B') and 2µm in (A').

enrichment of GFP-FHOD1 1-339 in microvilli (Figure A.5 A'). This effect is not seen when GFP-FHOD1 569-1164 is expressed, which is completely cytoplasmic (Figure A.5B, B'). However, the localization of GFP-FHOD1 1-339 is still very weak and this fragment of FHOD1 cannot nucleate actin filaments. Thus even if is it slightly enriched in microvilli, it is unlikely acting on actin in this region.

What possible roles could this interaction between ezrin and FHOD1 serve? Considering that FHOD1 prefers interacting with a closed, inactive confirmation of ezrin it is possible that FHOD1 is somehow effecting ezrin regulation. Determining a role for FHOD1 and other proteins that prefer the inactive conformation of ezrin is an interesting avenue to pursue.

References

Alberts, A. S. (2001). Identification of a carboxyl-terminal diaphanous-related formin homology protein autoregulatory domain. J. Biol. Chem. *276*, 2824–2830.

Barret, C., Roy, C., Montcourrier, P., Mangeat, P., and Niggli, V. (2000). Mutagenesis of the Phosphatidylinositol 4,5-Bisphosphate (Pip2) Binding Site in the Nh2-Terminal Domain of Ezrin Correlates with Its Altered Cellular Distribution. J. Cell Biol. *151*, 1067–1080.

Bretscher, A. (1989). Rapid phosphorylation and reorganization of ezrin and spectrin accompany morphological changes induced in A-431 cells by epidermal growth factor. J. Cell Biol. *108*, 921–930.

Fievet, B. T., Gautreau, A., Roy, C., Del Maestro, L., Mangeat, P., Louvard, D., and Arpin, M. (2004). Phosphoinositide binding and phosphorylation act sequentially in the activation mechanism of ezrin. J. Cell Biol. *164*, 653–659.

Garbett, D., LaLonde, D. P., and Bretscher, A. (2010). The scaffolding protein EBP50 regulates microvillar assembly in a phosphorylation-dependent manner. J. Cell Biol. *191*, 397–413.

Gary, R., and Bretscher, A. (1995). Ezrin self-association involves binding of an N-terminal domain to a normally masked C-terminal domain that includes the F-actin binding site. Mol. Biol. Cell *6*, 1061–1075.

Hanono, A., Garbett, D., Reczek, D., Chambers, D. N., and Bretscher, A. (2006). EPI64 regulates microvillar subdomains and structure. J. Cell Biol. *175*, 803–813.

Kühn, S., and Geyer, M. (2014). Formins as effector proteins of Rho GTPases. Small GTPases *5*.

Niggli, V., Andréoli, C., Roy, C., and Mangeat, P. (1995). Identification of a phosphatidylinositol-4,5-bisphosphate-binding domain in the N-terminal region of ezrin. FEBS Lett. *376*, 172–176.

Reczek, D., Berryman, M., and Bretscher, A. (1997). Identification of EBP50: A PDZ-containing phosphoprotein that associates with members of the ezrin-radixin-moesin family. J. Cell Biol. *139*, 169–179.

Schulte, A., Stolp, B., Schönichen, A., Pylypenko, O., Rak, A., Fackler, O. T., and Geyer, M. (2008). The human formin FHOD1 contains a bipartite structure of FH3 and GTPase-binding domains required for activation. Structure *16*, 1313–1323.

Viswanatha, R., Ohouo, P. Y., Smolka, M. B., and Bretscher, A. (2012). Local phosphocycling mediated by LOK/SLK restricts ezrin function to the apical aspect of epithelial cells. J. Cell Biol. *199*, 969–984.

Viswanatha, R., Wayt, J., Ohouo, P. Y., Smolka, M. B., and Bretscher, A. (2013). Interactome analysis reveals ezrin can adopt multiple conformational States. J. Biol. Chem. *288*, 35437–35451.

Appendix B
Identifying novel partners of the Cobl localization domain (Cobl-648-899) in both JEG-3 and HEK293T cells

Overview

This appendix contains results from two independent SILAC experiments that sought to determine novel binding partners of the actin nucleator Cordon Bleu. Cordon Bleu (Cobl) was the focus of Chapter 3 and featured a SILAC experiment that identified novel interacting partners that bound to the COBL domain of Cobl (Cobl-COBL, AA 1-408). Due to technical difficulties, this experiment had to be performed in HEK293T cells, which don't have microvilli on their apical domain, as creating a JEG-3 stable cell line was not possible at that time. Another issue is that the COBL domain is not involved in localization to microvilli. A novel localization domain has been identified for Cobl (Chapter 3, (Wayt and Bretscher, 2014)), which is a 250 amino acid region that is still able to localize to microvilli in JEG-3 cells. Thus I created both JEG-3 and HEK393T stable cell lines that expressed a minimum region of Cobl that was required for localization to microvilli (AA 648-899). This appendix contains the results of two SILAC experiment, one in JEG-3 cells and one in HEK293T cells, utilizing Cobl-LD (AA 648-899) to determine novel interacting partners for Cobl. I also confirm two top candidates from the JEG-3 SILAC experiment by immunoprecipitations. These potential lists of candidates might be useful for someone who wished to pursue this line of research in the future.

Materials and Methods

Antibodies and Reagents

The mouse FLAG antibody and resin was from Sigma-Aldrich (St. Louis, MO), and the mouse GFP antibody was from Santa Cruz Biotechnology (Santa Cruz, CA). Goat anti-mouse secondary antibodies conjugated to horseradish peroxidase were from Jackson ImmunoResearch Laboratories (West Grove, PA).

Plasmids

Murine GFP-Cobl-FL was a kind gift from M. Kessels (Research Institute of the FSU Jena, Jena, Germany). Cobl FL and truncations were cloned into a modified PQCXIP (BD Biosciences) backbone that has an N-terminal 3xFLAG to create FLAG constructs. 3xFlag-Cobl- COBL (1-408), 3xFlag-Cobl-CT (409-1337), 3xFlag-Cobl-LD (648-899). The internal deletion of the Cobl localization domain (Δ 648-899) was generated by two steps of overlapping PCR and inserted into the modified PQCXIP to create 3xFlag-CoblΔLD. AnnexinA2 (Addgene) and PP55alpha (Addgene) were cloned into pEGFP-C2.

Cell Culture and Transfection

JEG-3, and HEK293T cells (American Type Culture Collection, Manassas, VA) were maintained in a 5% CO_2 humidified atmosphere at 37°C. JEG-3 cells were cultured in MEM (Thermo Fisher Scientific, Lafayette, CO) with 10% fetal bovine serum (FBS), and HEK293T in DMEM with 5% FBS. JEG-3 cells were transfected with polyethylenimine (Polysciences, Warrington, PA) and 1–2 μg plasmid DNA, as described (Hanono *et al.*, 2006). HEK293T cells were co-transfected with Lipofectamine 2000 (Invitrogen) according to the manufacturers' instructions. For generation of

stable JEG-3 and HEK293T cell lines expressing 3xFLAG-Cobl-LD or 3xFLAG-empty vector, Phoenix-AMPHO cells were cotransfected with the above constructs in pQCXIP in addition to a plasmid encoding VSV-G using polyethylenimine. The infected HEK293T cells were then selected and maintained with 2 μg/ml puromycin (Sigma-Aldrich).

Immunoprecipitations and Western Blotting

HEK293T cells transiently co-expressing 3xFLAG-Cobl constructs and either GFP-ANAX2 or GFP-PP55alpha constructs for 24 hours were lysed in lysis buffer (25 mM Tris, pH 7.4, 5% glycerol, 150 mM NaCl, 50 mM NaF, 0.1 mM Na_3VO_4, 10 mM β-glycerol phosphate, 8.7 mg/ml paranitrophenylphosphate, 0.3% Triton X-100, and protease inhibitor tablet [Roche]) and immunoprecipitated with M2 FLAG resin (Sigma-Aldrich) for 2 hours. Immunoprecipates were than washed 4 times in wash buffer (Lysis buffer but with 0.2% Triton X-100 and no protease inhibitor tablet) and eluted from the FLAG resin with 200μg/ml 3xFLAG peptide. Eluates were than denatured with Laemmli buffer, resolved by SDS-PAGE, transferred to Immobilon-FL (EMD Millipore, Billerica, MA), blotted with specific antibody and visualized by ECL.

SILAC and mass spectrometry

For SILAC, HEK293T or JEG-3 cells stably expressing either 3xFLAG-Empty Vector or 3xFLAG-Cobl-LD were grown in MEM with 10% dialyzed FBS (Invitrogen) and either [^{12}C]arginine and lysine or [^{13}C]arginine and lysine, respectively, for three weeks to allow uniform labeling of all proteins. FLAG immunoprecipitations were performed as described above with modifications for mass spectrometry (Smolka *et al.*, 2007; Viswanatha *et al.*, 2012). Briefly, after immunoprecipitation, protein bound to FLAG resin was eluted in 50 mM Tris (pH 8.0) and 1%

SDS and then precipitated with 50% ethanol, 49.9% acetone, and 0.1% acetic acid. Protein samples were then mixed, trypsin digested (Promega, Madison, WI) overnight at 37°C and desalted in a C18 column (Waters, Milford, MA). The tryptic peptides were dehydrated in a speed vacuum and dissolved in 80% acetonitrile and 1% formic acid for fractionation by hydrophilic interaction chromatography. The resulting fractions were dried, dissolved in 0.1% trifluoroacetic acid, and injected into a mass spectrometer (Qexactive LC-MS/MS; Thermo Fisher Scientific). The data were analyzed using Proteome Discoverer (Thermo Fisher Scientific). Proteins were considered enriched if the ratio of Heavy:Light was above 2.0 and the score was above 20. Score is determined mathematically by the software and is considered an indication of how confidant the program is that the peptide from mass spectrometry belongs to the protein identified. PSMs is "Peptide Spectral Match" and is roughly the number of peptides identified in the mass spectrometry run. A hit with a low number of PSMs is not as confidently scored.

Results and Discussion

Use of SILAC-Mass spectrometry to discover novel Cordon Bleu interaction partners

To identify potential interacting proteins I utilized Stable Isotope Labeling of Amino acids in Cell Culture (SILAC) combined with quantitative mass spectrometry (see Fig. 3.8 in Chapter 3 for schematic). In outline, JEG-3 or HEK293T cells (in two independent experiments) stably expressing an empty vector control grown in light [^{12}C]arginine and lysine medium or 3x-FLAG-Cobl-LD (AA 648-899) grown in heavy [^{13}C]arginine and lysine medium were used to identify novel interacting partners. FLAG-immunoprecipitation was performed on both samples and the immunoprecipitates subsequently combined and trypsin digested. The digested samples were then subjected to quantitative mass spectrometry. Peptides identified as enriched in the control sample were considered background and peptides enriched in the 3xFLAG-Cobl-LD sample were considered potential interactors of the Cobl localization domain.

The top candidates identified by my analysis are shown in Table B.1 for HEK293T cells and Table B.2 for JEG-3 cells. To determine which proteins were potential candidates I chose proteins that had a Heavy:Light enrichment ratio above 2.0 and a score above 20 (see materials and methods for details). As seen in Table B.1, the top candidate in HEK293T cells is the microvillar protein ezrin with another member of the ERM family, radixin, also being significantly enriched. Other interesting proteins include Dynamin-2, which is involved in endocytosis (Grassart *et al.*, 2014) and Septin-7 which is located at the base of primary cilia and is suggested to play a role in actin cytoskeleton organization (Fliegauf *et al.*, 2014). This is potentially interesting because Cobl has also been localized to the base of primary cilia is zebrafish by others (Schüler *et al.*, 2013). Further verification will need to be done to determine if these proteins are true Cobl interacting proteins. This list could provide a nice starting point for future studies.

T**able B.1: Identifying binding partners for the Cobl localization domain (648-899) in HEK293T cells.** HEK293T cells stably expressing an empty vector control grown in light medium or 3x-FLAG-Cobl-LD (AA 648-899) grown in heavy medium were used to identify novel interacting partners. FLAG-immunoprecipitation was performed on both samples and the immunoprecipitates subsequently combined and trypsin digested. The digested samples were then subjected to quantitative mass spectrometry. Peptides identified as enriched in the control sample were considered background and peptides enriched in the 3xFLAG-Cobl-LD sample were considered potential interactors of the localization domain. Proteins are ranked highest to lowest in Heavy:Light enrichment. A score, determined by Proteome Discover, of 20 and a Heavy:Light ratio above 2.0 was used as a cutoff for determining potential interactors. Unique peptides represents the total number of unique peptides identified by mass spectrometry and #PSMs is number of Peptide Spectral Matches.

Protein	Score	Unique Peptides	# PSMs	Heavy: Light
Ezrin	49.91	8	18	5.490
14-3-3 Gamma	65.23	5	24	4.286
Phosphoserine aminotransferase	45.65	10	14	3.945
Septin-7	41.39	7	10	3.928
Phosphoglycerate kinase 1	158.91	15	42	3.839
Vesicle-fusing ATPase	47.21	12	16	3.689
Radixin	31.77	6	12	3.623
Isoform 3 of Sodium/potassium-transporting ATPase subunit alpha-1	110.54	22	38	3.130
Cyclin-dependent kinase 1	29.30	5	8	3.118
Isoform 2 of Dynamin-2	21.26	7	7	2.978
Isoform 3 of Exportin-2	118.12	20	33	2.707
Tyrosine-protein kinase CSK	35.25	9	11	2.256
Sorting nexin-2	34.77	8	12	2.217
Hypoxia up-regulated protein 1	76.65	15	20	2.148
Isoform 3 of Dynamin-1-like protein	30.82	6	9	2.097
Isoform 1 of Vinculin	115.56	25	35	2.047
Plastin-3	127.17	19	38	2.019

Table B.2. Identifying binding partners for the Cobl localization domain (648-899) in JEG-3 cells. JEG-3 cells stably expressing an empty vector control grown in light medium or 3x-FLAG-Cobl-LD (AA 648-899) grown in heavy medium were used to identify novel interacting partners. FLAG-immunoprecipitation was performed on both samples and the immunoprecipitates subsequently combined and trypsin digested. The digested samples were then subjected to quantitative mass spectrometry. Peptides identified as enriched in the control sample were considered background and peptides enriched in the 3xFLAG-COBL sample were considered potential interactors of the localization domain. Proteins are ranked highest to lowest in Heavy:Light enrichment. A score, determined by Proteome Discover, of 20 and a Heavy:Light ratio above 2.0 was used as a cutoff for determining potential interactors. Unique peptides represents the total number of unique peptides identified by mass spectrometry and #PSMs is number of Peptide Spectral Matches.

Protein	Score	Unique Peptides	# PSMs	Heavy:Light
Serine/threonine-protein phosphatase 2A 55 (PPP2R2A)	33.70	12	14	17.840
Protein S100-A10	16.32	1	5	5.246
Serine/threonine-protein phosphatase 2A 65 kDa regulatory subunit A alpha isoform (PPP2R1A)	52.76	13	20	4.441
Protein S100-A13	11.16	3	5	3.166
Annexin A2	97.37	20	36	2.523
Isoform 1A of Mitogen-activated protein kinase kinase kinase 7 (MAP3K7)	37.01	10	17	2.313
Kinesin-like protein KIF11	207.06	42	76	2.276
TGF-beta-activated kinase 1 and MAP3K7-binding protein (TAB1)	146.20	26	51	2.261
Four and a half LIM domains protein 2 (FHL2)	11.07	4	7	2.247
Serine/threonine-protein kinase RIO1 (RIOK1)	59.09	9	18	2.138
Protein S100-A16	12.16	2	5	2.133
Protein arginine N-methyltransferase 5 (PRMT5)	408.54	43	137	2.123
Serine/threonine-protein kinase 38- like	51.85	14	26	2.001
Protein phosphatase 1B (PPM1B)	694.30	44	229	1.993
Serine/threonine-protein kinase 38 (STK38)	219.82	27	83	1.971

However, because HEK393T cells do not have microvilli on their apical domain the same SILAC experiment as described above was repeated but with JEG-3 cells stably expressing Cobl-LD, the results of which can be seen in Table B.2. I wanted to compare the similarities and differences between the two cell types to determine cell specific interaction proteins. I also wanted to utilize a cell line that has Cobl localized to a very specific place, the base of microvilli, which might produce a list of candidates that were more likely to be relevant to microvilli. What is immediately striking is that the lists between the cell types are not at all similar, with vastly different proteins showing significant enrichment in Heavy:Light. I included several proteins whose enrichment was below 20 because they might be potentially interesting but would need to be verified before moving forward. The most significantly enriched Cobl interacting protein in JEG-3 cells is the regulatory subunit of the protein phosphatase 2A (PP55alpha), a serine/threonine phosphatase that has been implicated in the regulation of the microvillar protein EBP50 (Boratkó *et al.*, 2012). Interestingly, both the Ca^{2+} dependent lipid binding protein AnnexinA2 and its binding partner S100A10 were also enriched. AnnexinA2 is an interesting candidate because it has been localized to the luminal side of microvilli of the brush border (Danielsen *et al.*, 2003). AnnexinA2 has also been shown to interact with PP55alpha, which makes these top candidates even more intriguing. Because of these potential links to microvilli, these two proteins were selected to further verify by immunoprecipitation.

Immunoprecipitations confirm that AnnexinA2 and PP55alpha interact with Cobl

To validate the results of the SILAC analysis I co-expressed different FLAG-Cobl variants and GFP-AnnexinA2 (GFP-ANAX2) or GFP-PP55alpha in HEK293T cells, and then immunoprecipitated the FLAG epitope and blotted for the GFP-tagged construct. Despite being

identified as a potential binding partner for the localization domain of Cobl, AnnexinA2 was precipitated more efficiently with the full length version of Cobl (3xFlag-Cobl-FL) or the C-terminus of Cobl (3xFlag-Cobl-CT) than the localization domain alone (3xFlag-Cobl-LD)(Fig. B.1A). This suggests that there are other regions outside the Cobl LD that help mediate this interaction. In contrast, GFP-PP55alpha is recovered with similar affinity by both 3xFlag-Cobl-LD and 3xFlag-Cobl-FL (Fig. B.1B). Strikingly, the localization domain is not necessary for this interaction as a construct that lacks the localization domain (3xFlag-CoblΔLD) can still bind GFP-PP55alpha with some affinity. Determining if these proteins localize to microvilli in JEG-3 cells will be an important next step in validating whether these cells have a function within microvilli.

Collectively, these results suggest that there are many potential new binding partners of Cobl and understanding these interactions may reveal novel functions of Cobl within cells.

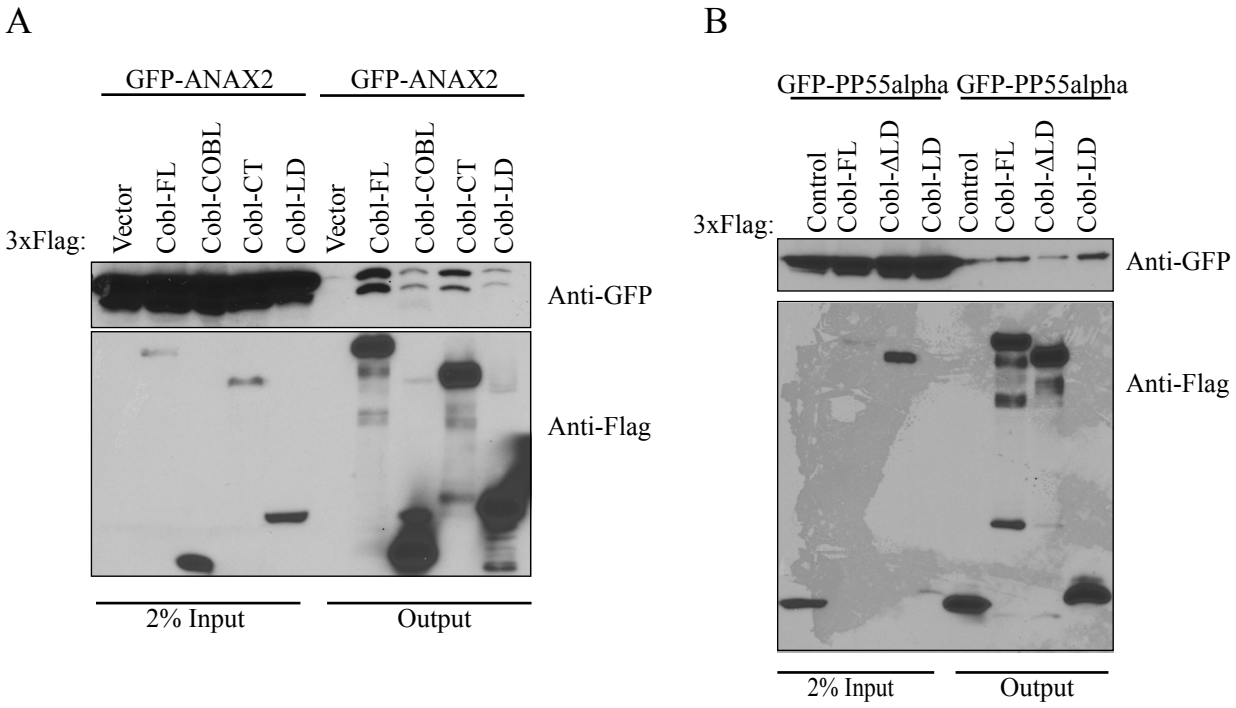

Figure B.1 AnnexinA2 and PP55alpha bind to Cobl in HEK293T cells. (A) 3x-Flag-Cobl constructs were co-expressed with GFP-ANAX2 in 293T cells for 48 hours, subjected to Flag immunoprecipitations(IP) and then subsequently blotted for GFP and Flag. (B) 3x-Flag-Cobl constructs were co-expressed with GFP-PP55alpha in 293T cells for 48 hours, subjected to Flag immunoprecipitations (IP) and then subsequently blotted for GFP and Flag.

References

Boratkó, A., Gergely, P., and Csortos, C. (2012). Cell cycle dependent association of EBP50 with protein phosphatase 2A in endothelial cells. PLoS One *7*, e35595.

Danielsen, E. M., van Deurs, B., and Hansen, G. H. (2003). "Nonclassical" secretion of annexin A2 to the lumenal side of the enterocyte brush border membrane. Biochemistry *42*, 14670–14676.

Fliegauf, M., Kahle, A., Häffner, K., and Zieger, B. (2014). Distinct localization of septin proteins to ciliary sub-compartments in airway epithelial cells. Biol. Chem. *395*, 151–156.

Grassart, A., Cheng, A. T., Hong, S. H., Zhang, F., Zenzer, N., Feng, Y., Briner, D. M., Davis, G. D., Malkov, D., and Drubin, D. G. (2014). Actin and dynamin2 dynamics and interplay during clathrin-mediated endocytosis. J. Cell Biol. *205*, 721–735.

Hanono, A., Garbett, D., Reczek, D., Chambers, D. N., and Bretscher, A. (2006). EPI64 regulates microvillar subdomains and structure. J. Cell Biol. *175*, 803–813.

Schüler, S., Hauptmann, J., Perner, B., Kessels, M. M., Englert, C., and Qualmann, B. (2013). Ciliated sensory hair cell formation and function require the F-BAR protein syndapin I and the WH2 domain-based actin nucleator Cobl. J. Cell Sci. *126*, 196–208.

Smolka, M. B., Albuquerque, C. P., Chen, S., and Zhou, H. (2007). Proteome-wide identification of in vivo targets of DNA damage checkpoint kinases. Proc. Natl. Acad. Sci. U. S. A. *104*, 10364–10369.

Viswanatha, R., Ohouo, P. Y., Smolka, M. B., and Bretscher, A. (2012). Local phosphocycling mediated by LOK/SLK restricts ezrin function to the apical aspect of epithelial cells. J. Cell Biol. *199*, 969–984.

Wayt, J., and Bretscher, A. (2014). Cordon Bleu serves as a platform at the basal region of microvilli where it regulates microvillar length through its WH2 domains. Mol. Biol. Cell.